GROUNDWATER HYDROGEN, OXYGEN, AND STRONTIUM ISOTOPE VARIATION OF HOUT BAY VALLEY, CAPE TOWN.

Warrick Daws (DWSWAR001)

Supervisor: Prof. Chris Harris

Co-supervisor: Prof. Judith Sealy

Abstract

Accessible groundwater can be an alternative water supply to meet water demands and elevate stress from existing water supply systems in semi-arid regions. Monitoring stable isotope compositions (δD and $\delta^{18}O$) in the hydrosphere can aid hydrogeologists in understanding groundwater processes. The δD and $\delta^{18}O$ of 148 water samples (groundwater, rainwater, and stream water) from Hout Bay, a coastal valley 20 km south-west of Cape Town are considered in this study. Groundwater samples from 65 boreholes/wellpoints is presented over two distinct phases (February/March 2020, and November 2020) with groundwater electrical conductivity and groundwater temperature measurements. Hout Bay groundwater δD and $\delta^{18}O$ range from -16.5‰ to -6.4‰ and -3.90‰ to -2.14‰ respectively and show no strong correlation with seasonality or elevation above sea level. Electrical conductivity of Hout Bay 2020 groundwater is relatively low ranging from 126 µS/cm to 2370 µS/cm. Hout Bay monthly rainwater amount, δD, and $\delta^{18}O$ were measured from March 2020 to February 2021. The weighted mean δD and $\delta^{18}O$ values of Hout Bay monthly rainwater from March 2020 to February 2021 are -6.2‰ and -2.38‰ respectively. The δD and $\delta^{18}O$ values of Hout Bay rainwater cluster around the local meteoric water line established for UCT, and show a strong amount effect (r = -0.92 for δD vs amount). Three possible explanations are proposed for the δD and $\delta^{18}O$ difference between Hout Bay monthly rainwater weighted mean from March 2020 to February 2021, and Hout Bay February/March 2020 and November 2020 groundwater. The first is that intense rainfall events preferentially recharge groundwater with low δD and $\delta^{18}O$ values. The second explanation is that Hout Bay groundwater might have retained more negative δD and $\delta^{18}O$ values from rainwater recharge prior to March 2020. Lastly, recharge from mountain peaks at higher elevation than the Hout Bay groundwater sample locations add a component of more negative δD and $\delta^{18}O$ to Hout Bay groundwater than proximal rainwater. Nine samples from Hout Bay February/March 2020 groundwater sample collection were analysed for strontium isotope composition ($^{87}Sr/^{86}Sr$) to determine the applicability of strontium to trace the source of groundwater. The $^{87}Sr/^{86}Sr$ ratios in Hout Bay groundwater vary from 0.710 to 0.731. There is a strong negative correlation between $^{87}Sr/^{86}Sr$ and $\delta^{18}O$ (r = -0.91). The low end of the $^{87}Sr/^{86}Sr$ data

array appears to be of marine origin but the corresponding $\delta^{18}O$ values of ~-2.9‰ do not reflect that of seawater. Minor interactions of Hout Bay groundwater with Cape Granite produce relatively high $^{87}Sr/^{86}Sr$ ratios while lower $^{87}Sr/^{86}Sr$ ratios similar to that of modern seawater are attributed to dissolution of the marine sediments of the Quaternary Witzand Formation and marine aerosols in sea spray. Higher rainwater amounts are proposed to increase $^{87}Sr/^{86}Sr$ ratios of higher elevation groundwater sample locations by diluting the dissolution of marine aerosols in rainwater.

Acknowledgements

Thank you to Prof. Chris Harris for patience and understanding. It was a pleasure to learn from you through this project. I am immensely appreciative of support from Prof. Judith Sealy. Mardi and Mark Cairns, I am grateful for the continued motivation and guidance. I am fortunate to have had close friends bolster me through this project. Isotope analysis was conducted by Joshua Mirkin at UCT. Funding for this research came from the National Research Foundation. Waters analysis costs were covered by a CIMERA grant.

Table of Contents

Chapter 1 Introduction

Water that exists and moves underground through subsurface soil and rock is referred to as groundwater. An aquifer is a porous or permeable rock formation that allows groundwater to flow through it. Groundwater exists as a subsurface water reservoir that is tapped into through boreholes, wellpoints, and springs. Groundwater plays a crucial part in the water cycle and makes up 0.79% of the Earths surface water balance (Kotwicki, 2009). Groundwater makes up 95% of the utilizable (excluding icecaps) freshwater balance on Earth (Freeze and Cherry, 1979).

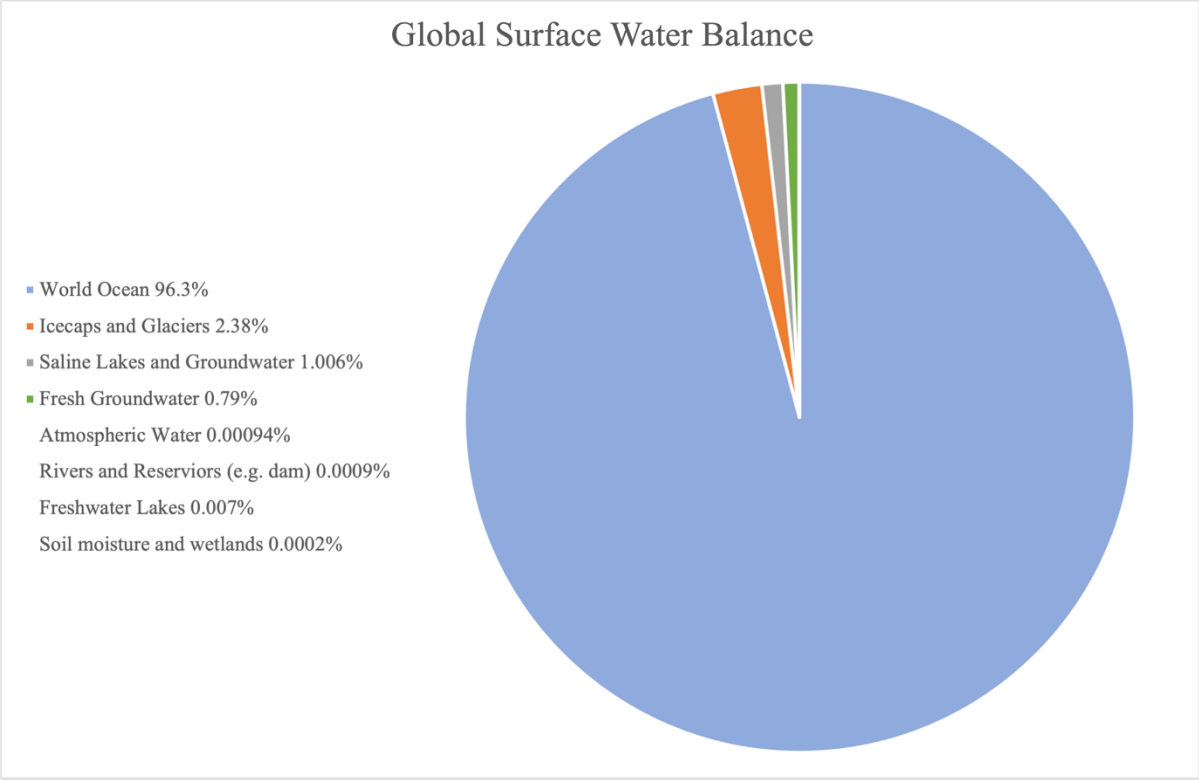

Fig 1.1 Global surface water balance after Kotwicki (2009).

South Africa is considered semi-arid receiving an average of 465 mm of rainfall annually (Pitman, 2011). Access to clean drinking water is an issue that many South Africans deal with regularly (Department of Environmental Affairs, 2013). The Western Cape province receives predominantly winter rainfall from May to August (Fig. 1.2). Cape Town's experiences a Mediterranean-type climate with temperature averages ranging from 13°C in rainy winters to 21°C in dry summers (International Atomic Energy Agency and World Meteorological Organization, 2006). The majority of Cape Town's drinking water supply is stored as surface water in dams. Existing water resources are subject to the possible adverse effects of climate change. Recently, Cape Town experienced one of its worst drinking water crises (Otto et al., 2018).

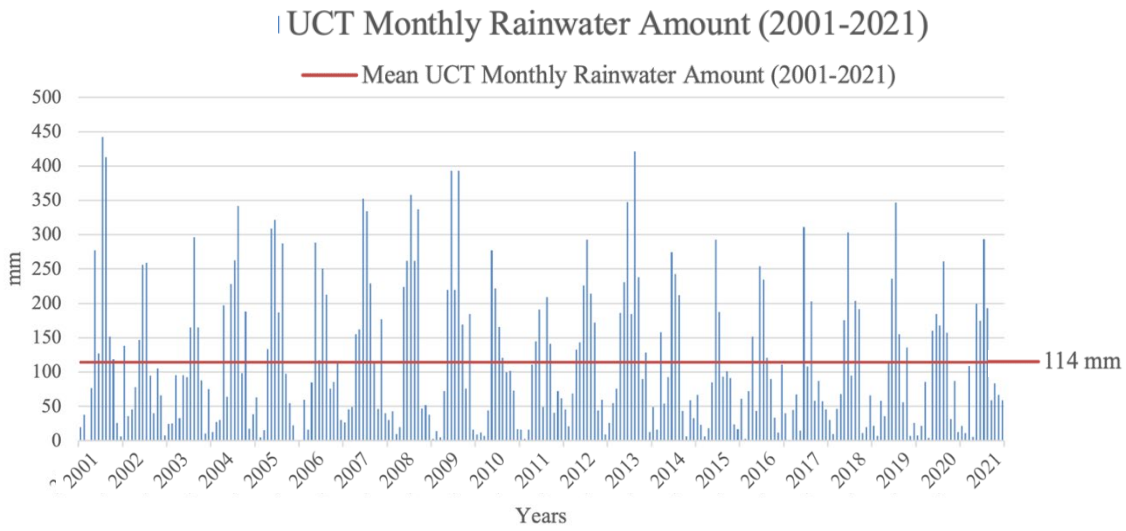

Fig 1.2 UCT monthly rainfall amount from January 2001 to December 2021 with a mean value of 114 mm for rainwater collected at 33°57'32.18"S 18°27'37.71"E. Reliable long term monthly data (δD, $\delta^{18}O$, and rainwater amount) collected at UCT by proficient individuals is accessible from June 1995 to December 2021 in the UCT data base. UCT is approximately 8 km from Hout Bay.

The City of Cape Town experienced a water supply shortage from 2015 to 2018 due to low rainfall for several years in the catchment areas for major dams (Otto et al., 2018; Enqvist and Ziervogel, 2019). Figure 1.2 shows historic Monthly rainwater amount collected at UCT for 20 years (January 2001-December 2021). There was no clear sign of meteorological drought due to lack of precipitation in Cape Town (Fig 1.2). The shortage put severe stress on water supply systems and strict water restrictions were implemented with tariff hikes to reduce water demand. To cope with the restrictions, many

households and industries turned to groundwater and rainwater as alternatives to surface water supply. In the many arid regions, groundwater is a fundamental source of drinking water and irrigation for agriculture (West et al., 2014). According to Cobbing and Hiller (2019), groundwater potential to elevate water supply is high in sub Saharan Africa. It is estimated that only 13% of municipal water in south Africa is groundwater (Riemann et al., 2012). Groundwater use is likely to increase as water demand increases.

$$\delta D = \frac{^{2}H/^{1}H_{(sample)} - ^{2}H/^{1}H_{(SMOW)}}{^{2}H/^{1}H_{(SMOW)}} * (1000)$$

$$\delta^{18}O = \frac{^{18}O/^{16}O_{(sample)} - ^{18}O/^{16}O_{(SMOW)}}{^{18}O/^{16}O_{(SMOW)}} * (1000)$$

Fig 1.3 The applied delta (δ) formulas that includes the ratio of heavy isotope to light and is adjusted to Vienna Standard Mean Ocean Water (SMOW) scale. H = hydrogen and O = oxygen

The stable isotope ratios of hydrogen, oxygen, and strontium have proved useful across a number of natural scientific disciplines including geology, hydrology, archaeology, and ecology (Craig, 1961; Dansgaard, 1964; Allison, 1988; West et al., 2006; Bowen and Good, 2015). For hydrogen and oxygen, the ratio of heavy isotope to light isotope is measured and reported in δ-notation relative to Standard Mean Ocean Water (SMOW) as in the equations above (Fig 1.3). The strontium isotope composition ($^{87}Sr/^{86}Sr$) of modern seawater is constant whereas the strontium isotope composition ($^{87}Sr/^{86}Sr$) of rocks is related to time-dependent radioactive decay of rubidium. An effective technique for monitoring groundwater is by using δD, $\delta^{18}O$, and $^{87}Sr/^{86}Sr$ composition to provide useful information about aquifer recharge and mixing of water bodies. An isoscape is a representation of geographical variation of isotopes (Bowen, 2010; West, et al 2014). Although it is concealed within the Earth's subsurface, groundwater generally behaves in a relatively predictable manner. Aquifers provide a framework for groundwater to flow through. It is therefore imperative to understand the geological controls on groundwater movement. Groundwater flow through aquifers is driven by hydraulic gradient. Physiochemical analysis (electrical conductivity and temperature) can provide insight on the processes

groundwater undergoes and broadly indicate water quality (Schot and van der Wal, 1992; de Montety et al., 2008). Point sources of pollution can be identified through chemical assessments of groundwater sample (Kjeldsen, 1993; Christensen et al., 2000). Degradation of groundwater quality by anthropogenic contaminants is avoidable through responsible human practices. Deuterium excess is a useful second-order parameter and can be used to infer relative humidity conditions during evaporation of water which ultimately forms precipitation (Gat, 1971; Pfahl and Sodemann, 2013). Similar isotope studies on the aquifers in the greater south-western Cape have been carried out (Weaver et al., 1999; Pietersen and Parsons, 2002; Harris et al., 2010; Miller et al., 2017, 2018; Diamond and Harris, 2019 Scott et al., 2020). These studies will be referred in the chapters that follow. There is no other previous isotopic groundwater study of this nature carried out in Hout Bay. Figure 1.4 is a Google Earth image of the Hout Bay river mouth entering the ocean. Rivers are surface expressions of groundwater and this represents the connectivity of water bodies. Fastidious monitoring of groundwater by hydrochemical means can allow for sustainable abstraction of groundwater resources and management of aquifer integrity. The sustainable use of groundwater requires monitoring of parameters at multiple intervals to observe seasonal trends and increase the accuracy of data.

Fig 1.4 Google Earth image on 15 August 2021 of the Hout Bay river mouth entering the ocean at 34° 2'44.88"S 18°21'22.57"E.

Aims and Objectives:

This study aims to establish the hydrogen, oxygen, and strontium isotope composition of Hout Bay groundwater. The seasonality of Hout Bay groundwater has not been investigated before this study. The source of recharge and the extent of recharge has not been published for Hout Bay groundwater. The quality of Hout Bay groundwater and the possible point sources of pollution as well as possible seawater ingress has not been accessed until this study. Data collected in this study could be incorporated into an isoscape and provide a great deal of insight into regional groundwater processes.

The key research questions that this thesis seeks to answer are:

1. Is there variation of δD and $\delta^{18}O$ in Hout Bay groundwater?
2. Is variation of δD and $\delta^{18}O$ in Hout Bay groundwater related to location (areal variation)?
3. Is variation of δD and $\delta^{18}O$ related to time of sample collection (seasonality)?
4. What are the possible causes of areal variation of parameters (δD, $\delta^{18}O$, electrical conductivity, groundwater temperature) measured in Hout Bay groundwater?
5. What are the possible causes of seasonal variation of parameters (δD, $\delta^{18}O$, electrical conductivity, groundwater temperature) measured in Hout Bay groundwater?
6. Are there correlations between parameters (δD, $\delta^{18}O$ electrical conductivity, groundwater temperature) measured in Hout Bay groundwater, Hout Bay rainwater, and Hout Bay stream water?
7. Are there major concerns over Hout Bay groundwater quality?
8. What do $^{87}Sr/^{86}Sr$ ratios of Hout Bay groundwater infer about groundwater in the study area?

Chapter 2 Background

This study focuses on of groundwater within the Hout Bay Valley in the Southern Peninsula of Cape Town, South Africa.

Fig 2.1 Hout Bay study area with topographical map adapted from OpenStreetMaps.

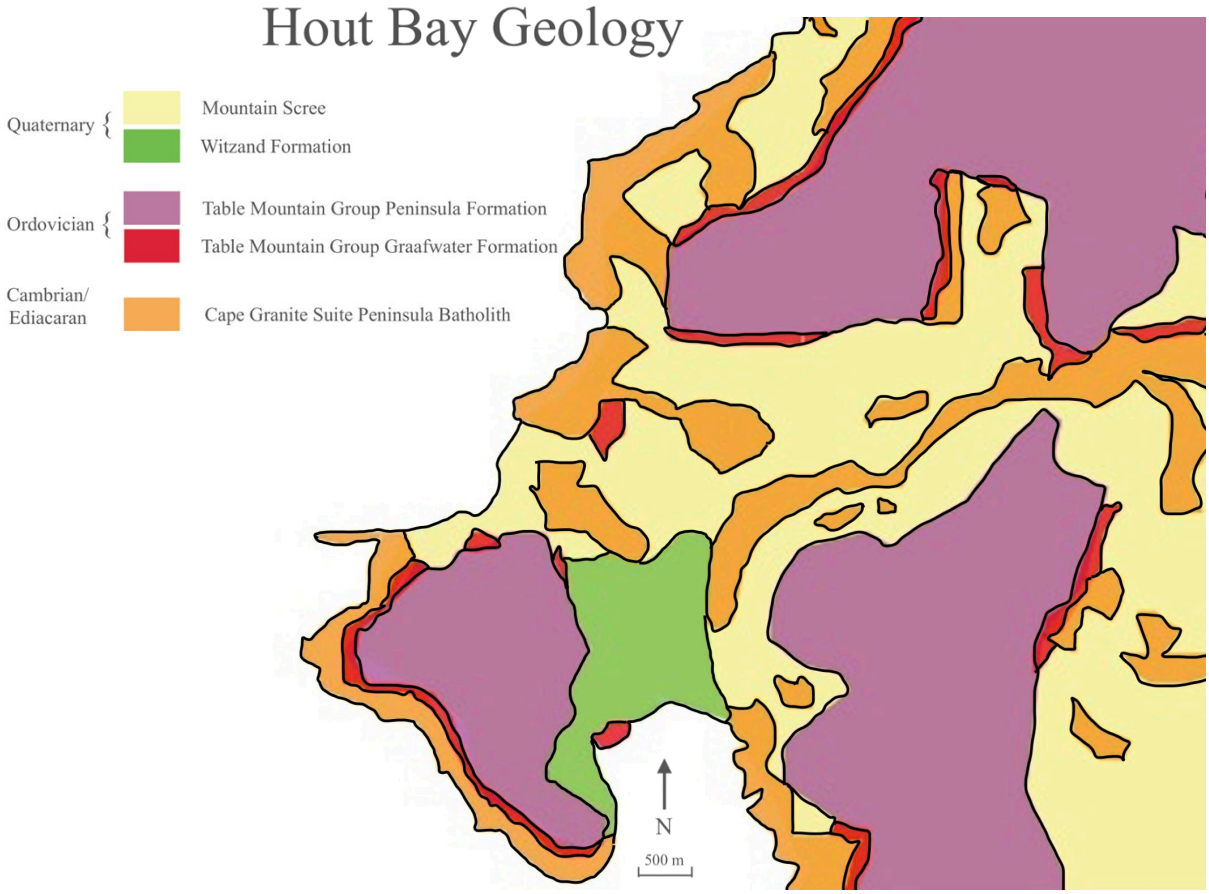

Fig 2.2 Geology of Hout Bay adapted from of Council for Geoscience (1990).

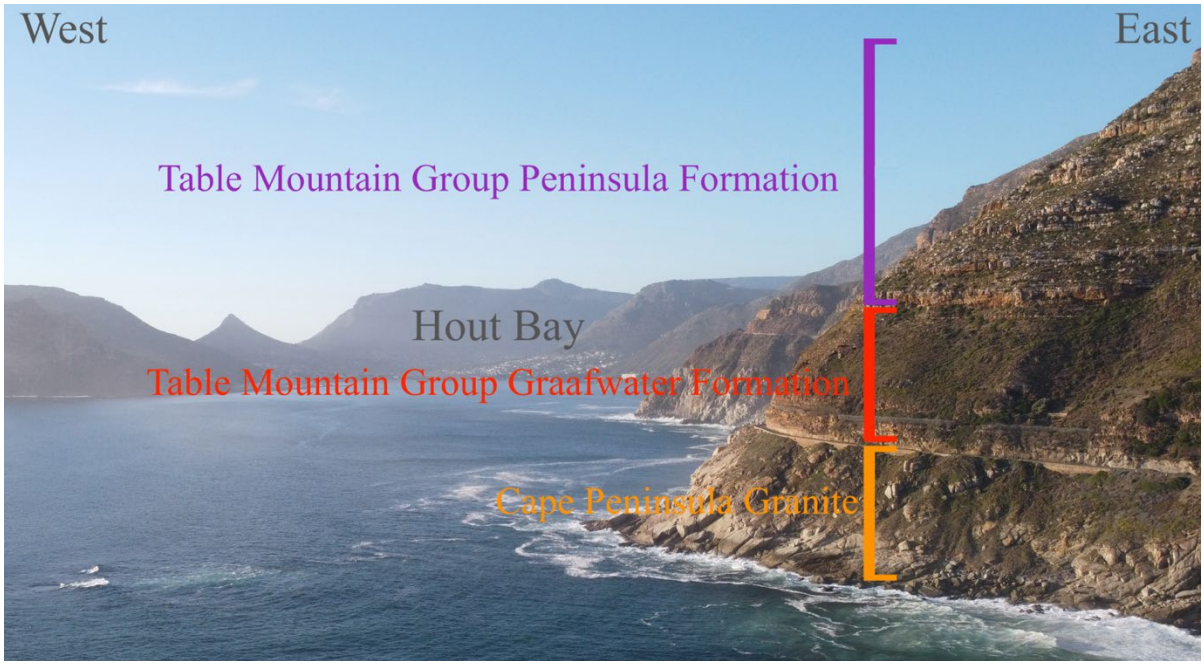

Fig 2.3 Drone image of Hout Bay showing outcrops of rock types. Drone image by Matthew Broekhuizen.

Study Area:

The groundwater sample collection area covered 14.53 km^2 in the Hout Bay suburb (Fig 2.1). Surround peaks rise to 857 mamsl to the North (Grootkop Peak), 928 mamsl to the South (Constantiaberg peak), 579 mamsl to the East (Vlakkenberg Peak), and 653 mamsl to the West (Karbonkelberg Peak) (Fig 2.1). The Hout Bay river flows through the centre of the valley and discharges into the Atlantic Ocean at Hout Bay beach (Fig 1.3). The valley slopes have a rich diversity of indigenous vegetation covering as well as what remains of some pine plantations. "Hout bay" is derived from "Houtbaai" (Wood Bay) which is what the Dutch settlers of the Cape colony named the area in 1653 due to the dense yellowwood forests in the area.

Local Geology:

Figure 2.2 shows the rock-types that outcrop in Hout Bay. The Cambrian S-type granites of the Cape Granite Suite formed during the Pan-African Saldania Belt Orogeny approximately 555 to 515 Ma (Scheepers and Schoch, 2006). The Peninsula Batholith forms the south-western portion of Cape Granite intrusions. Quartz, feldspars, and biotite dominate the mineralogy of the Peninsula Batholith and sedimentary enclaves are present (Scheepers, 1995; Schoch et al., 1997). The Cape Granite Suite intrusions are the basement rock for groundwater flow in Hout Bay (Theron, 1984). It crops out as rounded massive metaluminous boulders which are generally impermeable. Some fracture networks which form near fault zones allow groundwater to flow through them (Koning, 2013; Rodriquez et al., 2017).

Unconformably overlying the Cape Peninsula Granite Pluton is the Ordovician to Silurian Graafwater and Peninsula formations (Fig 2.4). These sedimentary packages were deposited approximately 485 to 444 Ma and form part of the Table Mountain Group (Rust, 1973). They outcrop to form the steep cliffs surrounding the Hout Bay valley. The Graafwater Formation consists of reddish fine grained shales and siltstones. The arenaceous medium to coarse grained sandstone of the Peninsula Formation is a thick horizontal unit (+-550 m) of highly fractured quartzites (Compton, 2004). Fracture networks offer

conduits for groundwater flow. Tectonic activity caused the jointing present in the Table Mountain Group and because the quartz-rich sandstone is very competent, these joints remain open to depths of 200 m below surface (Tankard et al., 1982). Numerous investigations into the potential of large scale abstraction of groundwater from the Table Mountain Group have been carried out around the Western Cape (Pietersen and Parsons, 2002; Cleaver, 2003; Colvin et al., 2009).

The Quarternary Witzand Formation of the Sandveld Group occurs on the lower slopes of the Karbonkelberg mountain peak (Fig 2.1; Fig 2.2). The Witzand Formation varies in thickness (+-30 m) and consists of well sorted fine grained calcareous unconsolidated sediments forming coastal dune plumes (Browning and Roberts, 2015).

The majority of the talus slopes of Hout Bay are made up of unconsolidated rock material that would have previously formed part of the Table Mountain Group and other weathered rock material (Diamond and Harris, 2019; Stapor Jr. et al., 1983). This unconsolidated rock material is referred to as Quaternary mountain scree (Fig 2.2).

The Table Mountain Group underwent compressional tectonics and then extensional tectonics. Deformation during the Permo-Triassic Cape Orogeny (290-220 Ma) caused the formation of the Cape Fold Belt and with it, the north-south striking faults of the Table Mountain Group in the study area (Johnston, 2000).

Weather:

Hout Bay experiences temperate Mediterranean climate where temperatures are moderately affected by ocean influences. Hout Bay generally experiences cool wet winters (May-August) and warm dry summers (November-February) (Fig 1.2). In summer the prevailing wind direction is from the south-east and in winter months is from the north-west. In Hout Bay, the heavy rains are carried by low pressure frontal systems that are driven by north-westerly winds in the winter months (May to August).

Stable Isotopes:

Atoms of the same element that have a difference in number of neutrons are known as the isotopes of an element. The result of varying numbers of neutrons is that isotopes of the same element can have varying atomic masses. Isotopes with fewer neutrons in the molecular nucleus are referred to as *light* while isotopes with higher amounts of neutrons are referred to as *heavy*. Differentiation of isotopes occurs during physiochemical processes such as evaporation and precipitation. The processes that lead to differentiation of hydrogen and oxygen isotope ratios are predictable (Craig, 1961; Dansgaard, 1964; Landwehr, 2014). Oxygen has 3 stable isotopes. Hydrogen has 2 stable and 1 radioactive.

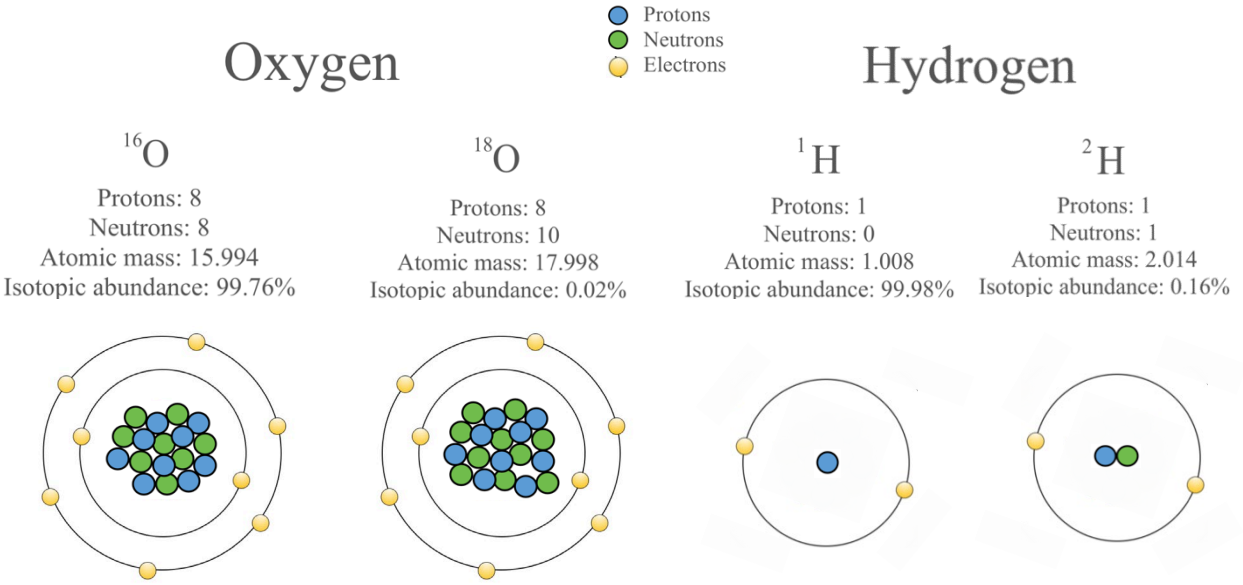

Fig 2.4 The stable isotopes of oxygen and hydrogen utilised in this study.

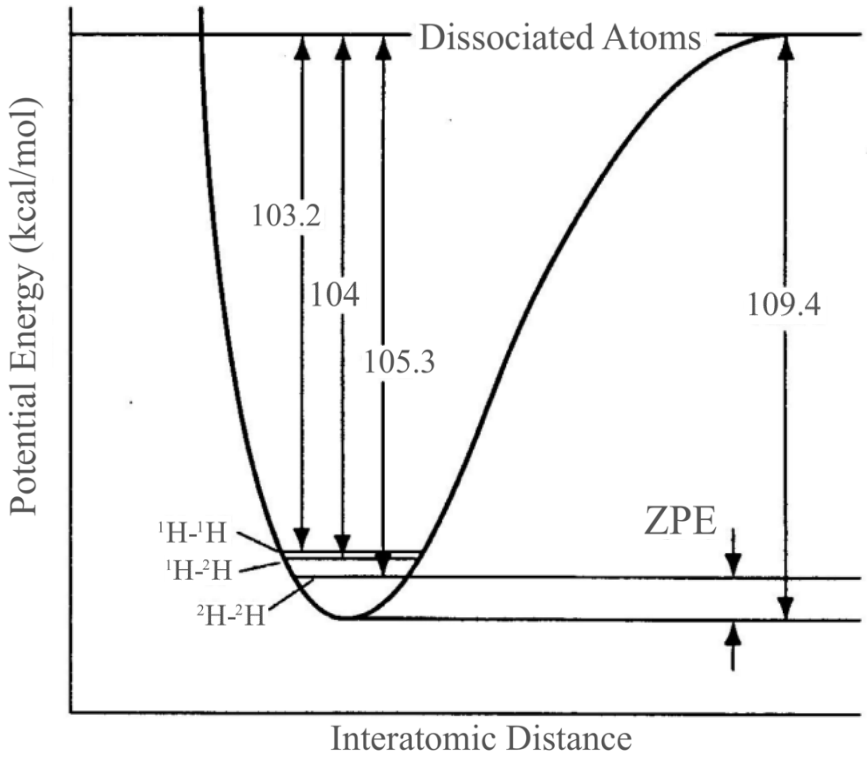

Fig 2.5 Zero point energy (ZPE) and energy required to dissociate various isotopes of hydrogen (^{1}H-^{1}H, ^{1}H-^{2}H, and ^{2}H-^{2}H) bonds.

The vibrational energy of an isotope is quantised by: E = ZPE + (hv/2) where h = Plancks constant, and v = vibrational frequency. The zero point energy (ZPE) of a molecule determines how much energy is required to dissociate a molecule. Hook's Law establishes that the vibrational frequency of an isotope is inversely proportional to its mass. From this, lighter isotopes require less potential energy to move to a higher energy level and therefore more readily dissociate than heavy isotopes. Greater fractionation occurs at lower temperatures. Isotopes fractionate based on dissociation energies and are caused by either equilibrium isotope exchange or kinetic effects. Equilibrium isotope exchange occurs where light isotopes have a preference for a phase. Kinetic effects are associated with processes such as evaporation where the velocities of isotopic molecules is different due to differing masses. Isotopes are more accurately represented as relative abundances of heavy isotope to light isotope rather than absolute abundances. The ratio of heavy isotopes relative to light isotopes in a measured sample is known as the delta value (Fig 1.3). The delta value is calculated relative to a known standard and expressed in per mille (‰). Vienna Standard Mean Ocean Water (V-SMOW) is a standard which reflects the accepted average isotope composition of seawater.

Geohydrology:

"The endless circulation of water between the ocean, atmosphere, and land is called the hydrological cycle" (Freeze and Cherry, 1979).

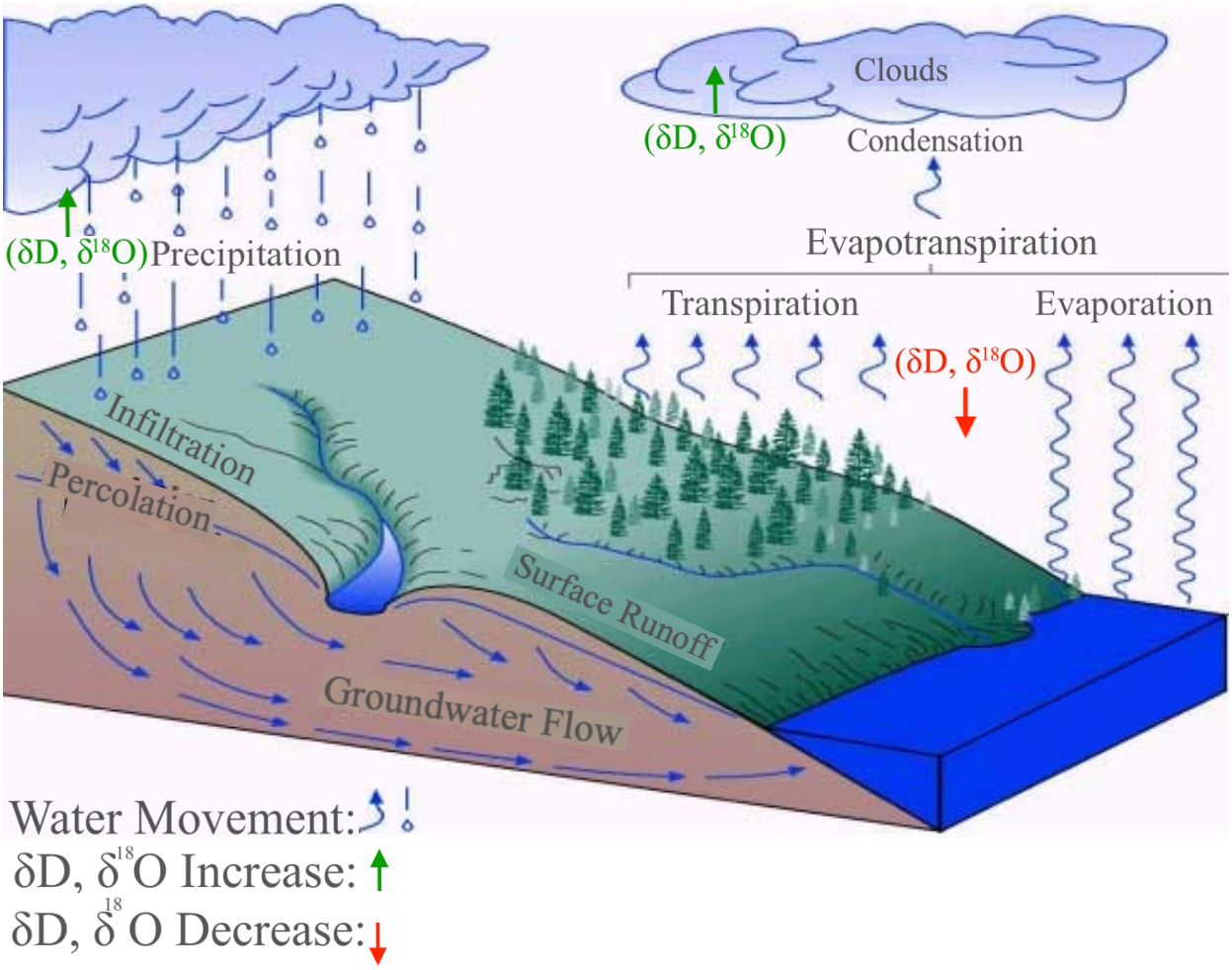

Fig 2.6 The hydrological cycle showing the flow of water through the hydrosphere with schematic changes in δD and $\delta^{18}O$. Imaged adapted from Spokane Aquifer Joint Board.

The hydrosphere is defined as a closed system of all the water confined to Earth. The hydrosphere consists of reservoirs that contain water (oceans, rivers, lakes icebergs, glaciers, and groundwater). The hydrological cycle is the pathway of water molecules through the hydrosphere between the reservoirs. Water moves through the hydrosphere in a very dynamic and somewhat predictable manner. Various water reservoirs hold water on Earth. Water moves between these reservoirs aided by processes such and evaporation and precipitation. Gravity, wind, heat, and pressure are the main drivers of processes that move water between reservoirs.

Aquifers can be recharged with water from various sources and some aquifers show interconnectivity. The Table Mountain Group rocks underwent slight greenschist metamorphism during the Cape Orogeny (Frimmel et al., 2001). The recrystallisation of quartz in the Table Mountain Group substantially reduced porosity and increased the rock competency. Brittle fractures in the Table Mountain Group form conduits which allow for water to flow through the rock. In Hout Bay, the Peninsula aquifer is made up of Table Mountain Group rocks. Mountain scree is geographically lower down the slopes of the Hout Bay Valley and forms the scree aquifer (Diamond and Harris, 2019; Stapor Jr. et al., 1983).

While groundwater is very simple by nature in that it is basically water stored below the Earth's surface, it is less straightforward to conceptualise because we cannot observe it without the aid of scientific investigative tools. Principles based on empirical data such as Darcy's Laws, allow determination of how water behaves in the subsurface (Freeze and Cherry, 1979). Isotope hydrology can be applied to understanding and characterising groundwater remotely.

Isotope Hydrology:

Hydrogen and oxygen stable isotopes in water fractionate in predictable ways through the hydrological system. Isotopic variation in the environment can be explained by a number of effects. Changes in isotope composition of water are caused by various environmental factors (climate, weather, and geography). Natural processes such as evaporation and precipitation alter the δD and $\delta^{18}O$ values of water. Evaporation of a surface reservoir results in the enrichment of heavy isotopes in that surface

reservoir. This enrichment is referred to as evapoconcentration and it increases the δD and $\delta^{18}O$ values of the surface reservoir (Gat, 1971). When water evaporates from the ocean surface, fractionation of isotopes causes the evaporated water vapour to be isotopically lighter than the ocean it evaporated from. The effect of evaporation on the isotope composition of a water body is dependent on the proportion of water that evaporates rather than the absolute amount of water that evaporates (Pfahl and Sodemann, 2013). After recharge, groundwater concealed within the Earth's surface is not subject to evaporative processes which could alter δD and $\delta^{18}O$. The groundwater isotope compositions of recharge water percolating through sand often differ to that of aquifers recharged by water percolating through crystalline rock (Gat, 1996). Evaporation and precipitation cause hydrogen and oxygen isotope fractionation however Gat (1971) understood plant transpiration to not result in isotope fractionation of hydrogen and oxygen.

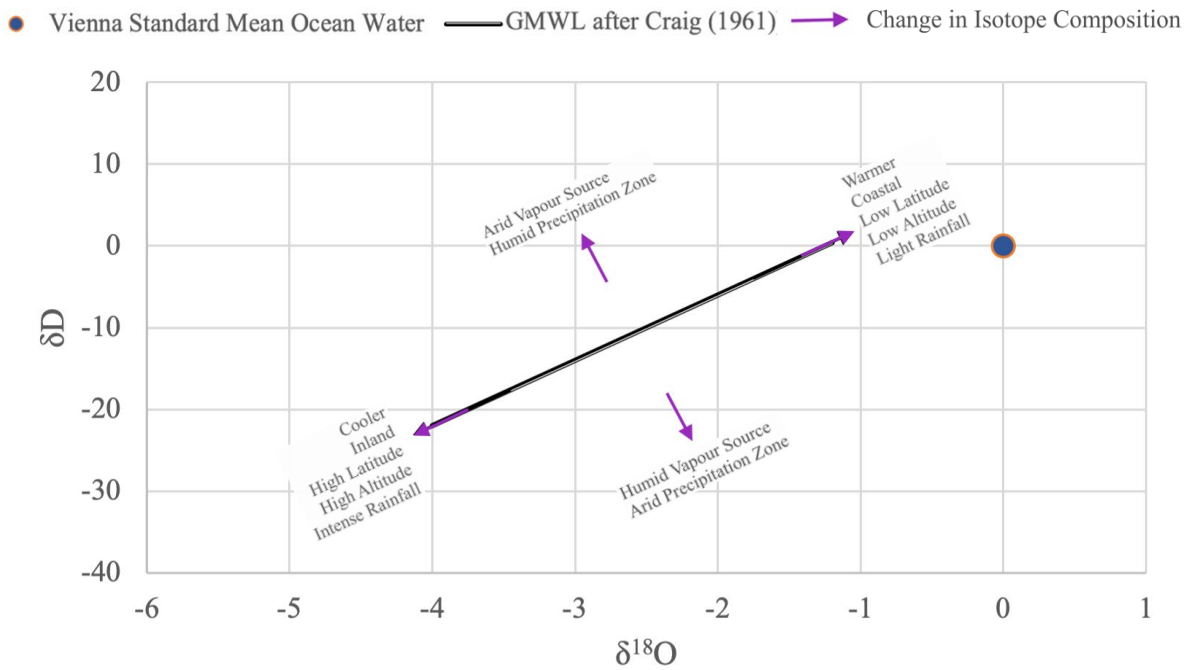

Fig 2.7 General changes in δD and $\delta^{18}O$ composition from the Global Meteoric Water Line (GMWL) after Craig (1961) and Dansgaard (1964).

The Global Meteoric Water Line (GMWL) was first described by Craig (1961). Stable oxygen and hydrogen isotope values plotted against each other were found to have a trendline ($\delta D = 8*\delta^{18}0 + 10$). The Global Meteoric Water Line (GMWL) is ideal for describing the isotopic trends in continental regions in the northern hemisphere. Various fractionation effects have been found to alter δD and $\delta^{18}O$ values of precipitation and therefore the nature of the trendline.. Similar trendlines have been incorporated into isotope studies since Craig (1961) and as a result, led to a better understanding of δD and $\delta^{18}O$ behaviour in precipitation. Harris (2010) found the Local Meteoric Water Line for Cape Town to be $\delta D = 5.55*\delta^{18}O + 6.11$ from rainwater collected at UCT from 1996 to 2008.

Most of the effects which change δD and $\delta^{18}O$ values in rainwater are interrelated:

1. The temperature effect is believed to have the most influence on the δD and $\delta^{18}O$ values of a water body (Dansgaard, 1964). Areas that experience warmer climates result in precipitation that is enriched in the heavier isotopes of hydrogen and oxygen and vice versa for cooler climates (Fig 4.2).
2. The amount effect refers to the amount of rainwater that falls in a precipitation event. Areas that experience intense precipitation events are associated with rainfall that is enriched in light isotopes (Landwehr et al. 2014).
3. The altitude effect is as a result of how high above sea level the precipitation forms. At higher elevations, precipitation is found to be enriched in lighter isotopes (Fig 2.7). Temperature decreases with altitude which contributes to the effect.
4. The continental effect is a geographical effect which is dependent on the distance from the evaporative ocean source that the precipitation forms. As water vapour progresses further inland, the heavy isotopes fall out as precipitation first resulting in precipitation enriched in light isotopes further from the ocean (Fig 2.7).
5. The reservoir effect refers to the alteration of the isotopic ratios in precipitation by reservoirs that contribute to water vapour in the atmosphere. These reservoirs can include large rivers, lakes or dams. This is not considered in this study as there are no significantly large dams or lakes in close proximity to the study area.

Deuterium Excess:

Deuterium excess is measurable is defined by: Deuterium excess (d-excess) = $\delta D - 8*\delta^{18}O$. The relative mass difference between the light and heavy isotopes of hydrogen is greater than that of oxygen. The result is that hydrogen fractionates more so than oxygen during processes that produce phase changes such as evaporation and precipitation. Deuterium excess (d-excess) is a second-order parameter used to infer the conditions during evaporation of water from the ocean surface (Good et al., 2015). Deuterium excess can serve as a meteoric indicator of the relative humidity at sea surface during evaporation (Pfahl and Sodemann, 2013). Diffusive processes during evaporation over the ocean surface are affected by humidity and can result in a relative enrichment of deuterium in the evaporated water vapour (Merlivat and Jouzel, 1979). The gaseous water vapour is then advected away from the ocean surface before isotopic equilibrium can occur with ocean water. Sub-cloud secondary evaporation preferentially evaporates lighter isotopes and therefore decreases deuterium excess (Liu *et al.*, 2008; Chen *et al.*, 2015). Precipitation that undergoes sub-cloud secondary evaporation has been found to decrease the δD vs $\delta^{18}O$ line of best fit slope (Stewart, 1975).

Strontium Isotopes:

The decay of Rubidium (^{87}Rb) to Strontium (^{87}Sr) has a half-life of 4.72×10^{10} years (McMullen et al., 1966). Strontium (^{87}Sr) is continuously being produced by radioactive decay of rubidium (^{87}Rb) and therefore increasing the abundance of strontium (^{87}Sr) in rocks (Weaver et al., 1999). Cations exchange of strontium (Sr^{2+}) with calcium (Ca^{2+}) can occur in minerals. Therefore, the occurance of strontium-bearing minerals contributes to strontium concentrations in water. Strontium isotopes do not fractionate by the same surface processes as hydrogen and oxygen. As previously mentioned, δD and $\delta^{18}O$ are sensitive to fluctuations by processes such as evaporation and precipitation. Groundwater interacts with the aquifer rock it flows through and by chemical dissolution the groundwater inherits the strontium isotope compostion ($^{87}Sr/^{86}Sr$) of the aquifer rock. Processes such as atmospheric deposition, biological cycling, also affect strontium measured in groundwater (Clow and Mast, 1997). The present day $^{87}Sr/^{86}Sr$ ratio of seawater is relatively constant is accepted to be 0.7092 (Elderfield,

1985). Scott et al. (2020) noted that in near coast groundwater, strontium in sea spray dissolves into rainwater that recharges aquifer systems. Strontium isotope ($^{87}Sr/^{86}Sr$) data along with δD, $\delta^{18}O$, and electrical conductivity data has proved useful in the determination of seawater influences on groundwater (Weaver, 1999; McNutt, 2000; Jørgensen et al. 2008).

Chapter 3 Methodology

This chapter describes the methodology that was followed and the materials used to get accurate and precise data from water samples. This includes sampling methods, analytical methods, and the error of the data obtained.

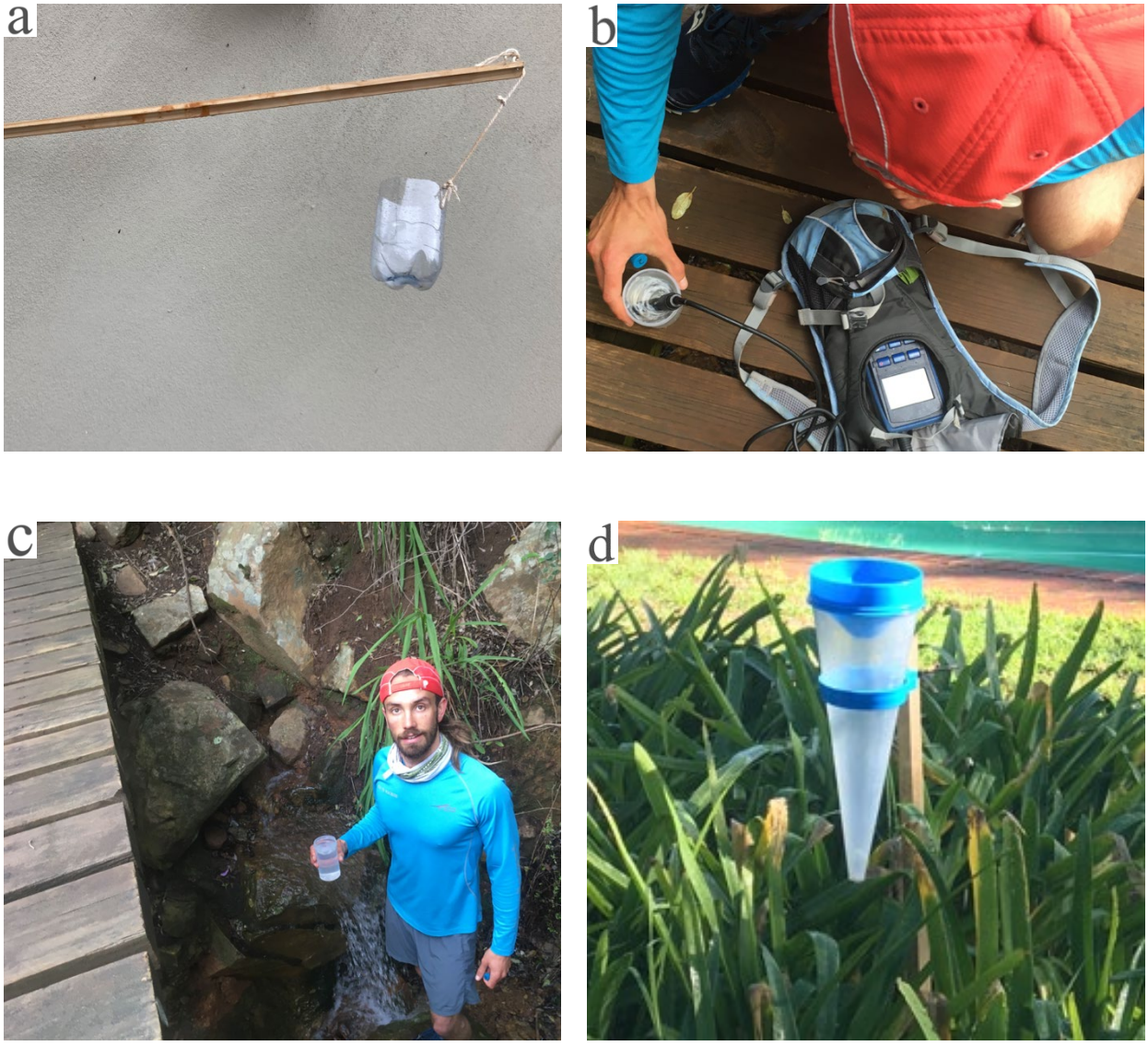

Fig 3.1 a Polyethylene terephthalate sample collection extension. **b** Infield electrical conductivity and temperature measurement. **c** Hout Bay stream sample collection. **d** rainwater collection in Hout Bay rain gauge.

Fig 3.2 Sample locations in Hout Bay. The location of the UCT rain gauge is on the small map with the label “UCT Rainwater”.

Hydrogen and oxygen stable isotope analysis was conducted on 148 water samples from the Hout Bay valley during this study. Electrical conductivity and groundwater temperature were recorded during sample collection in the field. The groundwater sample collection took place over two distinct phases (February/March 2020, and November 2020). Correlations between groundwater sample data was investigated to fingerprint groundwater behaviour. Nine samples from Hout Bay February/March 2020 groundwater sample collection were analysed for strontium isotope ratios ($^{87}Sr/^{86}Sr$). From February 2020 to February 2021, Hout Bay monthly rainwater amount was measured and a sample analysed for stable isotope ratios (δD, $\delta^{18}O$). Fourteen stream water samples were collected from Hout Bay mountain streams on 17/18 August 2020 (Fig 3.1 c). Groundwater deuterium excess (d-excess) was calculated based on δD and $\delta^{18}O$ values. The data was put into tables and used to produce figures which aim to graphically represent data.

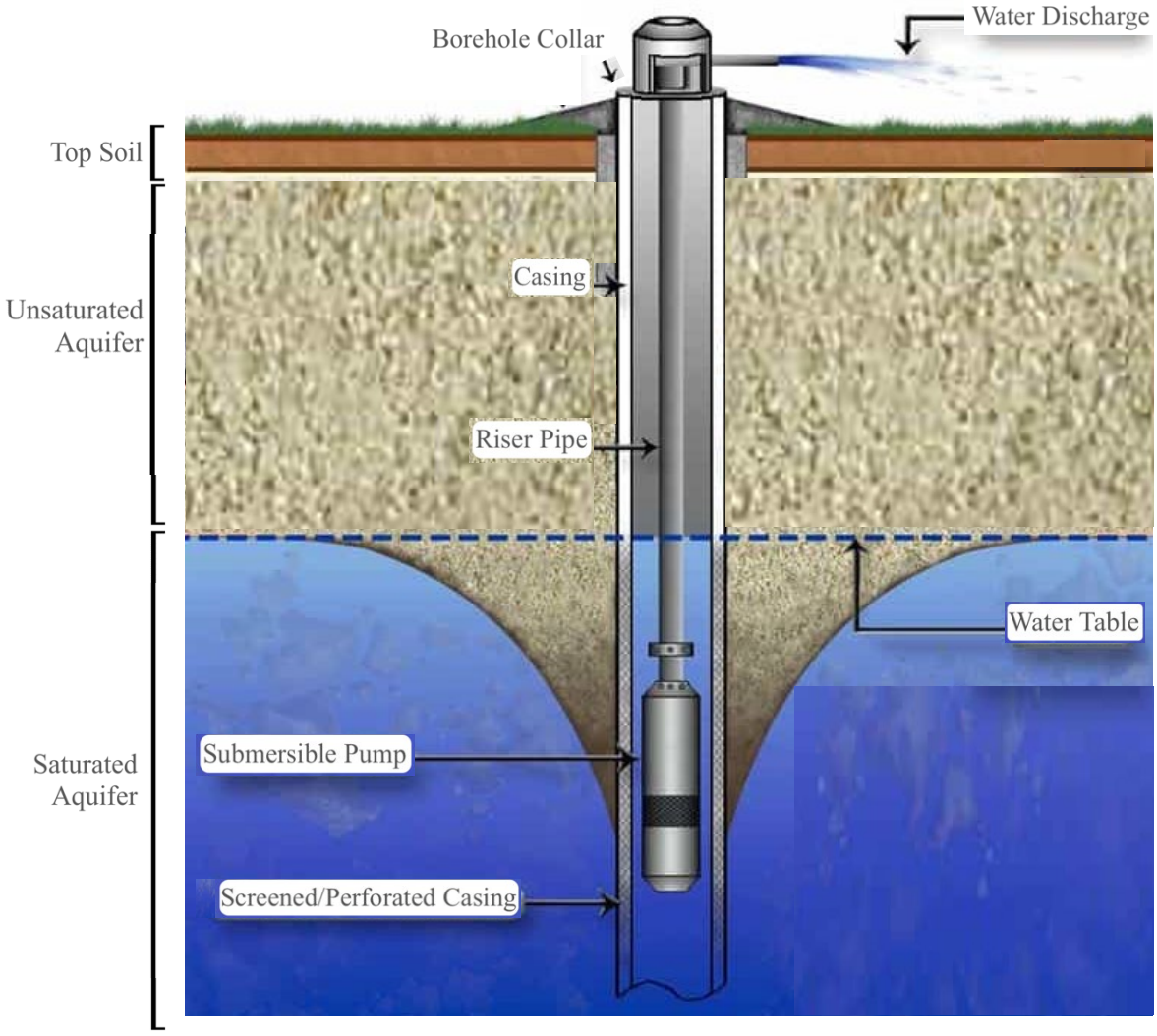

Fig 3.3 Groundwater abstraction from a borehole adapted from RPM Drilling.

Groundwater Sampling:

Groundwater samples were accessed through boreholes and wellpoints. A wellpoint is differentiated from a borehole by having a pump above ground surface as opposed a submersible pump found inside a borehole. Generally, a wellpoint is shallower than 10 m below ground surface. Public participation was necessary for access to private boreholes/wellpoints. Social platforms and personal connections were helpful in gaining access to residential boreholes/wellpoints in Hout Bay. Groundwater samples were acquired by traditional door-to-door requests for a water sample from Hout Bay residents. Access was granted to 64 boreholes/wellpoints in the Hout Bay valley for groundwater sampling over this study. Borehole locations included private residential homes and public institutions such as schools (Fig 3.1). Fifty-eight samples were collected before (February/March) and sixty-three samples were collected after (November) the winter rain in 2020. Electrical conductivity and temperature of groundwater were recorded at each sample location while a sample was collected for isotope analysis at UCT. The mean surface elevation above mean sea level for Hout Bay groundwater sample locations is 64 mamsl (metres above mean sea level).

Prior to sample collection, the borehole/wellpoint pump was activated and allowed to pump for 5 minutes. As a result, water that may have been sitting in the borehole casing after the pump was last activated may be flushed out with groundwater. After flushing, a sample was collected as close to the borehole collar as possible to best represent the groundwater (Fig 3.3). In some cases, this required a device that can reach into a water storage tank to reach the water inlet (Fig 3,1 a). In other cases, a groundwater sample could be collected directly from the borehole/wellpoint. Prior to sample collection, a clean sample bottle was rinsed 3 times with the groundwater flowing out of the borehole/wellpoint. The sample bottle was filled and sealed to prevent evaporation of the sample. Each sealed sample was labelled with the appropriate sample #. Once a sample was secured for isotope analysis, more groundwater was collected for electrical conductivity and temperature analysis. This took place in the field using a TeltraCon350i probe on a WTW-conductivity multimeter and a plastic beaker that was rinsed three times with borehole water (Fig 3.1 c). Standards of potassium chloride were used to

calibrate the electrical conductivity meter and produced electrical conductivity readings (1.41 mS/cm, 0.76 mS/cm) that validated data (Adamson, 2006). The surface elevation was of samples was acquired from Google Earth Pro by inputting borehole surface coordinates. The depth of borehole data was dependent on information provided by the individual who assisted with borehole access. This information was not available for all sample locations. In some cases, the individual who assisted with borehole access did not know (or have any means to know) the borehole depth.

Stream water Sampling:

Water sample collection in this study was limited by the location of established boreholes/wellpoints. To broaden the geographical scope of this study, fourteen water samples were collected from streams in Hout Bay during a storm event (Fig 3.1 d). The sample collection took place on 17/18 August 2020 and the procedure was the same as the sample collection procedure for *Groundwater Sampling* as stated above. The purpose of stream water collection is to observe any correlations with groundwater data.

Electrical Conductivity:

Electrical conductivity readings are used to infer the salinity of water (Anderson and Cummings, 1999). Groundwater interacts with aquifer rock to dissolve salts into solution and has been estimated to contribute 50% of the salt loading of rivers into the oceans (Zektser and Loaiciga, 1993). The concentration of dissolved ions in solution has a strong linear correlation with electrical conductivity which make electrical conductivity readings a good indication of water quality. Lower electrical conductivity indicates better water quality (Pal et al., 2015).

Rainwater Sampling:

Monthly rainwater was collected in a rain gauge (Fig 3.1 d) in Hout Bay for a year at 34°00'51.29" S 18°21'49.56" E (Fig 3.2). After rainfall events, rainwater collected in the rain gauge in Hout Bay was transferred to a clean bottle allocated for a month and sealed. The rainwater volume was recorded at the end of the month from March 2020 to February 2021. A well-mixed sample representative of the month's rainwater was collected in a 50 ml glass sample bottle and sealed for stable isotope analysis (δD, $\delta^{18}O$) at UCT approximately 8 km away. The δD and $\delta^{18}O$ weighted mean for Hout Bay monthly rainwater was calculated using monthly rainfall amount as the weighting.

Analytical Methods:

Water samples were analysed for hydrogen and oxygen isotope ratios (δD and $\delta^{18}O$) using a L2120-i Picarro wavelength scanned cavity ring-down (WS CRD) spectrometer. Chemcorrect was applied to assess data validity as found in West et al. (2014). Adam Cape Town Millipore (ACTMP) and Rocky Mountain Water (RMW) were the working standards for δD and $\delta^{18}O$ analysis. Bottled water can serve as a working standard for δD and $\delta^{18}O$ analysis (Bowen et al., 2005). Evian water sourced at the Cachat spring in France was run as was an additional check for δD and $\delta^{18}O$ analysis in this study. Spangenberg and Vennemann (2008) accepted δD =73.1‰ +-1.2‰ and $\delta^{18}O$ =10.2 ‰ +-0.3‰. Bottled Evian water was analysed following the same procedure as sample water at UCT (Table 3.3). Analysis of Evian water produced mean δD and $\delta^{18}O$ values of -71.6‰ (σ = 0.4‰) and 10.24‰ (σ = 0.13‰) respectively in 2020. Error is considered as 0.8‰ and 0.26‰ for δD and $\delta^{18}O$ respectively.

Strontium isotope composition ($^{87}Sr/^{86}Sr$) was measured on a NuPlasma mass spectrometer and referenced to a NIST987 standard ($^{87}Sr/^{86}Sr$ = 0.710). Rubidium interference was corrected for by comparing strontium isotope ratios to $^{85}Rb/^{87}Rb$ and ^{85}Sr values. Instrument-induced fractionation was addressed by comparing $^{87}Sr/^{86}Sr$ values to $^{86}Sr/^{88}Sr$ = 0.1194.

Terraclimate Temperature Data:

Terraclimate is a high resolution model that was utilised in the absence of historical measured temperature data for Hout Bay. Terraclimate temperatures were verified by comparison with measured temperatures from Kirstenbosch reported by Harris *et al.* (2010). Terraclimate modelled temperature data for Kirstenbosch correlated well with measured temperatures at Kirstenbosch (Fig 3.5). Terraclimate modelled maximum and minimum daily temperatures are assumed to closely approximate real ambient maximum and minimum daily temperatures (Fig 3.6). Terraclimate temperature data for Hout Bay was utilised in to observe ambient temperature effects on rainwater isotopes (Fig 4.).

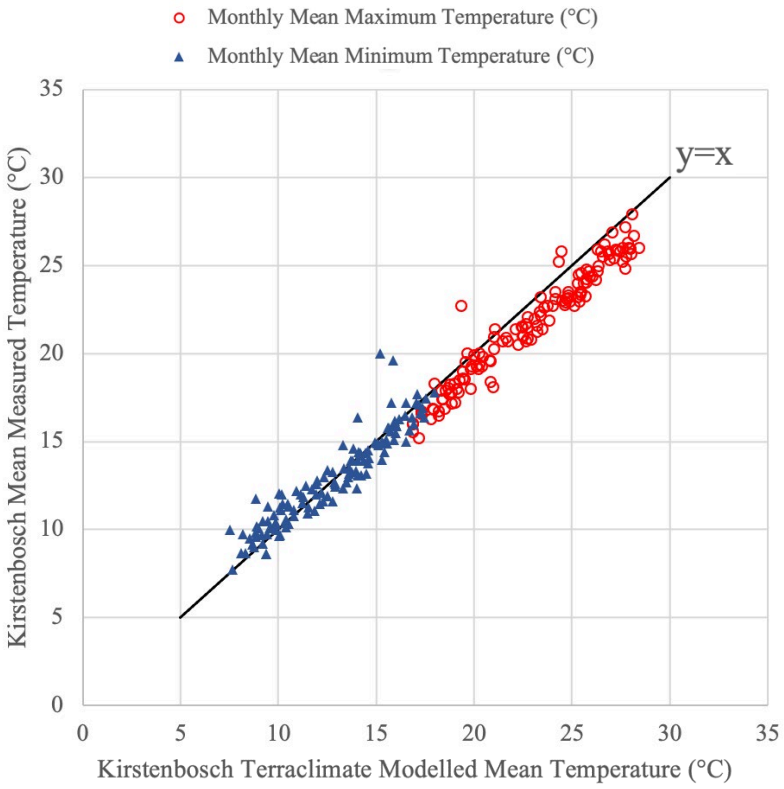

Fig 3.5 Month average daily maximum and minimum Kirstenbosch Terraclimate modelled temperature vs month average daily maximum and minimum Kirstenbosch measured temperature (January 1997- December 2007).

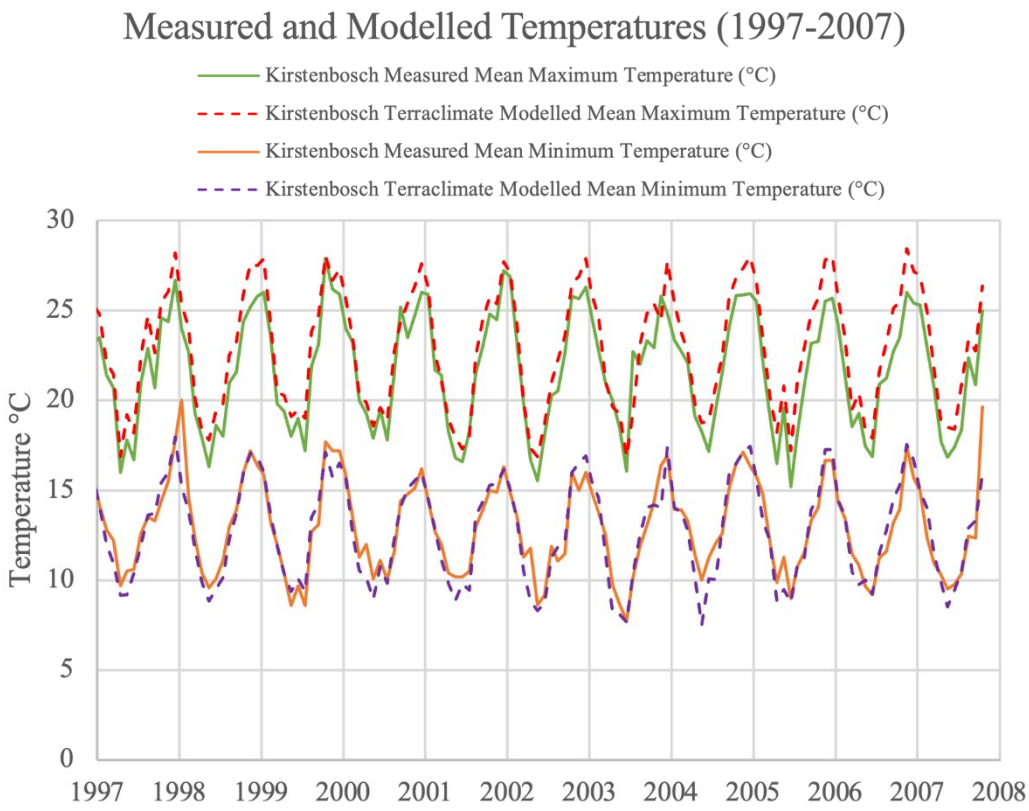

Fig 3.6 Month average daily maximum and minimum Terraclimate modelled temperature and month average daily maximum and minimum Kirstenbosch measured temperature (January 1997- December 2007).

Analysed data was compiled in Microsoft excel sheets and put into plots to give the reader graphical context. Hout Bay groundwater samples that were collected in February/March 2020 and November 2020 were included in groundwater statistical calculations (minimum, maximum, range, mean, standard deviation). Pearson's correlation coefficient (r) shows the correlation between data. Spread of data was quantified on Microsoft excel by range ($Value_{Maximum}$- $Value_{Minimum}$) and standard deviation (σ) of all the data (St dev. P). A Jupyter v3.7.5 notebook served as an interface for pythons matplotlib functionality to create figures and the Pandas library to import and manage data. Open Street Maps base maps were adjusted to a Plate Carree projection through the Cartopy library for graphical representation of areal variation of Hout Bay groundwater (Fig 4.3). Correlations between groundwater samples were investigated to fingerprint groundwater behaviour and figures were produced which aim to express the data. The relevant compiled results of this study are presented in chapter 4.

Chapter 4 Results

The range of δD and $\delta^{18}O$ values of Hout Bay 2020 groundwater is 10.1‰ and 1.76‰ respectively. Differences in parameters (δD, $\delta^{18}O$ electrical conductivity, groundwater temperature) measured in groundwater is observed from February/March 2020 to November 2020 in Hout Bay groundwater samples. In this chapter, δD, $\delta^{18}O$, deuterium excess, electrical conductivity, and temperature of groundwater is presented with rainwater and stream water data.

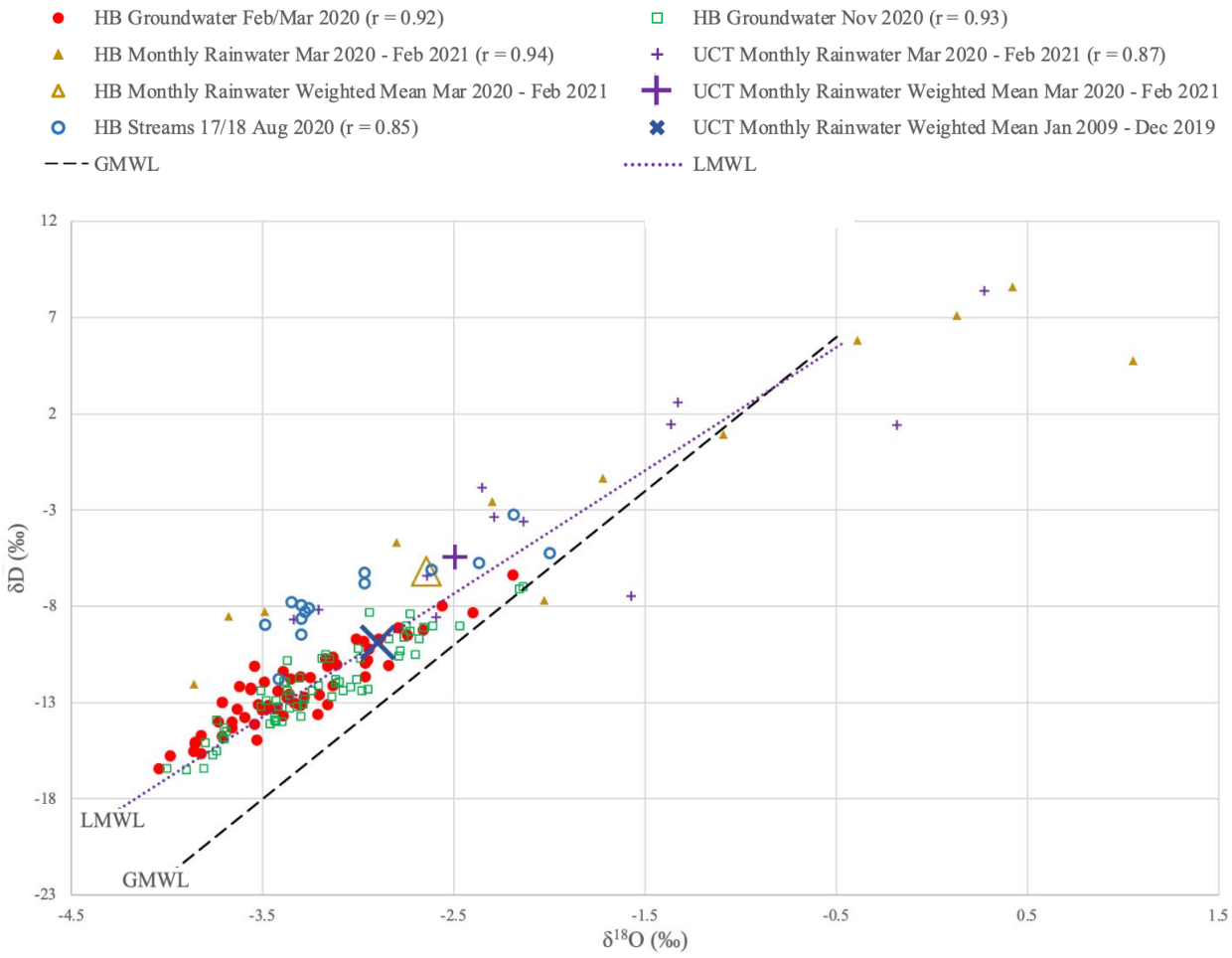

Fig 4.1 δD vs $\delta^{18}O$ for water samples collected at Hout Bay (HB); boreholes in February/March and November 2020, streams on 17/18 August 2020, monthly rainwater from March 2020 to February 2021, and the weighted mean for monthly rainwater from March 2020 to February 2021. The $\delta^{18}O$ and δD values for monthly rainwater collected at UCT from March 2020 to February 2021 as well as the weighted mean for UCT monthly rainwater from March 2020 to February 2021 and January 2009 to December 2019 is plotted for interpretation purposes. The Global Meteoric Water Line (GMWL) after Craig (1961) and the Local Meteoric water Line (LMWL) after Harris (2010) feature for reference.

Figure 4.1 shows the δD vs $\delta^{18}O$ values from the 60 borehole samples collected in February/March forming a trendline ($\delta D = 4.8\delta^{18}O+3.8$, r = 0.92). In November, 64 boreholes were accessed for sample collection forming a trendline ($\delta D = 5.1\delta^{18}O+4.3$, r = 0.93) as on Figure 4.1. Monthly rainwater δD and $\delta^{18}O$ values for rain gauges at Hout Bay and UCT from March 2020 to February 2021 are the most highest isotope values considered in this study. The Hout Bay rainwater weighted mean δD (-6.8‰) and $\delta^{18}O$ (-2.95‰) are more negative than UCT rainwater weighted mean δD (-5.8‰) and $\delta^{18}O$ (-2.56‰). The δD weighted mean for Hout Bay rainwater is less negative than all Hout Bay groundwater samples except for February/March HB39 (-6.4‰). Fourteen stream water samples collected during a rainfall event on 17/18 August 2020 are plotted on Figure 4.1. The δD and $\delta^{18}O$ mean values for Hout Bay groundwater ($\delta D_{Feb/Mar}$ = -12.4‰, δD_{Nov} = -12.2‰, $\delta^{18}O_{Feb/Mar}$ = -3.31‰, $\delta^{18}O_{Nov}$ = -3.21‰) are more negative than those for streams (δD = -7.4‰, $\delta^{18}O$ = -3.0). The Hout Bay groundwater δD vs $\delta^{18}O$ values plot close to the Local Meteoric Water Line (LMWL) (Harris et al., 2010). The Hout Bay groundwater δD plots above the Global Meteoric Water Line (GMWL) after Craig (1961), as on Figure 4.1.

Table 4.1 Groundwater δD, $\delta^{18}O$, electrical conductivity, deuterium excess, and groundwater temperature values from borehole water samples collected in February/March and November 2020.

Sample #	δD (‰)		$\delta^{18}O$ (‰)		EC (µS/cm)		Groundwater Temp (°C)		d-excess (‰)	
	Feb/Mar	Nov	Feb/Mar	Nov	Feb/Mar	Nov	Feb/Mar	Nov	Feb/Mar	Nov
HB1	-15.7	-16.4	-3.50	-3.81	423	366	21.2	21.1	14.9	14.1
HB2	-15.2	*NA*	-3.33	*NA*	278	*NA*	26.3	*NA*	15.6	*NA*
HB3	-13.2	-12.4	-3.42	-3.37	972	864	21.4	21.4	14.6	14.6
HB4	-11.1	-12.8	-3.36	-3.28	633	1146	24.1	20.8	14.2	13.4
HB5	-9.8	-9.6	-3.21	-2.76	381	383	20.1	19.8	13.9	12.5
HB6	-10.7	-10.7	-2.74	-2.99	422	378	21.1	19.3	14.4	13.2
HB7	-16.5	-16.5	-3.47	-3.90	457	401	19.4	22.2	15.9	14.7
HB8	-15.6	-15.5	-3.63	-3.74	442	363	20.7	24.1	15.3	14.4
HB9	-15.8	-14.8	-3.30	-3.71	385	407	21.8	19.9	16.1	14.9
HB10	-13.0	-12.9	-2.84	-3.48	366	335	18.9	22.2	16.7	14.9
HB11	-11.0	-10.3	-3.30	-2.78	1010	1002	21.6	18.7	12.7	11.9
HB12	-10.2	-9.7	-3.28	-2.84	1258	1271	22.0	20.8	13.3	13.0
HB13	-10.8	-12.3	-2.66	-2.95	1247	1200	21.3	20.4	12.8	11.3
HB14	-12.8	-12.2	-3.35	-3.04	1292	1202	20.2	20.1	14.2	12.1
HB15	-14.8	-14.9	-3.49	-3.70	554	465	20.8	22.0	14.9	14.7
HB16	-14.2	-14.0	-3.52	-3.43	1700	1446	22.2	21.7	14.2	13.4
HB17	-9.7	-9.0	-2.79	-2.47	883	752	19.9	19.9	13.4	10.8
HB18	-11.4	-11.7	-2.19	-3.31	259	232	17.8	19.0	15.7	14.8
HB19	-11.1	-10.7	-2.96	-3.19	208	198	20.0	22.5	17.2	14.8
HB20	-11.7	-11.8	-3.82	-3.01	243	243	19.5	20.0	14.3	12.3
HB21	-11.1	-11.8	-3.53	-3.12	1900	1761	20.0	19.6	13.8	13.2
HB22	-13.4	-13.2	-3.73	-3.32	434	454	23.5	20.1	14.6	13.4
HB23	-13.1	-13.2	-3.20	-3.42	892	802	21.3	21.2	13.6	14.2
HB24	-12.4	-12.6	-3.59	-3.36	1045	914	24.6	21.2	14.9	14.3
HB25	-12.6	-13.2	-3.17	-3.51	1180	1004	23.6	20.7	14.3	14.9

Sample #	δD (‰)		$\delta^{18}O$ (‰)		EC (µS/cm)		Groundwater Temp (°C)		d-excess (‰)	
	Feb/Mar	Nov	Feb/Mar	Nov	Feb/Mar	Nov	Feb/Mar	Nov	Feb/Mar	Nov
HB26	-13.6	-13.7	-3.39	-3.30	1056	962	22.6	19.4	12.1	12.7
HB27	-9.5	-9.7	-2.56	-2.68	1207	1209	21.8	21.9	12.4	11.7
HB28	-13.3	-14.0	-3.01	-3.40	1541	1358	25.5	20.0	14.4	13.2
HB29	-13.4	-12.7	-3.56	-3.14	825	824	26.3	22.6	15.7	12.4
HB30	-13.2	-12.4	-3.13	-2.98	248	225	23.7	21.2	13.2	11.4
HB31	-11.1	-10.6	-3.66	-2.79	890	863	20.3	20.2	11.6	11.7
HB32	-11.7	-11.9	-3.56	-3.10	509	449	19.2	19.6	14.7	12.9
HB33	-12.7	-13.1	-3.85	-3.29	898	768	21.9	21.8	13.5	13.2
HB34	-9.3	-9.3	-3.16	-2.73	778	627	25.4	20.6	12.0	12.5
HB35	-11.8	-11.9	-2.40	-3.39	240	233	20.7	19.4	15.0	15.2
HB36	-12.0	-12.9	-3.66	-3.43	348	304	25.4	23.8	16.0	14.5
HB37	-13.1	-14.3	-3.43	-3.70	378	343	24.8	21.6	15.0	15.3
HB38	-9.1	-10.5	-3.71	-2.70	560	547	20.3	18.9	13.2	11.1
HB39	-6.4	-7.0	-3.62	-2.14	611	421	20.6	19.4	11.1	10.1
HB40	-11.7	-10.2	-2.96	-3.00	935	879	21.9	21.9	12.0	13.8
HB41	-14.7	-14.1	-3.82	-3.46	649	498	20.6	20.7	15.8	13.6
HB42	-15.0	-12.4	-3.53	-3.08	213	203	20.2	20.1	13.3	12.2
HB43	-14.0	-8.3	-3.73	-2.94	239	297	20.0	23.0	15.8	15.2
HB44	-12.6	-12.1	-3.20	-3.21	540	518	19.5	20.5	13.0	13.6
HB45	-13.8	-13.9	-3.59	-3.74	643	600	20.1	18.2	14.9	16.0
HB46	-10.7	-10.7	-3.17	-3.15	166	149	18.7	17.7	14.6	14.5
HB47	-13.7	-13.9	-3.39	-3.44	945	847	19.4	20.2	13.4	13.6
HB48	-8.0	-15.1	-2.56	-3.80	1977	1160	20.4	16.1	12.5	15.3
HB49	-9.7	-9.1	-3.01	-2.66	716	578	25.1	18.3	14.4	12.2
HB50	-12.3	-11.9	-3.56	-3.38	357	360	19.3	21.5	16.2	15.1

Sample #	δD (‰)		$\delta^{18}O$ (‰)		EC (µS/cm)		Groundwater Temp (°C)		d-excess (‰)	
	Feb/Mar	Nov	Feb/Mar	Nov	Feb/Mar	Nov	Feb/Mar	Nov	Feb/Mar	Nov
HB51	-12.2	-8.4	-3.13	-2.73	379	1038	20.2	19.6	12.9	13.4
HB52	-14.3	-14.5	-3.66	-3.69	445	406	19.3	18.0	14.9	15.0
HB53	-12.4	-12.4	-3.56	-3.51	361	335	18.2	18.6	16.1	15.7
HB54	-15.1	-15.7	-3.85	-3.76	525	471	25.0	22.9	15.7	14.4
HB55	-13.1	-12.4	-3.16	-3.24	961	846	21.3	21.3	12.1	13.5
HB56	-8.4	-10.8	-2.40	-3.37	135	126	17.3	18.1	10.8	16.2
HB57	-14.0	-13.8	-3.66	-3.44	1707	1752	25.1	18.6	15.3	13.7
HB58	-13.3	-13.3	-3.43	-3.36	2370	2180	23.9	24.9	14.1	13.6
HB59	-13.0	-7.1	-3.71	-2.16	826	632	19.7	20.0	16.7	10.2
HB60	-12.2	*NA*	-3.62	*NA*	365	*NA*	20.1	*NA*	16.8	*NA*
HB61	*NA*	-16.4	*NA*	-4.00	*NA*	200	*NA*	*NA*	*NA*	15.6
HB62	*NA*	-9.0	*NA*	-2.61	*NA*	739	*NA*	22.9	*NA*	11.9
HB63	*NA*	-10.5	*NA*	-3.17	*NA*	194	*NA*	17.0	*NA*	14.9
HB64	*NA*	-9.0	*NA*	-2.75	*NA*	2920	*NA*	18.5	*NA*	13.0
HB65	*NA*	-12.0	*NA*	-3.12	*NA*	1496	*NA*	16.1	*NA*	13.0

EC: electrical conductivity
d-excess: deuterium excess = $\delta D - 8 * \delta^{18}O$
Temp: temperature
NA means a value is unknown either due to technical reasons or because a sample was not acquired.

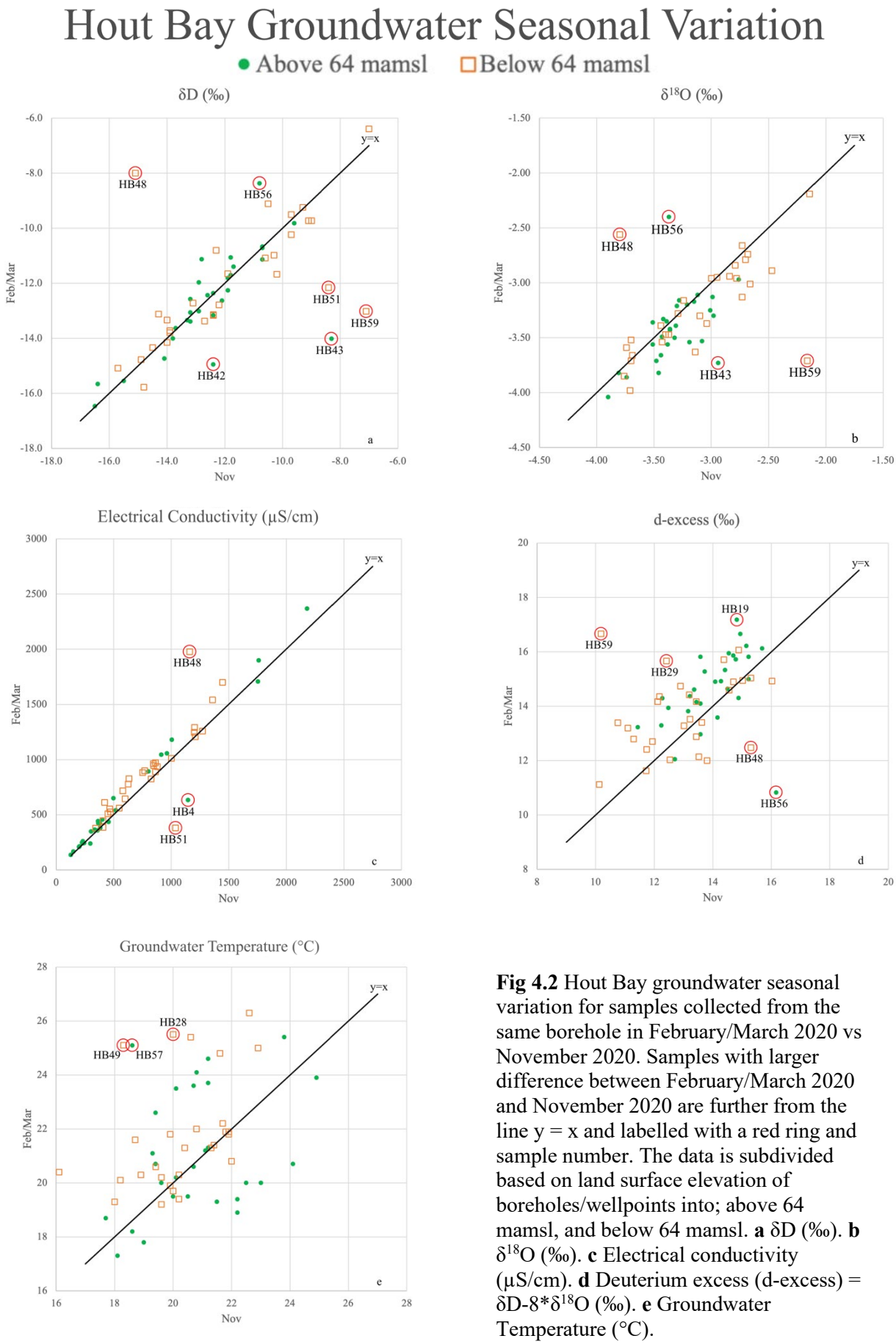

Fig 4.2 Hout Bay groundwater seasonal variation for samples collected from the same borehole in February/March 2020 vs November 2020. Samples with larger difference between February/March 2020 and November 2020 are further from the line y = x and labelled with a red ring and sample number. The data is subdivided based on land surface elevation of boreholes/wellpoints into; above 64 mamsl, and below 64 mamsl. **a** δD (‰). **b** $\delta^{18}O$ (‰). **c** Electrical conductivity (µS/cm). **d** Deuterium excess (d-excess) = $\delta D - 8*\delta^{18}O$ (‰). **e** Groundwater Temperature (°C).

Groundwater Seasonal Variation:

The mean values for δD and $\delta^{18}O$ of Hout Bay groundwater increase within error from February/March 2020 (δD = -12.4‰, $\delta^{18}O$ = -3.31‰) to November 2020 (δD = -12.2‰, $\delta^{18}O$ = -3.21‰). The range of $\delta^{18}O$ values increase from February/March 2020 (1.85‰) to November 2020 (1.86‰). There is a decrease in range of δD (10.1‰ to 9.5‰) and deuterium excess (6.4‰ to 6.0‰) from February/March 2020 to November 2020. Hout Bay groundwater mean deuterium excess decreases from February/March 2020 (14.3‰) to November 2020 (13.5‰). For Hout Bay groundwater February/March 2020 samples, the electrical conductivity and groundwater temperature mean values are 740.12 µS/cm (range: 2235 µS/cm = 2370 µS/cm-135 µS/cm) and 21.45 °C (range: 9.0 °C = 26.3 °C-17.3 °C) respectively. The mean of Hout Bay groundwater electrical conductivity and groundwater temperature for samples collected in November 2020 is 699.96 µS/cm3 (range: 2054 µS/cm = 2920 µS/cm-126 µS/cm) and 20.56 °C (range: 8.8 °C = 24.9 °C-16.1 °C) respectively.

Figure 4.2 shows the variation at each Hout Bay groundwater location between February/March 2020 and November 2020. If the data point on Figure 4.2 is to the right of the line y = x, the value was higher in February/March 2020. If the data point on Figure 4.2 is to the left of the line y = x, the value was higher in November 2020. For HB42, δD increases from -15.0‰ to -12.4‰. For HB43, δD and $\delta^{18}O$ notably increase from February/March 2020 to November 2020. For HB48, δD, $\delta^{18}O$ and electrical conductivity decrease from February/March 2020 to November 2020. For HB51, δD and electrical conductivity increases from February/March 2020 to November 2020. At HB56, δD decreases (-8.4‰ to -10.8‰), $\delta^{18}O$ decreases (-2.40‰ to-3.37‰), and deuterium excess increases (10.8‰ to 16.2‰) from February/March 2020 to November 2020 whereas at HB59, δD and $\delta^{18}O$ increase and deuterium excess decreases. Deuterium excess decreases from February/March 2020 to November 2020 at HB19 (17.2‰ to 14.8‰) and HB29 (15.7‰ to 12.4‰). Groundwater temperature decreases between February/March 2020 and November 2020 at HB49 (25.1 °C to 18.3 °C), HB57 (25.1 °C to 18.6 °C), and HB28 (25.5 °C to 20.0 °C). Electrical conductivity increases at HB4 (633 µS/cm to 1146 µS/cm),

and at HB51 (379 µS/cm to 1038 µS/cm) from February/March 2020 and November 2020. The majority of points sit above the line y = x for deuterium excess, electrical conductivity, and groundwater temperature.

δD

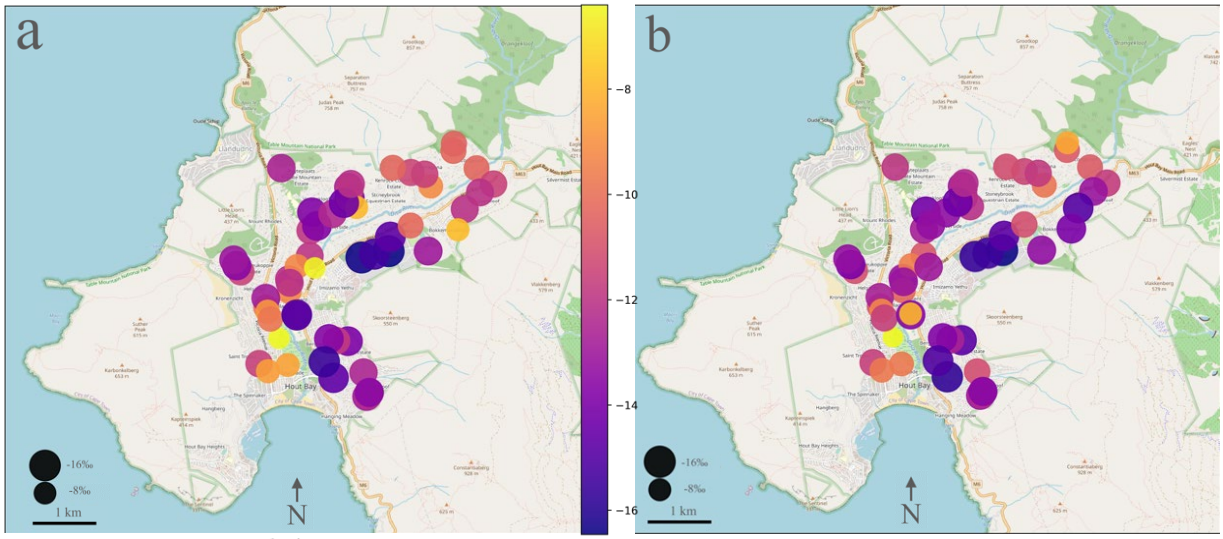

Feb/Mar Nov

$\delta^{18}O$

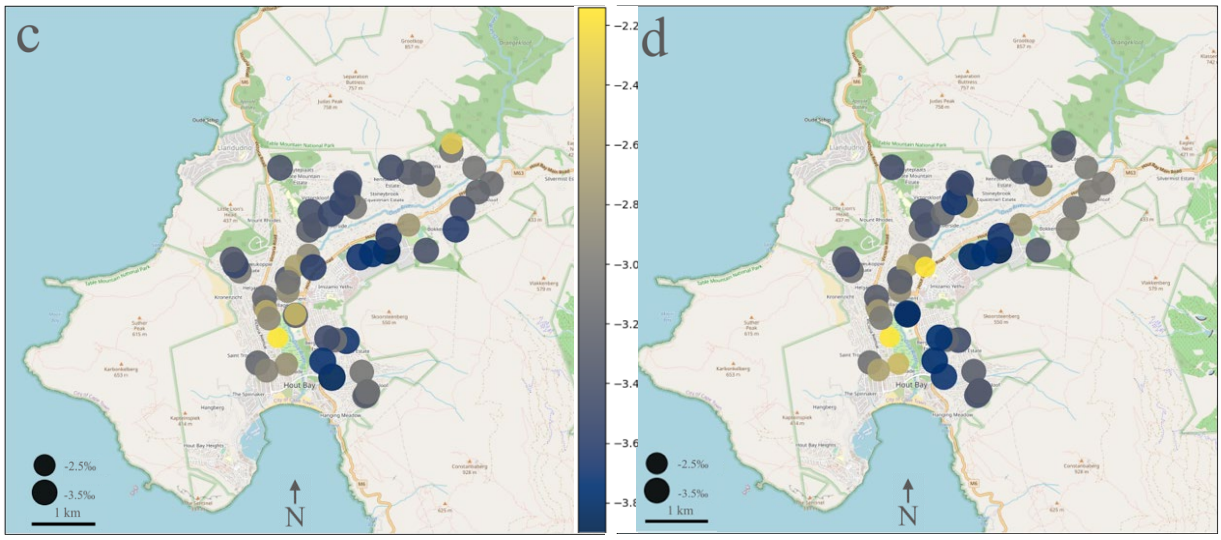

Feb/Mar Nov

Electrical Conductivity

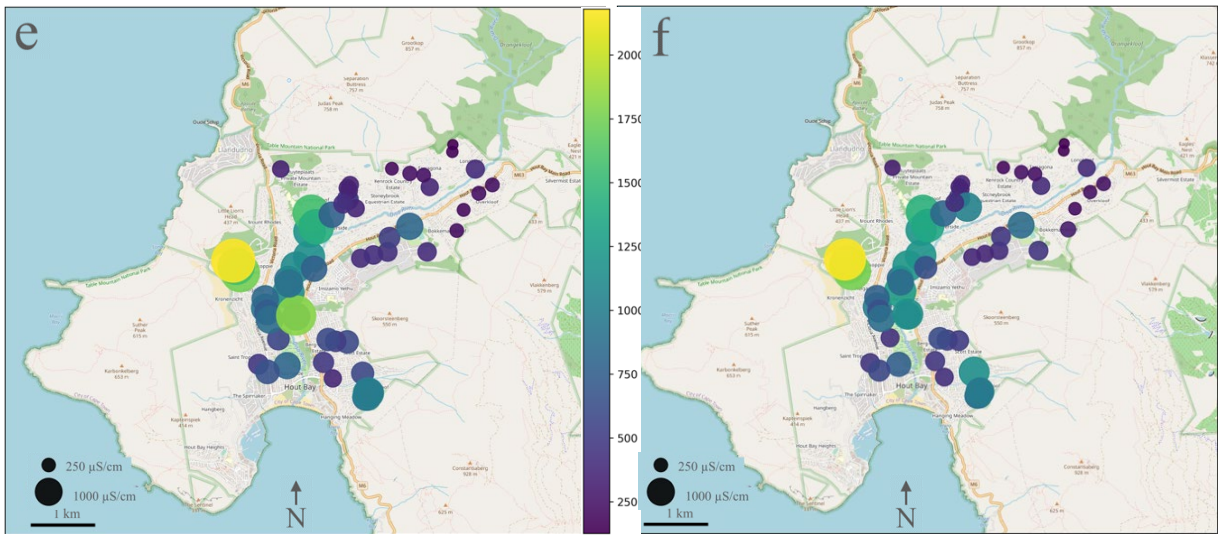

Feb/Mar Nov

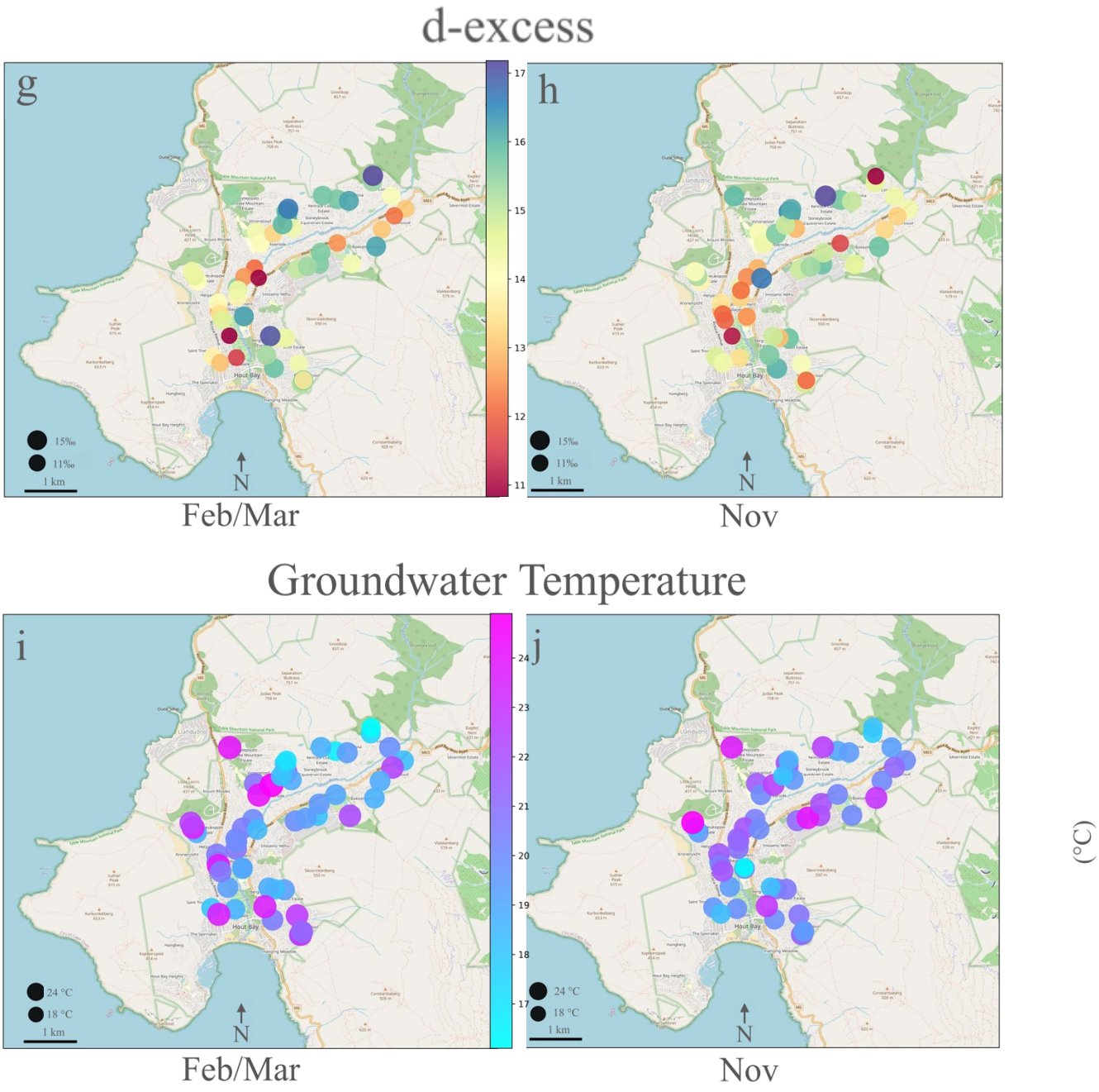

Fig 4.3 Plots of Hout Bay groundwater February/March 2020 (left) and November 2020 (right); δD (**a**, **b**), $\delta^{18}O$ (**c**, **d**), electrical conductivity (**e**, **f**), deuterium excess (d-excess) = δD-8*$\delta^{18}O$ (**g**, **h**), and groundwater temperature (**i**, **j**).

Groundwater Areal Variation:

Figure 4.3 shows the areal variation observed across all measured variables in Hout Bay groundwater samples collected in February/March 2020 and November 2020. Hout Bay groundwater δD and $\delta^{18}O$ values showed similar patterns of variation (Fig 4.3 a, b, c, d). Samples collected from boreholes/wellpoints south-east of the Hout Bay river had more negative δD and $\delta^{18}O$ values than those collected north-west of the Hout Bay River. Samples collected on the south-east slope of the Hout Bay valley (HB1, HB8, HB15, HB22, HB27) are in close proximity to one another and have negative δD and $\delta^{18}O$ values relative to the other boreholes in Hout Bay (Fig 4.3 a, b). The electrical conductivity groundwater trend for Hout Bay is increasing from north-east to south-west. The highest groundwater electrical conductivity values are west of the valley on Little Lions Head mountain slope (Fig 4.3 e, f). Groundwater deuterium excess values tend to be lower in the centre of Hout Bay valley (HB1, HB11, HB27, HB33, HB34, HB48, HB59) at elevations below 30 mamsl (Fig 4.3 g, h). The lowest groundwater temperatures recorded are at the boreholes on the north slopes high up the Hout Bay valley (HB18, HB19, HB46, HB56) with a surface elevations above 120 mamsl (Fig 4.3 i, j).

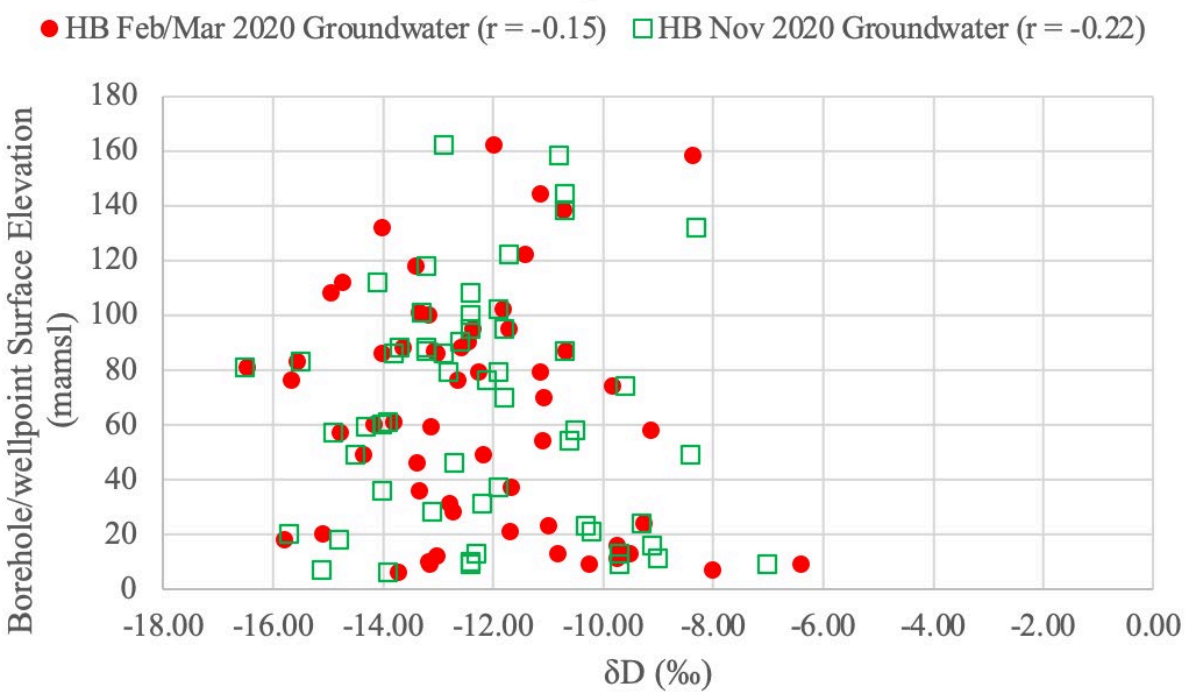

Fig 4.4 Borehole/wellpoint surface elevation vs δD for Hout Bay (HB) groundwater samples collected in February/March 2020 and November 2020.

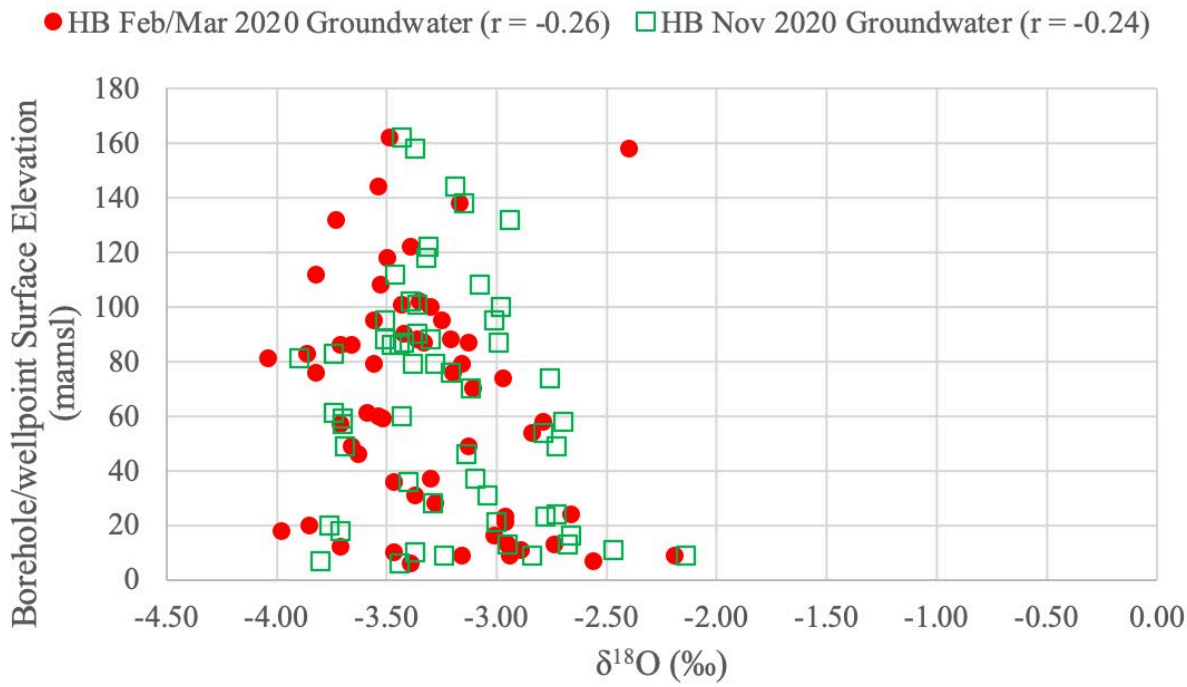

Fig 4.5 Borehole/wellpoint surface elevation vs $\delta^{18}O$ for Hout Bay (HB) groundwater samples collected in February/March 2020 and November 2020.

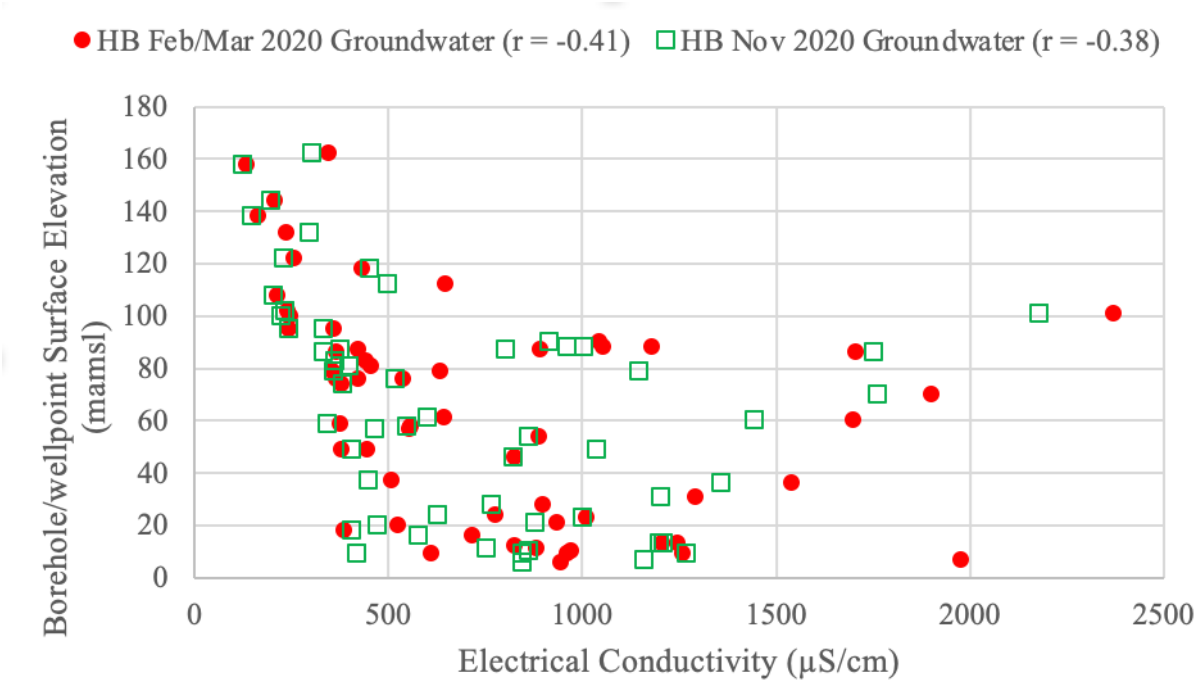

Fig 4.6 Borehole/wellpoint surface elevation vs electrical conductivity for Hout Bay (HB) groundwater samples collected in February/March 2020 and November 2020.

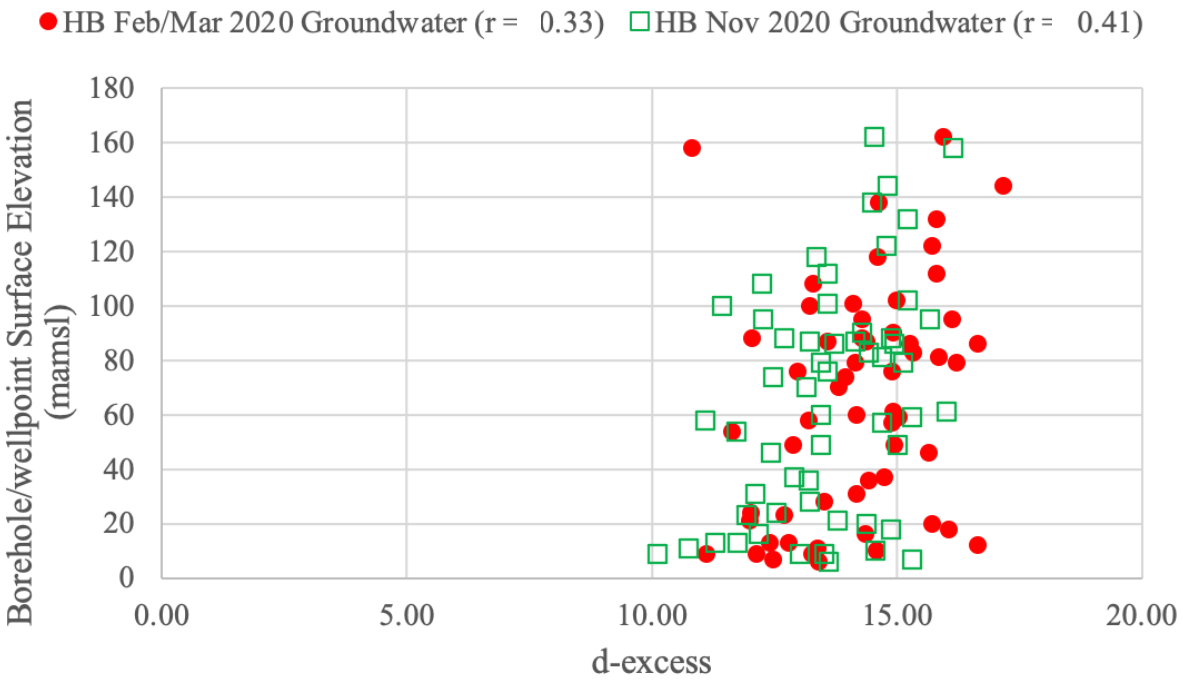

Fig 4.7 Borehole/wellpoint surface elevation vs deuterium excess (d-excess) for Hout Bay (HB) groundwater samples collected in February/March 2020 and November 2020.

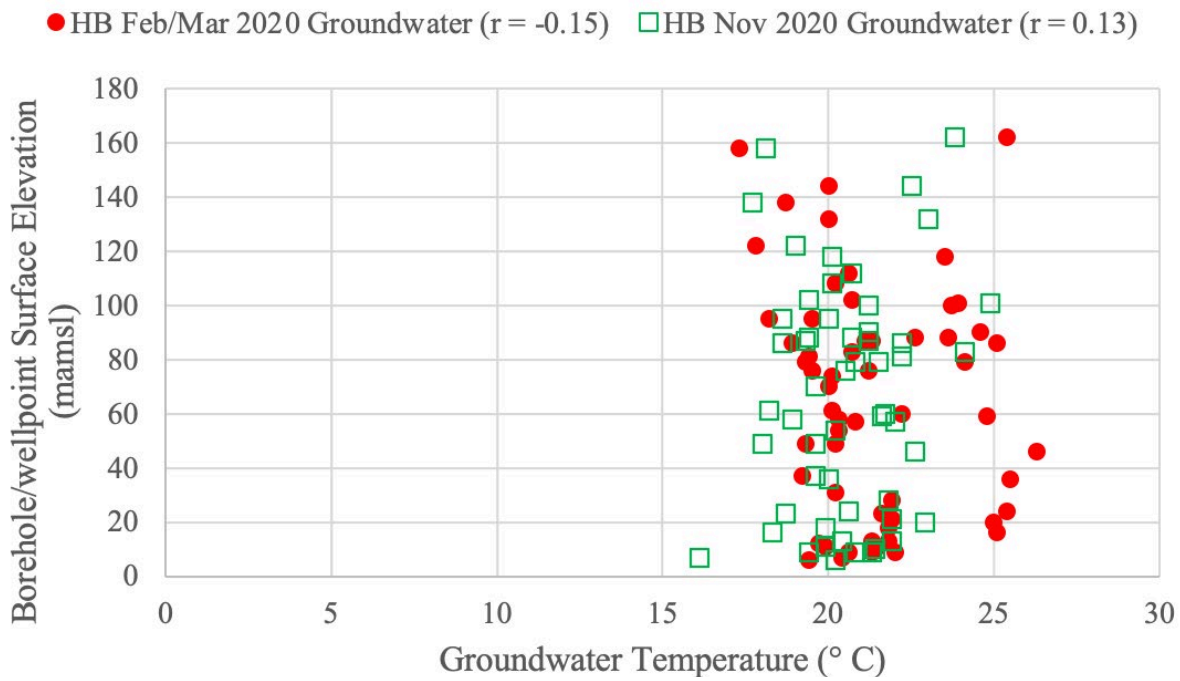

Fig 4.8 Borehole/wellpoint surface elevation vs groundwater temperature for Hout Bay (HB) groundwater samples collected in February/March 2020 and November 2020.

The correlation (r) between δD and $\delta^{18}O$ of Hout Bay groundwater February/March 2020 and November 2020 samples and boreholes/wellpoint surface elevation is weak (Fig 4.4; Fig 4.5). The correlation (r) between boreholes/wellpoint surface elevation, and electrical conductivity and deuterium excess of Hout Bay groundwater February/March 2020 and November 2020 samples is is moderate (Fig 4.6; Fig 4.7).

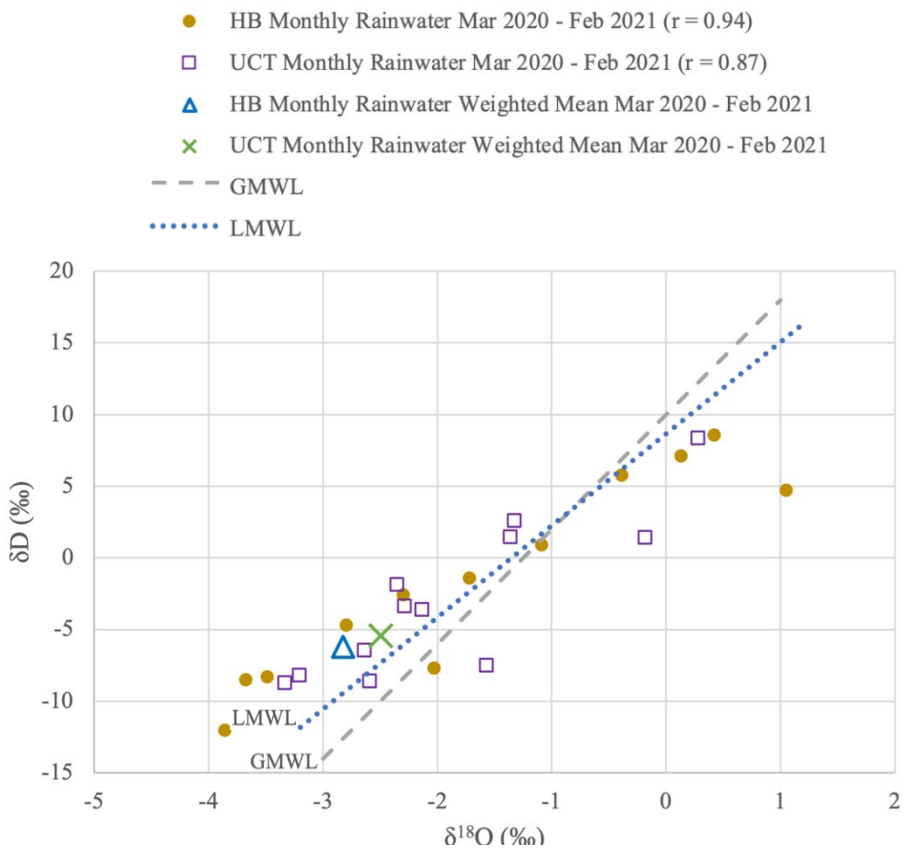

Fig 4.9 δD vs $\delta^{18}O$ rainfall data for monthly Hout Bay (HB) and UCT rain gauge samples from March 2020 to February 2021. The Global Meteoric Water Line (GMWL) after Craig (1961) and the Local Meteoric water Line (LMWL) after Harris (2010) feature for reference.

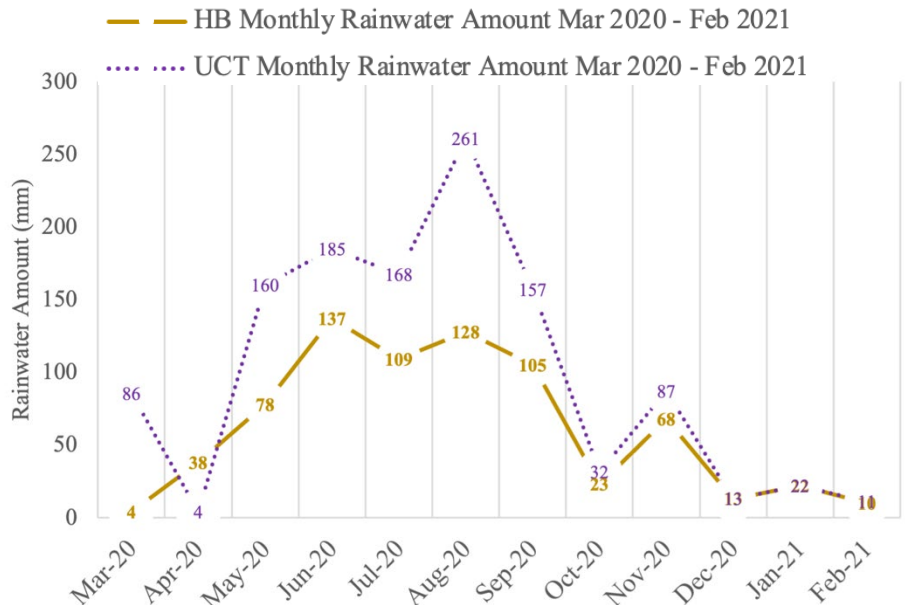

Fig 4.10 Monthly rainfall amount for rain gauges at Hout Bay (HB) and UCT from March 2020 to February 2021. The numerical data point on the plot is monthly rainfall amount (mm).

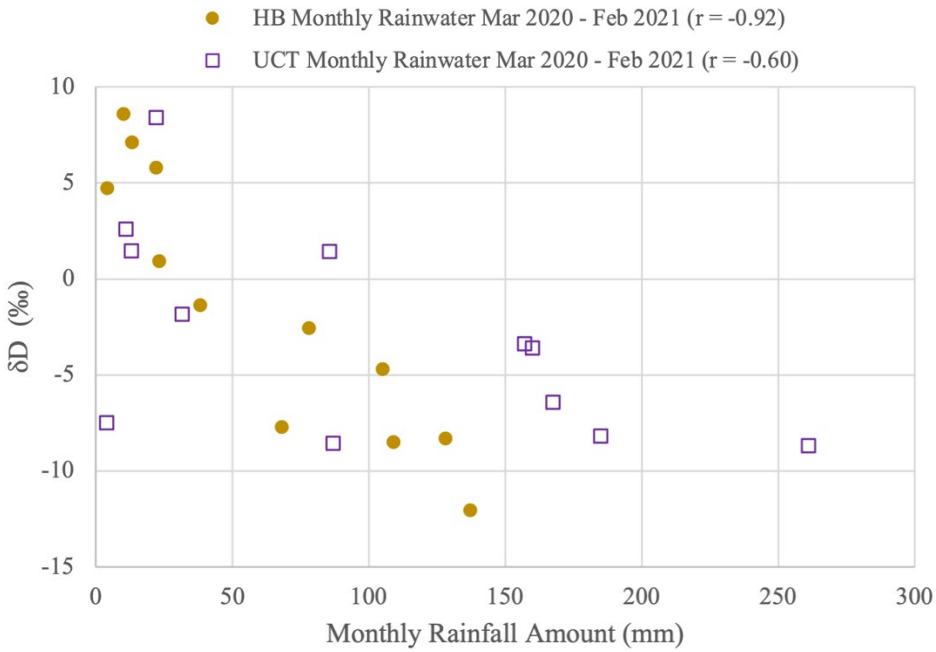

Fig. 4.11 δD vs monthly rainfall amount for rain gauges at Hout Bay (HB) and UCT from March 2020 to February 2021.

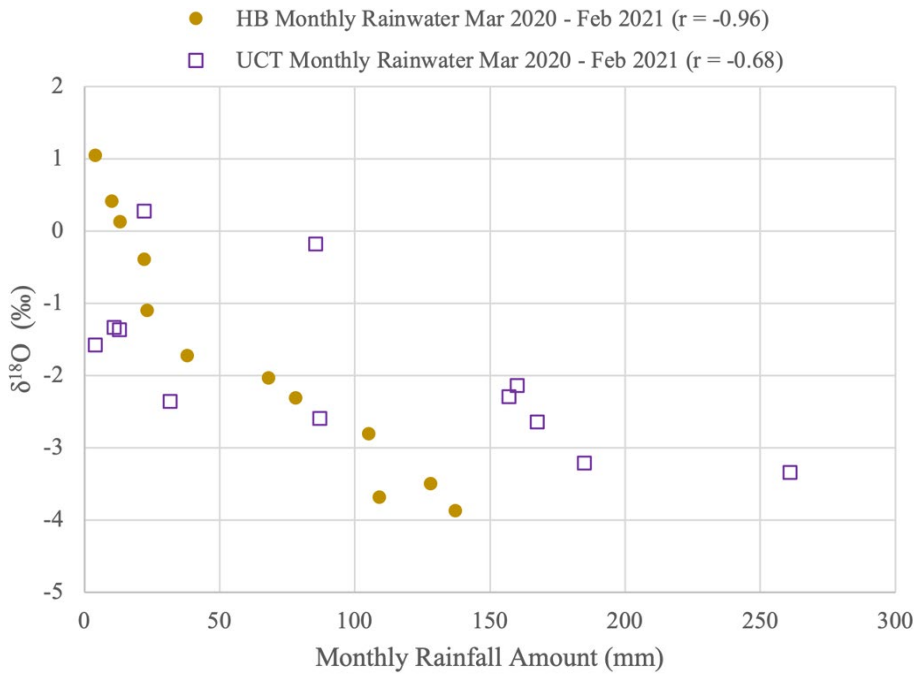

Fig. 4.12 $\delta^{18}O$ vs monthly rainfall amount for rain gauges at Hout Bay (HB) and UCT from March 2020 to February 2021.

Table 4.2 Hout Bay Terraclimate modelled mean monthly temperature (maximum and minimum) and monthly Hout Bay rainwater isotope ratios (δD and $\delta^{18}O$) from March-December 2020.

Month:	Max Temp (°C):	Min Temp (°C):	δD (‰):	$\delta^{18}O$ (‰):
Mar-20	24.56	14.34	4.8	1.05
Apr-20	22.47	12.62	-1.4	-1.72
May-20	20.13	11.44	-2.6	-2.3
Jun-20	17.95	9.72	-12.0	-3.86
Jul-20	17.91	8.75	-8.5	-3.68
Aug-20	17.26	8.74	-8.3	-3.49
Sep-20	18.72	9.52	-4.7	-2.8
Oct-20	20.97	11.29	0.9	-1.09
Nov-20	22.47	12.75	-7.7	-2.03
Dec-20	24.43	14.32	7.1	0.13

Temp: temperature

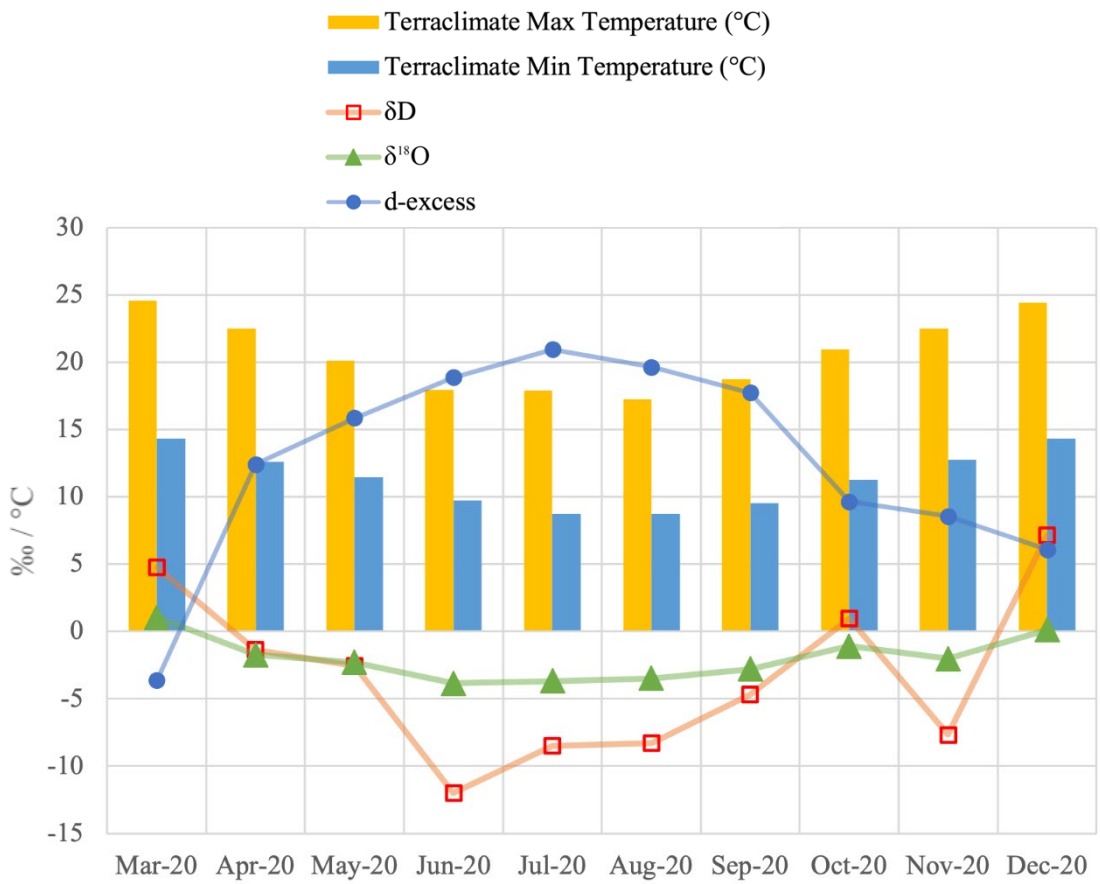

Fig 4.13 Plot of Hout Bay monthly rainwater (δD, $\delta^{18}O$, and deuterium excess) vs month (March 2020 to February 2021) and Hout Bay Terraclimate modelled mean monthly temperature (maximum and minimum) and from March 2020 to February 2021.

Rainwater:

Hout Bay rainwater δD vs $\delta^{18}O$ values from March 2020 to February 2021 correlate on Figure 4.4 (r = 0.94). UCT monthly rainwater δD and $\delta^{18}O$ values during the same months are plotted on Figure 4.4 for comparison (r = 0.87). The weighted mean for Hout Bay rainwater δD, $\delta^{18}O$, and deuterium excess is -6.2‰, -2.83‰, and 16.4‰ respectively. The cumulative rainwater amount from March 2020 to February 2021 was greater at UCT (1185 mm) than at Hout Bay (735 mm). The mean monthly rainwater amount collected at Hout Bay from March 2020 to February 2021 is 61 mm (range: 4 mm - 137 mm). The mean monthly rainwater amount collected in UCT from March 2020 to February 2021 is 99 mm (range: 4 mm - 261 mm). The monthly rainfall amount at UCT was greater than Hout Bay except for the months of April and December 2020 and January 2021. Rainfall amount increased from October to November at UCT and Hout Bay. Hout Bay monthly rainwater amount (MRA) correlates with δD on Figure 4.11(r = -0.92). University of Cape Town (UCT) monthly rainwater amount (MRA) correlates with δD on Figure 4.11 (r = -0.60). Hout Bay monthly rainwater amount (MRA) correlates with $\delta^{18}O$ on Figure 4.12 (r = -0.96). University of Cape Town (UCT) monthly rainwater amount (MRA) correlates with $\delta^{18}O$ on Figure 4.12 (r = -0.68). The weighted mean represents an average for rainwater collected at Hout Bay and UCT from March 2020 to February 2021 (Fig 4.14).

Stream Water:

Table 4.3 Hout Bay 17/18 August 2020 stream water

Sample #	δD (‰)	$\delta^{18}O$ (‰)	d-excess (‰)	EC (µS/cm)	Stream Temp (°C)
S1	-8.6	-3.30	17.8	189	12.5
S2	-5.2	-2.00	10.8	194	9.8
S3	-5.7	-2.37	13.2	177	11.1
S4	-8.1	-3.26	18.0	150	13.1
S5	-3.2	-2.19	14.3	112	9.9
S6	-9.4	-3.30	17.0	143	12.0
S7	-6.2	-2.97	17.5	191	10.4
S8	-6.1	-2.62	14.9	174	12.7
S9	-7.9	-3.30	18.5	160	11.2
S10	-7.8	-3.35	19.1	169	9.1
S11	-6.8	-2.97	17.0	235	12.0
S12	-8.3	-3.28	18.0	204	9.1
S13	-11.8	-3.42	15.6	237	15.8
S14	-8.9	-3.49	19.0	185	12.2
Min	-11.8	-3.49	10.8	112	9.1
Max	-3.2	-2.00	19.1	237	15.8
Mean	-7.4	-2.99	16.5	180	11.5
St. dev. P	2.0	0.47	2.3	32.4	1.8
Range	8.54	1.49	8.27	125	6.7

EC: electrical conductivity
d-excess: deuterium excess = $\delta D - 8 * \delta^{18}O$
Temp: temperature

This groundwater study was limited by the location of already established boreholes. During a storm event on 17/18 August 2020, 14 water samples were collected from mountain streams to observe any correlations with ground water data. The δD mean is -7.4‰ with a standard deviation of 2‰ and the $\delta^{18}O$ mean is -3‰ with a standard deviation of 0.5‰. The mean deuterium excess value is 16.5‰ with a standard deviation of 2.3‰. EC values range from 112 µS/cm - 237 µS/cm. S14 is a surface stream and S13 is a spring that flowed out of the ground to join the S14 stream. S14 was collected above the collection point for S13. δD vs $\delta^{18}O$ for stream samples produced a r = 0.85 (Fig 4.1).

Groundwater Strontium Isotopes:

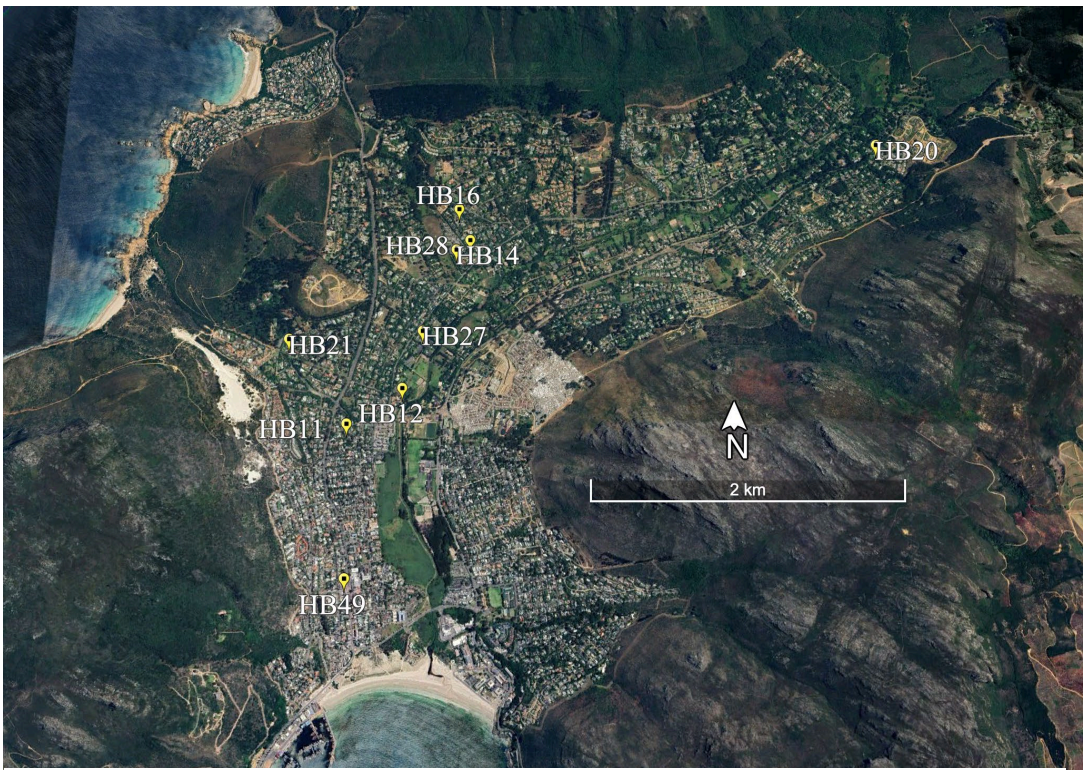

Fig. 4.17 Google Earth image of strontium isotope sample locations for Hout Bay February/March 2020 groundwater samples: HB11, HB12, HB14, HB16, HB20, HB21, HB27, HB28, HB49.

Table 4.4 Strontium sample locations for Hout Bay February/March 2020 groundwater; $^{87}Sr/^{86}Sr$, $\delta^{18}O$ (‰), electrical conductivity (µS/cm), borehole/wellpoint surface elevation (mamsl), and distance from ocean (m).

Sample #:	$^{87}Sr/^{86}Sr$:	$\delta^{18}O$ (‰):	Electrical Conductivity (µS/cm):	Surface Elevation (mamsl):	Distance from Ocean (m):
HB11	0.7098	-2.96	1010	23	1922
HB12	0.7108	-2.94	1258	9	2148
HB14	0.7247	-3.37	1292	31	2199
HB16	0.7288	-3.54	1700	60	2195
HB20	0.7263	-3.25	243	95	4640
HB21	0.7193	-3.11	1900	70	1378
HB27	0.7121	-2.74	1207	13	2170
HB28	0.7312	-3.47	1541	36	2246
HB49	0.7095	-3.01	716	16	751
Modern Ocean	0.7092	0	~50000	0	0

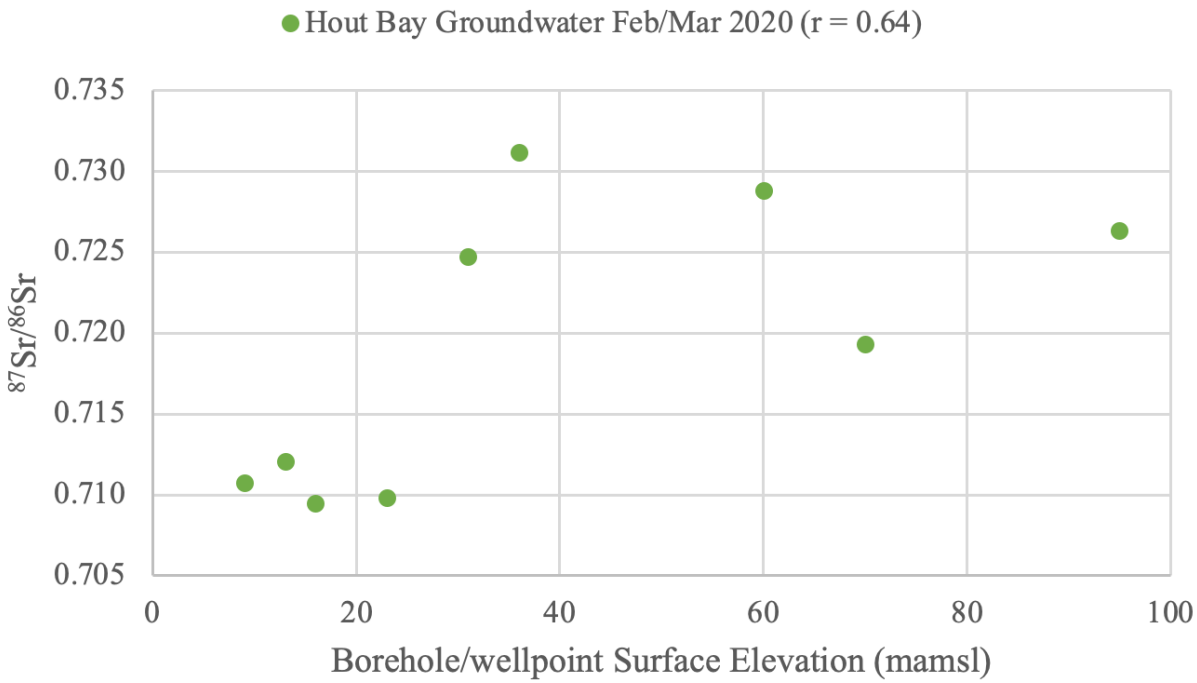

Fig. 4.18 Strontium isotope ratio ($^{87}Sr/^{86}Sr$) vs borehole/wellpoint surface elevation for Hout Bay February/March 2020 groundwater samples: HB11, HB12, HB14, HB16, HB20, HB21, HB27, HB28, HB49.

An exploratory study of nine selected samples from Hout Bay February/March 2020 groundwater was made (samples HB11, HB12, HB14, HB16, HB20, HB21, HB27, HB28, HB49. Unfortunately, it was not practical to measure the elemental strontium concentration in these samples. The mean strontium isotope ratio ($^{87}Sr/^{86}Sr$) for the samples analysed is 0.7192 with a standard deviation of 0.0083 and range of 0.0217. Hout Bay February/March 2020 groundwater samples have a moderately strong positive correlation (r = 0.64) between $^{87}Sr/^{86}Sr$ ratios and borehole/wellpoint surface elevation (Fig 4.18). The relationship between $^{87}Sr/^{86}Sr$ and stable isotopes will be discussed below.

0.70

Chapter 5: Discussion and Conclusions

It is estimated that only 13% of South Africa's tap water is sourced from groundwater (Riemann et al., 2012). The apparent cheapness and availability of groundwater reduces the value of its knowledge, and its invisibility reduces the trust in its value. Fastidious management can allow for sustainable use of groundwater resources. An in-depth Hout Bay groundwater study of such as this study has not been published before. The lack of prior isotope data in Hout Bay makes the data in this study valuable to the growing isotope database of the region and may contribute to producing future isoscapes. Each Hout Bay groundwater sample was found to have a distinct isotope composition and differences are observed between February/March 2020 and November 2020 sample data. The δD, $\delta^{18}O$, deuterium excess, electrical conductivity, and temperature of Hout bay groundwater is interpreted and compared with rainwater and stream water data. The relationship between borehole/wellpoint location and variation of Hout Bay groundwater data is explained in this chapter. Lastly, strontium isotope ($^{87}Sr/^{86}Sr$) data of Hout Bay groundwater is discussed.

Rainwater:

Climate in the Western Cape is susceptible to fluctuations (Midgley *et al.*, 2005). The δD and $\delta^{18}O$ values of rainwater should be monitored over several years to gain accurate insight into the correlations between data sets because long term effects become more apparent over longer sample campaigns as observed at UCT. The weighted mean δD and $\delta^{18}O$ values of UCT monthly rainwater from January 1996 to December 2021 are -11.1‰ and -3.10‰ respectively (Table 5.1). The weighted mean δD and $\delta^{18}O$ values of UCT monthly rainwater from March 2020 to February 2021 are -5.4‰ and -2.50‰. Cape Town's Mediterranean climate experiences higher rainfall during southern hemisphere winter months. Monthly rainwater amount at Hout Bay and UCT is >100 mm from June 2020 to August 2020 (Fig 4.10). It is expected that monthly rainwater amount decreases from winter to summer. Interestingly, monthly rainfall amount increased from October 2020 to November 2020 at the Hout Bay and UCT rain gauges. A mean monthly rainwater amount of 61 mm was recorded at the Hout Bay rain gauge from March 2020 to February 2021 with a minimum of 4 mm and a maximum of 137 mm (Fig 4.10).

Low ambient temperatures and high rainwater amount during winter is associated with lower rainwater δD and $\delta^{18}O$ values than in summer (Dansgaard, 1964). Hout Bay rainwater δD and $\delta^{18}O$ values decrease during southern hemisphere winter months (June, July, August, and September) due to low ambient temperatures and high rainwater amounts (Fig 4.13). The Hout Bay monthly rainwater deuterium excess increased during southern hemisphere winter months (Fig 4.13). Terraclimate temperatures of Hout Bay are lowest (< 20 °C) for the winter months of June, July, August, and September in comparison to other months (Table 4.2). Lower ambient temperatures induce lower relative humidity during evaporation and therefore increase in deuterium excess values in precipitation. Hout Bay monthly rainwater deuterium excess values from June 2020 to September 2020 (17.73‰ to 20.95‰) is likely to be dominantly mediated by ambient temperature. In addition to this, less sub-cloud secondary evaporation occurs during intense winter rain events which may cause deuterium excess in Hout Bay monthly rainwater June 2020 to September 2020.

Table 5.1 Pearson's correlation coefficient (r) for monthly rainwater isotope composition (δD and $\delta^{18}O$) and monthly rainwater amount (MRA)from March 2020 to February 2021 at Hout Bay and UCT.

Dataset:	MRA vs δD (r):	MRA vs $\delta^{18}O$ (r):
Hout Bay monthly rainwater Mar 2020 – Feb 2021	-0.92	-0.96
UCT monthly rainwater Mar 2020 – Feb 2021	-0.60	-0.68
UCT monthly rainwater Jan 1996 – Dec 2021	-0.46	-0.51

r: Pearson's correlation coefficient
MRA: monthly rainwater amount
Data is more detailed on Figure 4.10 and Figure 4.11.

There is a much stronger correlation between rainwater isotope composition (δD and $\delta^{18}O$) and rainwater amount and for rainwater collected in Hout Bay compared to rainwater collected at UCT from March 2020 to February 2021 (Table 5.2). Intense winter weather systems move into the Western Cape from the north-west and the mountainous relief of the area causes orogenic rainfall. Hout Bay is closer to the ocean than UCT and receives less rainfall than UCT which may result in more coherent rainfall with a stronger correlation between rainwater amount and rainwater isotope composition.

Table 5.2 Weighted mean δD and $\delta^{18}O$ values of UCT monthly rainwater January 1996 to December 2021 for months that received; > 0mm, > 20 mm, >50 mm, > 60 mm, >80 mm, and >120 mm.

Dataset:	**δD weighted mean (‰):**	**$\delta^{18}O$ weighted mean (‰):**
UCT monthly rainwater Jan 1996 -Dec 2021 > 0 mm	-11.1	-3.10
UCT monthly rainwater Jan 1996 -Dec 2021 > 20 mm	-11.2	-3.13
UCT monthly rainwater Jan 1996 -Dec 2021 > 50 mm	-11.8	-3.22
UCT monthly rainwater Jan 1996 -Dec 2021 > 60 mm	-12.0	-3.26
UCT monthly rainwater Jan 1996 -Dec 2021 > 80 mm	-12.2	-3.29
UCT monthly rainwater Jan 1996 -Dec 2021 > 120 mm	-12.9	-3.40

The weighted mean of δD and $\delta^{18}O$ values of monthly rainwater collected in Hout bay between March 2020 to February 2021 is -6.2‰ and -2.38‰ respectively. Hout Bay groundwater δD and $\delta^{18}O$ mean values in February/March 2020 (δD = -12.4, $\delta^{18}O$ = -3.31) and November 2020 (δD = -12.2, $\delta^{18}O$ = -3.21) are more negative than Hout Bay March 2020 to February 2021 rainwater weighted mean δD and $\delta^{18}O$ values. The mean surface elevation of Hout Bay groundwater sample locations is 64 mamsl. The rain gauge where Hout Bay rainwater was collected is at 81 mamsl in a central position in the study area (Fig 3.2). Hout Bay monthly rainwater weighted mean δD vs $\delta^{18}O$ is more indicative of light, low altitude rainfall than the δD vs $\delta^{18}O$ data arrays of Hout Bay February/March 2020 and November 2020 groundwater (Fig 4.1). There are three possible reasons for the δD and $\delta^{18}O$ difference between Hout Bay 2020 groundwater and Hout Bay March 2020 to February 2021 rainwater collected during this study:

1. Intense rainfall events result in high rainwater amounts and produce precipitation with low δD and $\delta^{18}O$ values as observed in monthly rainwater collected at UCT from January 1996 to December 2021 (Dansgaard, 1964; Table 5.2). The δD and $\delta^{18}O$ values of groundwater tends to be more similar to the isotope composition of intense rainfall events than light rainfall events because high rainwater amounts associated with intense rainfall events contribute larger volumes of water to groundwater recharge. Therefore, the dominant δD and $\delta^{18}O$ component of Hout Bay groundwater is more negative than the rainfall in the study area.
2. Hout Bay rainwater in years prior to this study may have recharged Hout Bay groundwater with more negative δD and $\delta^{18}O$ rainwater than Hout Bay March 2020 to February 2021 rainwater

and subsequently still dominate δD and $\delta^{18}O$ values of Hout Bay groundwater. The weighted mean δD and $\delta^{18}O$ values for rainwater collected at Hout Bay and UCT from March 2020 to February 2021 are similar (Fig 4.1). The δD vs $\delta^{18}O$ data point UCT monthly rainwater weighted mean from January 2009 to December 2019 plots much closer to the cluster of Hout Bay groundwater δD vs $\delta^{18}O$ data arrays (Fig 4.1). If Hout Bay rainwater δD and $\delta^{18}O$ values were similar to UCT rainwater δD and $\delta^{18}O$ values from January 2009 to December 2019, Hout Bay groundwater might have retained more negative δD and $\delta^{18}O$ values from rainwater recharge prior to March 2020.

3. There may be a distal high elevation component to Hout Bay groundwater recharge. This is not ruling out that groundwater is locally recharged in Hout Bay. Rather, high elevation groundwater recharge from precipitation on mountain peaks that surround Hout Bay add a component of more negative δD and $\delta^{18}O$ to Hout Bay groundwater due to altitude effect (Dansgaard, 1964). Hout Bay stream samples were collected at higher elevation (207 mamsl to 405 mamsl) than groundwater sample locations (6 mamsl to 162 mamsl) and have similar δD and $\delta^{18}O$ values to Hout Bay monthly rainwater weighted mean from March 2020 to February 2021 (Fig 4.1).

The three scenarios explained above may work together to affect the difference between Hout Bay groundwater and Hout Bay rainwater δD and $\delta^{18}O$ values. Constraining the dominant cause of difference between Hout Bay rainwater and groundwater would require monitoring Hout Bay rainwater for a longer period than this study allowed.

Stream Water:

Water from streams in Hout Bay was collected during an intense rainfall event that caused increased surface runoff. Stream water is fed by water flowing from the mountain peaks surrounding Hout Bay. The mean measured Hout Bay stream water temperature (11.4 °C) is lower than groundwater temperatures for February/March 2020 (21.5 °C) and November 2020 (20.5 °C). Water is a good

conductor of heat and as groundwater flows through the aquifer, latent heat from the Earth causes groundwater temperature to be greater than stream water temperature. The electrical conductivity of Hout Bay February/March 2020 and November 2020 groundwater is generally greater than that of Hout Bay stream water (Table 4.1). Sample S13 water was collected from a stream that emerges as a groundwater from a spring whereas sample S14 is a surface stream. Groundwater dissolves minerals and salts during its flow path which increases electrical conductivity (Anderson and Cummings, 1999). Hout Bay stream water samples S13 and S14 are in very close proximity to one another. Stream water emerging from the ground at S13 as a spring has higher electrical conductivity than the surface water collected at S14. The water from S13 is likely to interact with subsurface Earth material and therefore increase electrical conductivity through dissolution.

Table 5.3 The minimum, maximum, range, standard deviation, and mean of Hout Bay 2020 groundwater data.

	δD (‰)		**$\delta^{18}O$ (‰)**		**EC (µS/cm)**		**Groundwater Temp (°C)**		**d-excess (‰)**	
	Feb/ Mar	Nov	Feb/ Mar	Nov	Feb/ Mar	Nov	Feb/ Mar	Nov	Feb/ Mar	Nov
Min	-16.5	-16.5	-3.85	-3.90	135	126	17.3	16.1	10.8	10.1
Max	-6.4	-7.0	-2.19	-2.14	2370	2180	26.3	24.9	17.2	16.2
Range	10.1	9.5	1.66	1.76	2235	2054	9.0	8.8	6.4	6.0
σ	2.1	2.2	0.39	0.39	493	444	2.2	1.7	1.5	1.4
$\bar{x}$	-12.4	-12.2	-3.31	-3.21	740	700	21.5	20.5	14.3	13.5

Min: minimum
Max: maximum
σ: standard deviation
$\bar{x}$: mean

Groundwater Temperature:

The mean groundwater temperature decreases by 1.0 °C from February/March 2020 (21.5 °C) to November 2020 (20.5 °C). The majority of Hout Bay groundwater temperature values sit above the line y = x on Figure 4.2 e, highlighting generally higher groundwater temperatures in February/March 2020 compared to November 2020. A Terraclimate model of Hout Bay produced the lowest ambient maximum daily temperatures (< 20 °C) for the winter months of June, July, August, and September in

comparison to other months (Fig 4.13). Colder ambient temperatures experienced during winter months before November 2020 sampling may have led to lower groundwater temperatures. Hout Bay groundwater temperature ranges from 9.0 °C in February/March 2020 to 8.8 °C in November 2020. No clear correlation was observed between groundwater temperature and other data considered in this study.

Groundwater Electrical Conductivity:

Drinking water supply in Cape Town has an electrical conductivity of approximately 150 µS/cm and seawater has an electrical conductivity of approximately 50000 µS/cm measured on a WTW-conductivity multimeter. There is a moderate correlation between borehole/wellpoint surface elevation and electrical conductivity of February/March 2020 (r = -0.41) and November 2020 (r = -0.38) Hout Bay groundwater (Fig 4.6). During subsurface flow, groundwater inherits chemical constituents as dissolved ions from aquifer matrix interactions which in turn increase groundwater electrical conductivity along groundwater flow path. Groundwater electrical conductivity in Hout Bay increases from north-east to south-west (Fig 4.3 e, f). This trend of increasing groundwater electrical conductivity follows the flow of the Hout Bay River from inland towards the ocean. The mean electrical conductivity of Hout Bay 2020 groundwater decreases by 40 µS/cm from February/March 2020 (740 µS/cm) to November 2020 (700 µS/cm). High rainfall experienced before November 2020 sample collection may have had a dilution effect on groundwater electrical conductivity causing a decrease in electrical conductivity values. The dilution of groundwater and resulting decrease of groundwater electrical conductivity is clear on Figure 4.2 c where the majority of the data points sit above the line y = x. Groundwater flows under hydraulic gradient that is generally driven by gravity. The groundwater from shallow wellpoint HB48 (5 m) is at a school field that gets irrigated (Fig 3.2). It is likely that HB48 being at low elevation in the valley (6 m) receives groundwater recharge from various surrounding higher elevation groundwater and therefore is susceptible to changes in water chemistry. For HB48, groundwater electrical conductivity notably decreases from February/March 2020 to November 2020 (Fig 4.2 c). Groundwater from HB4 underwent an increase in electrical conductivity from 633 µS/cm

to 1146 µS/cm between February/March 2020 and November 2020 (Fig 4.2 c). Interestingly, the electrical conductivity increases from February/March 2020 to November 2020 at HB51 (Fig 4.2 c). Electrical conductivity in Hout Bay groundwater is relatively low to when compared to similar studies conducted in the region. Finlayson (2022) generally found higher electrical conductivity values ($\bar{x}$ = 1520 µS/cm, range: 110 µS/cm – 58700 µS/cm) in a groundwater study of areas east of Hout Bay. Electrical conductivity can be viewed as a preliminary quality assessment. Day et al. (2020) found that the quality of surface water bodies in Cape Town has been deteriorating. Tredoux et al. (2004) noted the importance of monitoring groundwater quality. Hout Bay February/March and November 2020 groundwater electrical conductivity results indicate Hout Bay groundwater quality varies and is generally of intermediate to good quality.

Seasonality of Groundwater Data

Differences in Hout Bay groundwater δD and $\delta^{18}O$ values observed between February/March 2020 and November 2020 could be expected due to seasonal fluctuations in rainwater δD and $\delta^{18}O$ values (Fig 4.13). The mean values for Hout Bay groundwater δD and $\delta^{18}O$ vary slightly from February/March 2020 and November 2020. Groundwater is a dynamic resource that is susceptible to change (Schot and van der Wal, 1992; Jat, Khare and Garg, 2009). Numerous factors could affect differences observed in Hout Bay groundwater data between February/March 2020 and November 2020. The data points encircled on Figure 4.2 a, b, c, d, and e showed the most difference between February/March 2020 and November 2020. Each data point on Figure 4.2 is subdivided and depicted as >64 mamsl or <64 mamsl. The flow of groundwater through scree aquifers on the slopes of Table Mountain is likely to be stratified (Diamond and Harris, 2019). Shallow groundwater flow is fast and superficially recharged whereas deeper groundwater flow is much slower after being recharged by intense rainfall events. Samples collected below 64 mamsl show more variation between February/March 2020 and November 2020 data than samples collected above 64 mamsl due to receiving more varied low elevation proximal recharge (Fig4.2). This has been referred to as selection effect by Diamond and Harris (2019).

Sample location HB48 is a shallow wellpoint that is used in conjunction with a deeper borehole (HB47). Groundwater abstracted from HB47 and HB48 is used for irrigation of school grounds most intensively during drier summer months. The groundwater is exposed to the atmosphere through irrigation sprinklers. Exposure to the atmosphere allows for evaporative loss of lighter isotopes while the residual water infiltrates the ground as recharge. Evaporation during summer irrigation may have caused the δD and $\delta^{18}O$ values to be lower in February/March 2020 at HB48 compared to November 2020.

The δD and $\delta^{18}O$ values at HB56 decreased from February/March to November (Fig 4.2 a, b). The months preceding Hout Bay groundwater November 2020 sample collection received more intense rainfall than the months preceding February/March 2020 sample collection (Fig 1.2). Hout Bay 2020 monthly rainwater amount for May, June, July, and August is greater than 105 mm. For the remainder of months in 2020, Hout Bay monthly rainwater amount is less than 78 mm (Fig 4.10). The ambient cooler winter temperatures (~9 °C to 17 °C) with higher rainfall (> 100 mm/month) may have recharged groundwater at HB56 and HB48 with isotopically lighter water prior to Hout Bay groundwater November 2020 sample collection. It is unclear what caused δD and $\delta^{18}O$ to increase from February/March 2020 to November 2020 at HB42 and HB51. The δD and $\delta^{18}O$ values observed in Hout Bay groundwater at HB43 from February/March 2020 are coherent with an evaporitic groundwater recharge (Fig 4.2). The HB59 groundwater is from a shallow wellpoint that is likely to receive recharge by water that evaporates.

Areal Variation of Groundwater Hydrogen and Oxygen Isotopes:

The δD and $\delta^{18}O$ values of Hout Bay 2020 groundwater cluster around the LMWL produced by Harris (2010) for rainwater collected at UCT from 1996 to 2008 (Fig 4.1). The δD and $\delta^{18}O$ values of Hout Bay 2020 groundwater showed areal variation in the boreholes/wellpoints dataset. Figure 2.7 is a useful guide in determining what may cause δD and $\delta^{18}O$ variation in Hout Bay groundwater. Areal variation patterns of Hout Bay 2020 groundwater δD and $\delta^{18}O$ (Fig 4.3 a, b, c, d) are similar because they are affected by the same factors. A number of natural factors can affect δD and $\delta^{18}O$ composition in

groundwater including; latitude, relative humidity, ambient temperature, precipitation distance from the ocean, precipitation amount, and altitude of precipitation formation in clouds (Craig, 1961; Dansgaard, 1964). Hout Bay is surrounded by mountain peaks that rise to 867 mamsl in the north and 928 mamsl in the south (Fig 2.1). The high elevation mountain peaks surrounding Hout Bay are above steep cliffs that form a valley topography. The mountainous relief surrounding Hout Bay is shaped predominantly by underlying lithology. Figure 2.3 shows the steep relief of the Table Mountain Group that forms the structure of the Hout Bay valley topography. Table Mountain Group rocks outcrops as cliffs with the majority of lower slopes covered in alluvium composed of mountain scree (Fig 2.2). The Earth material that makes up the mountain scree forms an unconsolidated aquifer overlying a fractured Cape Granite basement. Most boreholes/wellpoints in Hout Bay abstract groundwater flowing through mountain scree. A few boreholes in Hout Bay were drilled into Cape Granite. The boreholes abstracting groundwater from Cape Granite were strategically drilled based on hydrological surveys involving structural data and geophysics. The mountainous geographical relief of Cape Town induces orographic rainfall in what is considered a semi-arid region. Orogenic rainfall results in an altitude effect on isotopes in precipitation compared to groundwater which in turn recharges lower elevation aquifers with a high altitude δD and $\delta^{18}O$ composition as previously mentioned. Generally, areal δD and $\delta^{18}O$ variation in Hout Bay groundwater is likely to be due to varied δD and $\delta^{18}O$ precipitation and mixing of groundwater. Variation of δD and $\delta^{18}O$ in precipitation recharge is attributed to the topographical relief of the Hout Bay valley. Some δD and $\delta^{18}O$ compositions of Hout Bay groundwater is affected by anthropogenic inputs such as recharge by irrigation water. Similar isotope investigations have been carried out in the areas surrounding Hout Bay. The date of sampling must be considered when comparing isotope values from other studies. Groundwater δD and $\delta^{18}O$ values reported by Finlayson (2022) east of Hout Bay in the southern suburbs of Cape Town are more positive than Hout Bay 2020 groundwater δD and $\delta^{18}O$ values. This difference in δD and $\delta^{18}O$ values is likely due to the proximity of the ocean to Hout Bay as well as generally lower elevation of boreholes/wellpoints in Hout Bay compared to the southern suburbs.

Hout Bay Groundwater Sectors

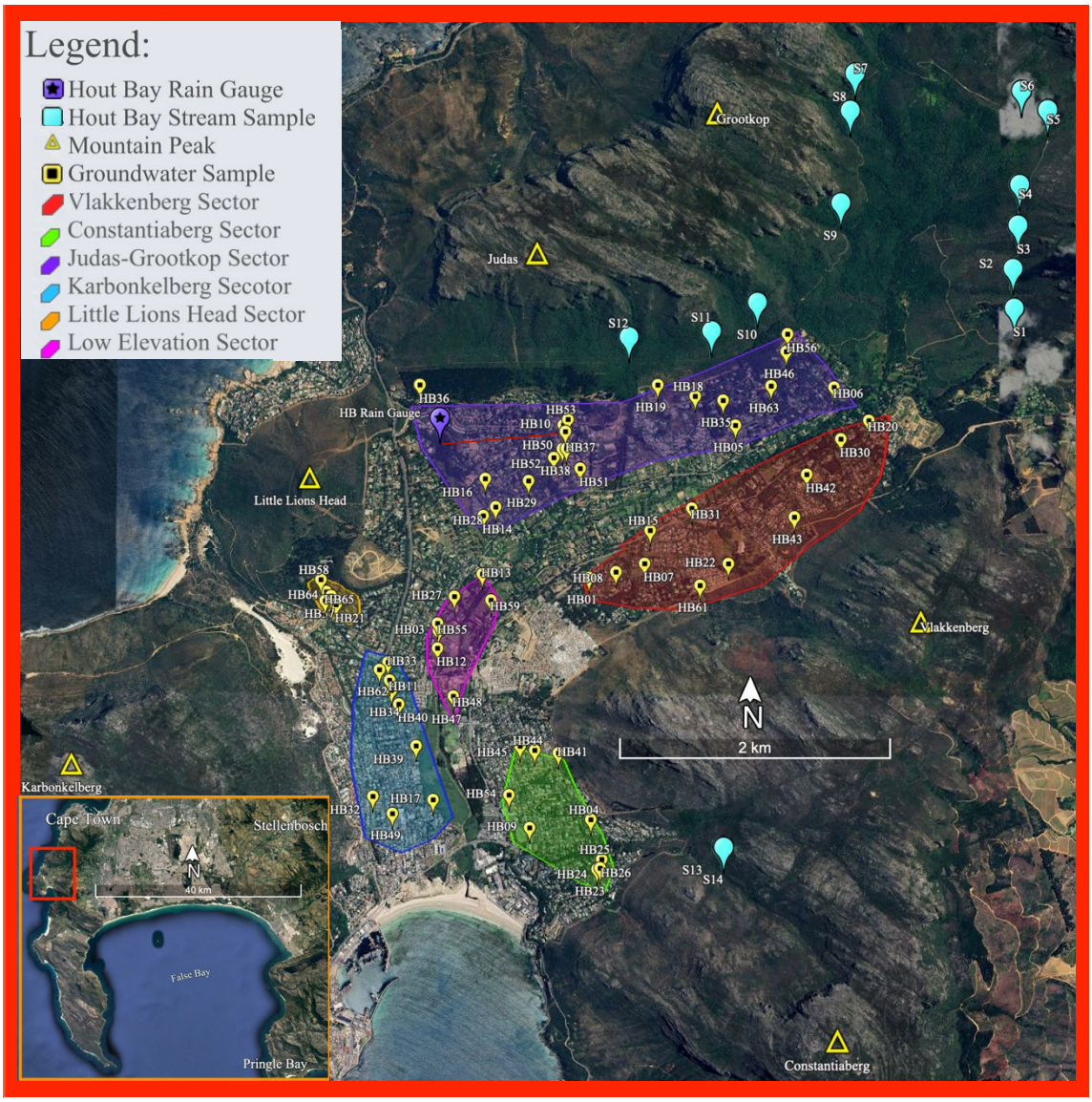

Fig 5.1 Google Earth image of Hout Bay with locations of; Hout Bay rain gauge, Hout Bay stream samples, mountain peaks, Hout Bay groundwater samples, and the Hout Bay groundwater sectors.

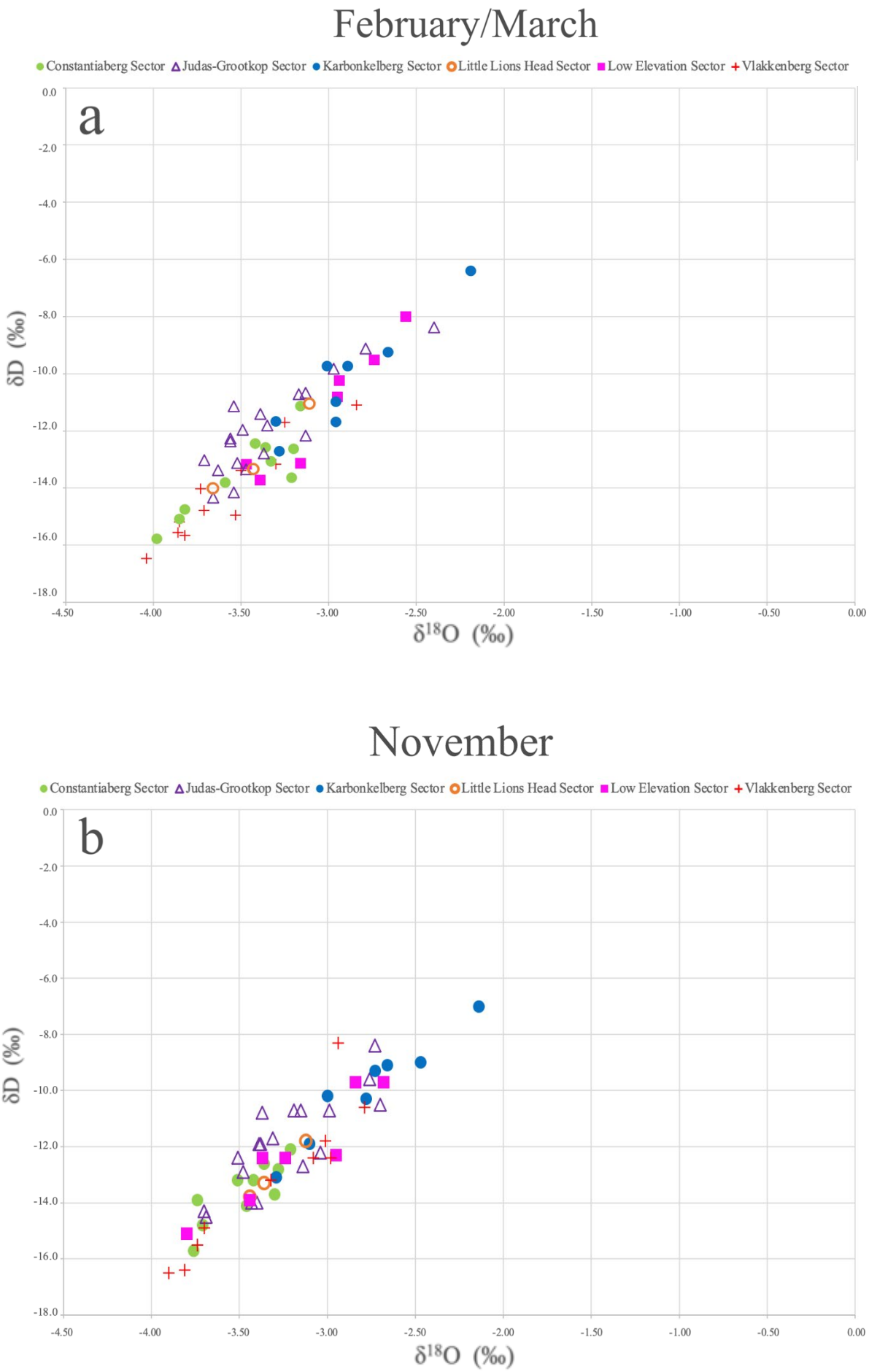

Fig 5.2 δD vs $\delta^{18}O$ of Hout Bay groundwater sectors: **a** February/March 2020, **b** November 2020.

The weak correlations between borehole/wellpoint surface elevation and Hout Bay groundwater δD ($r_{Feb/Mar}$ = -0.15, r_{Nov} = -0.22) and $\delta^{18}O$ ($r_{Feb/Mar}$ = -0.26, r_{Nov} = -0.24) were weak (Fig 4.4; Fig 4.5). Hout Bay groundwater sample locations were subdivided into sectors to access if areal variation of groundwater δD and $\delta^{18}O$ is related to geographical location. Sectors are assigned to Hout Bay groundwater samples locations based on the closest mountain peak above the groundwater sample location (Fig 5.2). The coherence of areal isotope variation and geographical location in Hout Bay groundwater is supported by the data arrays on Figure 5.3 a and Figure 5.3 b. Subtle differences in δD and $\delta^{18}O$ distinguish Hout Bay groundwater sectors.

The Constantiaberg and Vlakkenberg sectors are on the southern slopes of the Hout Bay valley (Fig 5.1). The δD and $\delta^{18}O$ values of groundwater from Constantiaberg and Vlakkenberg sectors are more negative than δD and $\delta^{18}O$ values from the other Hout Bay groundwater sectors (Fig 5.3). All groundwater sample locations in the Constantiaberg and Vlakkenberg sectors except HB9 and HB54 are above 50 mamsl. The Karbonkelberg sector is at a low elevation (<30 mamsl) and is in close proximity to the ocean. The δD and $\delta^{18}O$ values of groundwater from the Karbonkelberg sector are more positive than the other sectors (Fig 5.3). The groundwater from the low elevation sector receives gravity driven groundwater recharge from surrounding higher elevation groundwater as well as direct infiltration from precipitation. The spread of groundwater δD and $\delta^{18}O$ values from the Low Elevation sector is intermediate between Vlakkenberg, Constantiaberg, and Karbonkelberg and could represent mixing of Hout Bay groundwater sectors (Fig 5.3). The Judas-Grootkop sector includes a broadly spread array of δD and $\delta^{18}O$ values (Fig 5.3). The variation between Hout Bay groundwater sectors suggests that the altitude at which precipitation forms over Hout Bay and distance from the ocean is influences areal variation observed in Hout Bay groundwater δD and $\delta^{18}O$ values.

Groundwater Deuterium Excess:

The mean deuterium excess for Hout Bay groundwater in 2020 decreases within error by 0.8‰ from February/March (14.3‰) to November (13.5‰). Sub-cloud secondary evaporation occurs where

falling precipitation evaporates before reaching the Earth's surface. Precipitation that undergoes sub-cloud secondary evaporation has been found to decrease the slope of δD vs $\delta^{18}O$ line of best fit (Stewart, 1975). The line of best fit for plot of Hout Bay groundwater δD vs $\delta^{18}O$ in February/March 2020 and November 2020 have slope gradients less than that of the Global Meteoric Water Line (Fig 4.1). The deuterium excess decreases at HB19, HB29, and HB59 from February/March to November which could be caused by increased relative humidity during intense rainfall or that samples experienced evaporation. The groundwater at HB48 has a deuterium excess more indicative of contamination by irrigation water in February/March 2020 (12.5‰) than November 2020 (15.3‰). Wellpoint HB48 is at a private school where irrigation of sports fields with a combination of groundwater from HB47 borehole (40 m depth) and HB48 wellpoint (5 m depth) takes place. The evaporative signature of deuterium excess in February/March 2020 in comparison to HB48 November 2020 is consistent with irrigation being the cause.

Groundwater Strontium Isotopes:

Strontium isotopes do not fractionate in the same manner as hydrogen and oxygen isotopes. The strontium isotope composition ($^{87}Sr/^{86}Sr$) of groundwater can therefore provide insight into processes involving aquifer interaction and mixing of groundwater. Strontium isotope composition ($^{87}Sr/^{86}Sr$) analysis was conducted on spatially spread samples from Hout Bay February/March 2020. Only nine samples were selected to represent the larger data set because $^{87}Sr/^{86}Sr$ analysis is expensive. Elemental strontium concentration data was not obtained due to problems with analytical instruments. Strontium concentration of groundwater is expected to be low due to the low pH of groundwater in the study area and lack of carbonate rock-types (Weaver et al., 1999). The low $^{87}Sr/^{86}Sr$ ratios of Hout Bay groundwater samples HB11, HB12, HB27, and HB49 are similar to the modern seawater $^{87}Sr/^{86}Sr$ ratio; 0.7092 (Elderfield, 1986).

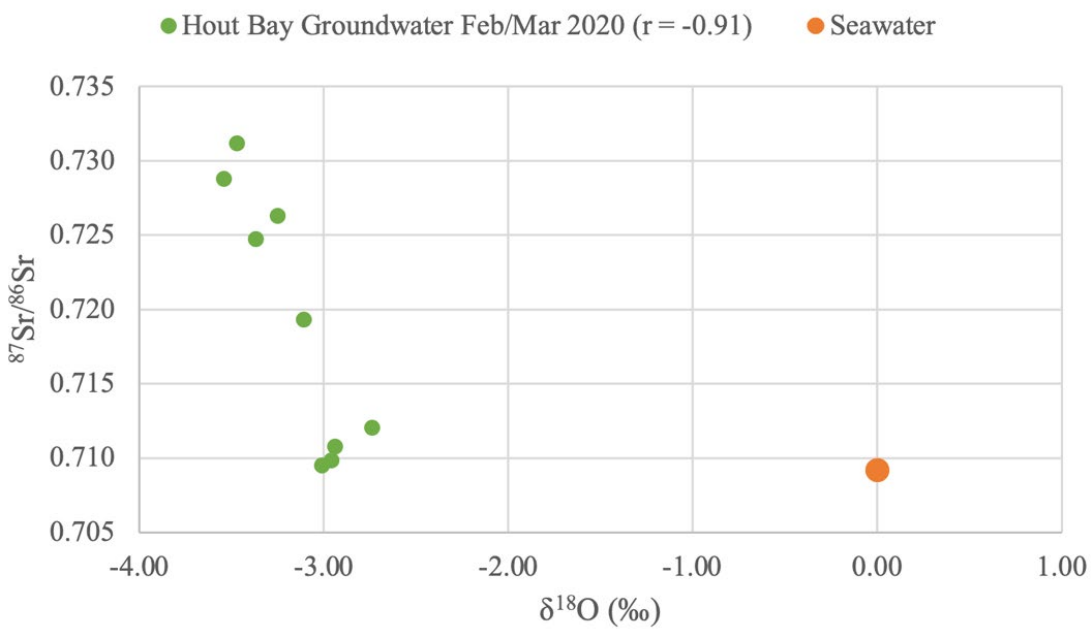

Fig. 5.3 Strontium isotope ratio ($^{87}Sr/^{86}Sr$) vs $\delta^{18}O$ (‰) for seawater and Hout Bay February/March 2020 groundwater samples: HB11, HB12, HB14, HB16, HB20, HB21, HB27, HB28, HB49.

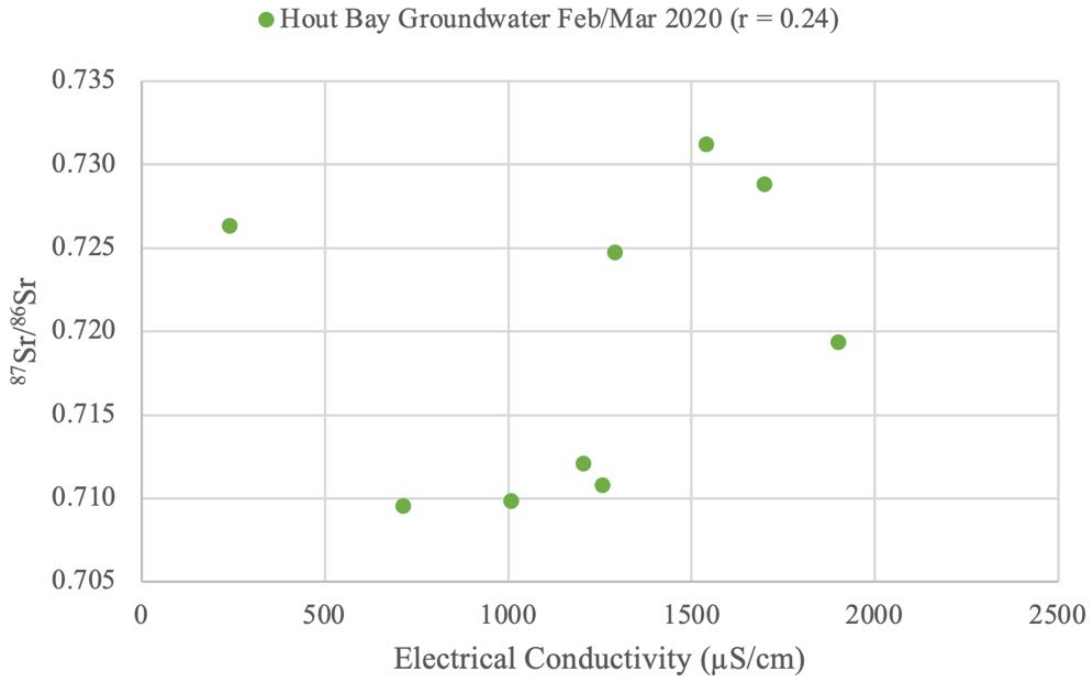

Fig. 5.4 Strontium isotope ratio ($^{87}Sr/^{86}Sr$) vs electrical conductivity (µS/cm) for Hout Bay February/March 2020 groundwater samples: HB11, HB12, HB14, HB16, HB20, HB21, HB27, HB28, HB49.

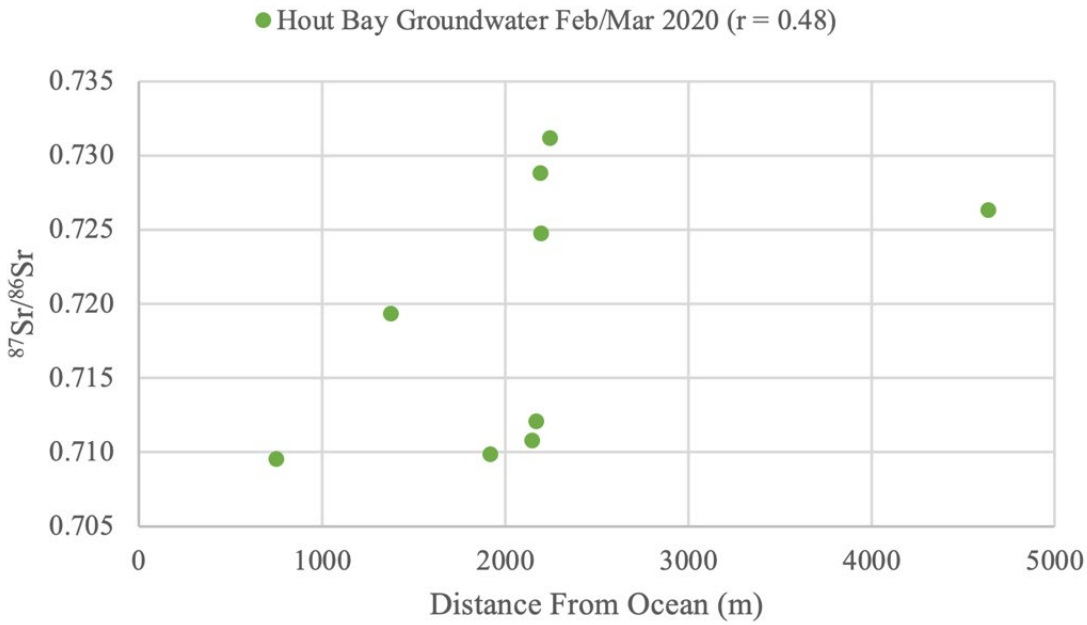

Fig. 5.5 Strontium isotope ratio ($^{87}Sr/^{86}Sr$) vs distance from ocean for Hout Bay February/March 2020 groundwater samples: HB11, HB12, HB14, HB16, HB20, HB21, HB27, HB28, HB49.

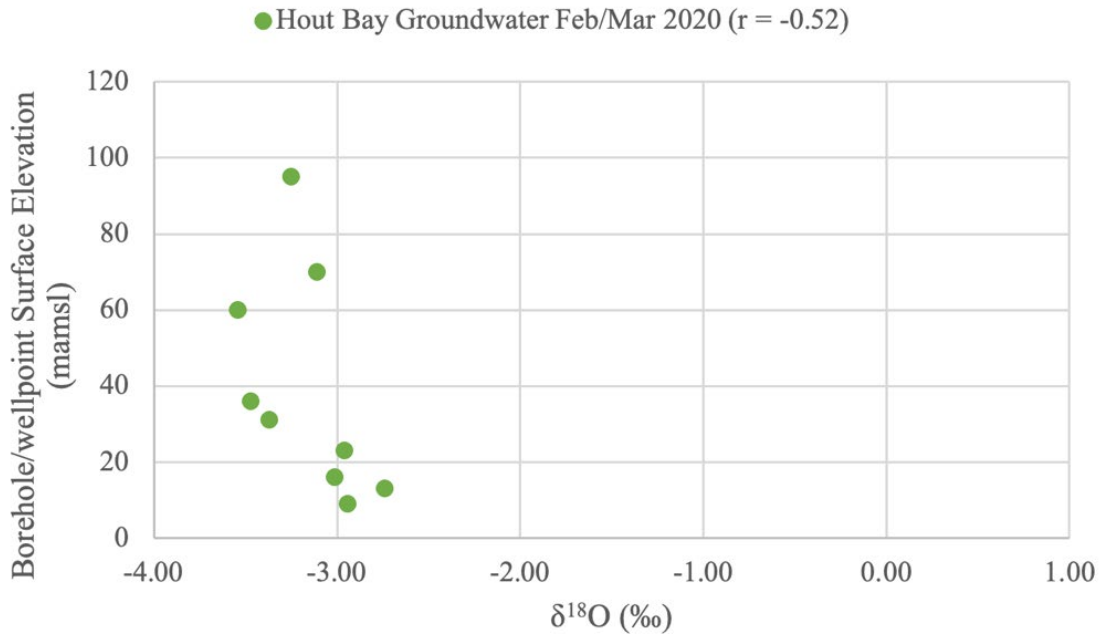

Fig. 5.6 $\delta^{18}O$ vs borehole/wellpoint surface elevation for Hout Bay February/March 2020 groundwater samples: HB11, HB12, HB14, HB16, HB20, HB21, HB27, HB28, HB49.

Hout Bay groundwater $^{87}Sr/^{86}Sr$ ratios do not correlate strongly with Hout Bay groundwater electrical conductivity (r = 0.24) suggesting that strontium in Hout Bay groundwater is not solely derived from the same source chemical constituents that reflect the electrical conductivity of Hout Bay groundwater (Fig 5.4). A combination of various mechanisms may affect $^{87}Sr/^{86}Sr$ ratio variation in Hout Bay groundwater as discussed below:

1. Dissolution of strontium bearing minerals in Cape Granite or the Table Mountain Group by groundwater.
2. Seawater strontium that has entered the groundwater system by seawater ingress.
3. Dissolution of strontium from shell and sand material of the Quaternary Witzand Formation by groundwater.
4. Dissolution of strontium in marine aerosol from sea spray.

Mechanism 1 is possible but unlikely. The $^{87}Sr/^{86}Sr$ ratios of Cape Granite (0.7701- 1.1602) are distinct from that of modern seawater; 0.7092 (Allsopp and Kolbe, 1965; Elderfield, 1986). The Table Mountain Group contains negligible amounts of strontium (Midgley et al., 2012) and is therefore unlikely to contribute strontium to Hout Bay groundwater. The elevation of the Cape Granite unconformity was noted as ~260 mamsl at Constantia Nek by Harris et al., (1999) which is the western limit of Hout Bay. The elevation of the Cape Granite unconformity outcrops at approximately 165 mamsl in the north of Hout Bay at Suikerbossie and just above sea-level below Karbonkelberg mountain peak in the in the south (Council for Geoscience, 1990) . Hout Bay groundwater from samples HB14, HB16, HB20, and HB28 may have minor interactions with Cape Granite to produce relatively high $^{87}Sr/^{86}Sr$ ratios (~0.730).

Hout Bay groundwater strontium isotope ratio ($^{87}Sr/^{86}Sr$) shows a good correlation (r = -0.91) with $\delta^{18}O$ values (Fig 5.3). Seawater does not plot on the data array of $^{87}Sr/^{86}Sr$ vs $\delta^{18}O$ (Fig 5.3). The $\delta^{18}O$ values (~-3.00‰) of Hout Bay groundwater with similar $^{87}Sr/^{86}Sr$ ratios to modern seawater are more negative than modern seawater. The $^{87}Sr/^{86}Sr$ ratios of most of the Hout Bay groundwater samples are higher than modern seawater (Table 4.4). It is therefore unlikely that seawater ingress as mentioned in

mechanism 2 above is a source of strontium in Hout Bay groundwater, although it should be noted that strontium concentration is required to model mixing contributions of water bodies.

The $^{87}Sr/^{86}Sr$ ratios in the sediments of the Quaternary Witzand Formation found in other regions of the Western Cape are close to that of modern ocean $^{87}Sr/^{86}Sr$ ratios (Franeschini and Compton, 2004). Groundwater borehole/wellpoint HB11, HB12, HB27, and HB49 are situated on the Witzand Formation (Fig 2.2; Fig 4.17). The groundwater samples collected from HB11, HB12, and HB27 were abstracted from shallow wellpoints and the depth of borehole HB49 was not available. Groundwater in the Witzand Formation sediments north of the study area inherits low $^{87}Sr/^{86}Sr$ ratios (Mauger and Compton, 2011). Therefore, mechanism 3 could explain the dominant source of strontium in Hout Bay groundwater HB11, HB12, HB27, and HB49 to be largely from groundwater percolating through and dissolving strontium from shell and sand material of the Quaternary Witzand Formation sediments.

Mechanisims 3 and 4 are both possible and may work in tandem. The contribution of some sea spray to Hout Bay groundwater strontium is supported by the positive correlation ($r = 0.48$) between $^{87}Sr/^{86}Sr$ ratio with distance from the ocean (Fig 5.5). Hout Bay groundwater sample HB21 is relatively close to the ocean (1378 m) and has a relatively intermediate $^{87}Sr/^{86}Sr$ ratio, suggesting influence of both sea spray and minor dissolution of Cape Granite as groundwater sources of strontium. Near coast aquifer systems generally have $^{87}Sr/^{86}Sr$ ratios similar to modern ocean due to strontium in marine aerosols dissolving into precipitation from sea spray (Scott et al., 2020). The data presented here fit this interpretation, but the correlation between $^{87}Sr/^{86}Sr$ ratios and $\delta^{18}O$ values should allow a more nuanced interpretation given more data. Hout Bay groundwater $\delta^{18}O$ values increase with decreasing borehole/wellpoint surface elevation which is expected due to altitude and amount effects (Fig 5.6). Higher rainwater amounts are expected at higher altitudes and result in lower $\delta^{18}O$ values due to the altitude and amount effects (Dansgaard, 1964). Because of the altitude and amount effects, a correlation between $^{87}Sr/^{86}Sr$ ratio $\delta^{18}O$ values is be generated for Hout Bay groundwater. In larger rainfall events, the sea spray component will be diluted. This means that recharge at higher altitudes will be by larger rainfall events which have a lower concentration of strontium due to containing proportionally less sea

spray and lower $\delta^{18}O$ values. As a result, positive correlation (r = 0.64) is observed between $^{87}Sr/^{86}Sr$ ratio and borehole/wellpoint surface elevation (Fig 4.18)

There is no relationship between $^{87}Sr/^{86}Sr$ ratios and $\delta^{18}O$ values in groundwater on Eastern side of the Table Mountain Range (Finlayson, 2022) in contrast to what has been observed in the Hout Bay groundwater. The correlation between $^{87}Sr/^{86}Sr$ ratios and $\delta^{18}O$ values in groundwater in the Hout Bay area is presumably related to proximity to the ocean where strontium from different sources has less chance to mix. At present, limited strontium isotope data has been obtained on groundwater in the region. Such data will be important for strontium isoscapes currently being developed.

Limitations of this Study:

1. Groundwater sample locations were limited by the location of existing boreholes/wellpoints in Hout Bay and the willingness of the public to allow access to boreholes/wellpoints.
2. COVID-19 regulations interrupted Hout Bay February/March 2020 groundwater water sample collection campaign. When regulations eased, a sufficient number of additional samples were collected in November 2020 to formulate a MSc dissertation.
3. The depth of borehole/wellpoint data was dependent on information provided by the individual who assisted with access to the borehole/wellpoint. This information was not available for many boreholes.
4. No rainwater amount, δD, and $\delta^{18}O$ data for Hout Bay is available for prior to this study.

Recommendations for Future Research and Groundwater Management:

1. Monitoring the state of groundwater is necessary for managing and maintaining this valuable water resource. This includes monitoring sustainable abstraction and identifying any indicators of groundwater deterioration such as pollution and seawater ingress. Degradation of groundwater by anthropogenic contaminants is avoidable through responsible human practices.

Point sources of pollution can be identified through chemical assessments of groundwater samples. Demand for groundwater is likely to increase into the future.

2. Multiple years of sample data collection (groundwater, rainwater, and stream water) would outline trends allow for more intricate data analysis.
3. The collection of collect tap water samples to determine groundwater contamination by leaking water pipes.
4. More borehole/wellpoint sample locations nearer the ocean could enhance resolution of data to more accurately detect seawater ingress.

Summary of Conclusions:

1. A strong correlation between stable isotope composition (δD and $\delta^{18}O$) and rainwater amount of Hout Bay monthly rainwater from March 2020 to February 2021 is attributed to coherence of rainfall due to the proximity of Hout Bay to the ocean.
2. Three possible explanations are proposed for the δD and $\delta^{18}O$ difference between Hout Bay monthly rainwater from March 2020 to February 2021, and Hout Bay February/March 2020 and November 2020 groundwater. The first is that intense rainfall events preferentially recharge groundwater with low δD and $\delta^{18}O$ values. The second explanation is that Hout Bay groundwater might have retained more negative δD and $\delta^{18}O$ values from rainwater recharge prior to March 2020. Lastly, recharge from mountain peaks at higher elevation than the Hout Bay groundwater sample locations add a component of more negative δD and $\delta^{18}O$ to Hout Bay groundwater than proximal rainwater.
3. Differences in Hout Bay groundwater δD, $\delta^{18}O$, and deuterium excess from February/March 2020 to November 2020 are generally within error. Yearly monitoring of groundwater may make changes in more apparent.
4. Hout Bay groundwater February/March 2020 and November 2020 parameters (δD, $\delta^{18}O$, deuterium excess, electrical conductivity, and groundwater temperature) are different between sample locations which reflects areal variation of groundwater. The areal variation is attributed

to various effects such as altitude of recharge precipitation formation and anthropogenic contamination e.g. irrigation water.

5. The electrical conductivity of Hout Bay groundwater in February/March 2020 and November 2020 is indicates quality of groundwater varies, but generally groundwater quality should not be of immediate concern. A slight dilution effect occurs due to heavy rainfall over winter months.
6. The strontium isotope ratios ($^{87}Sr/^{86}Sr$) of Hout Bay groundwater shows that strontium in Hout Bay groundwater is derived from numerous sources. Minor interactions of Hout Bay groundwater with Cape Granite produce relatively high $^{87}Sr/^{86}Sr$ ratios while lower $^{87}Sr/^{86}Sr$ ratios similar to that of modern seawater are attributed to dissolution of the marine sediments of the Quaternary Witzand Formation and marine aerosols in sea spray. Higher rainwater amounts are proposed to increase $^{87}Sr/^{86}Sr$ ratios of higher elevation groundwater sample locations by diluting the dissolution of marine aerosols in rainwater.

References:

Adamson, J. 2006. *ECN Technical Note 3*. Available: http://www.ecn.ac.uk/measurements/technical-notes/preparation-of-conductivity-and- ph-solutions/view [2021, August 11].

Allison, G. B. 1988. A Review of Some of the Physical, Chemical and Isotopic Techniques Available for Estimating Groundwater Recharge. *Estimation of Natural Groundwater Recharge*, 222 pp. 49–72. doi: 10.1007/978-94-015-7780-9_4.

Allsopp, H. L. and Kolbe, P. 1965. Isotopic age determinations on the Cape Granite and intruded Malmesbury sediments, Cape Peninsula, South Africa, *Geochemica et Cosmochimica*, 29, pp. 1115-1130.

Anderson, H. and Cummings, D. 1999. *Measuring the salinity of water*. (Report no. LC0064). Victoria, Australia: Department of Sustainability and Environment.

Bowen, G. J. 2005. Stable hydrogen and oxygen isotope ratios of bottled waters of the world, *Rapid Communications in Mass Spectrometry*, 19(23), pp. 3442–3450. doi: 10.1002/rcm.2216.

Bowen, G. J. and Good, S. P. 2015. Incorporating water isoscapes in hydrological and water resource investigations, *Wiley Interdisciplinary Reviews: Water*, 2(2), pp. 107–119. doi: 10.1002/wat2.1069.

Brown, C., Colvin, C., Hartnady, C., Hay, R., Le Maitre, D. and Riemann, K. 2003. Ecological and environmental impacts of large-scale groundwater development in the Table Mountain Group (TMG) Aquifer system. Discussion document for scoping phase. WRC project K5/1327. (CSIR report no. ENV-S-C 2003-076). Stellenbosch, South Africa: CSIR Environmentek.

Browing, C. and Roberts, D. L. 2015. Lithostratigraphy of the Witzand Formation (Sandveld Group), South Africa, South African Journal of Geology, 118 (3) pp. 317–322.

Chen, F. 2015. Relationship between sub-cloud secondary evaporation and stable isotopes in precipitation of Lanzhou and surrounding area, *Quaternary International*, 380–381, pp. 68–74. doi: 10.1016/j.quaint.2014.12.051.

Christensen, T. H. *et al.* 2000. Characterization of redox conditions in groundwater contaminant plumes, *Journal of Contaminant Hydrology*, 45(3–4), pp. 165–241. doi: 10.1016/S0169-7722(00)00109-1.

Cleaver, G. 2003. Assessment of environmental impacts of groundwater abstraction from Table Mountain Group [TMG] aquifers on ecosystems in the Kammanassie Nature Reserve and environs: report to the Water Research Commission: WRC report 03/1115/1, *Amanzi*, 2004(1115), Available at: http://search.ebscohost.com/login.aspx?direct=true&db=awn&AN=SANB-032301&site=ehost-live.

Clow, D. W. and Mast, M. A. 1997. Strontium 87/strontium 86 as a tracer of mineral weathering reactions and calcium sources in an Alpine/Subalpine Watershed, Loch Vale, Colorado, *Subsurface Hydrology,* 33(6), pp. 1335–1351.

Cobbing, J. and Hiller, B. 2019.Waking a sleeping giant: Realizing the potential of groundwater in Sub-Saharan Africa, *World Development*, 122, pp. 597–613. doi: 10.1016/j.worlddev.2019.06.024.

Colvin, C. 2009. *Ecological and environmental impacts of large-scale groundwater development in the Table Mountain Group (TMG) aquifer system*. Water Research Comission.

Craig, H. 1961. Isotopic variations in meteoric waters, *Science*, 133(3465), pp. 1702–1703. doi: 10.1126/science.133.3465.1702.

Council for Geoscience. 1990. *Cape Town 3318* [Map]. Scale 1:250 000. 1:250 000 Geological Series. Pretoria, South Africa: Council for Geoscience.

Dansgaard, W. 1964. Stable isotopes in precipitation, *Tellus*, 16(4), pp. 436–468. doi: 10.3402/tellusa.v16i4.8993.

Day, L., Ollis, D., Ngobela, T. and Rivers-Moore, N. 2020. *Water quality of rivers and open waterbodies in the City of Cape Town: status and historical trends, with a focus on the period April 2015 to March 2020.* Cape Town, South Africa: City of Cape Town.

Department of Environmental Affairs. 2013. Annual Report 2013. Pretoria, South Africa: Department of Environmental Affairs

Diamond, R. 1997. Stable isotopes of the Thermal springs of the Cape Fold belt. MSc, *Unpublished*, pp. 1–82.

Diamond, R. E. and Harris, C. 2019. Stable isotope constraints on Hydrostratigraphy and aquifer connectivity in the Table Mountain Group, *South African Journal of Geology*, 122(3), pp. 317–330. doi: 10.25131/sajg.122.0021.

Dippenaar, M.A. 2016. Hydrological heritage overview: Cape Town. Pretoria, South Africa: The Water Research Commission.

Elderfield, H. 1986. Strontium isotope stratigraphy, *Palaeogeography, Palaeoclimatology, Palaeoecology*, 57, pp. 71-90.

Finlayson, R. 2022. Spatial analysis of the O-, H-, and Sr- isotope composition of Cape Town groundwater. MSc, *Unpublished.*

Franceschini, G. Compton J. S. 2004. Aeolian and marine deposits of the Tabakbaai Quarry area, western Cape, South Africa, *South African Journal of Geology*, 107, pp. 619-632.

Freeze, R.A. and Cherry, J.A. 1979. Groundwater, Prentice-Hall Inc., Engelwood Cliffs, Vol. 7632, 604.

Frimmel, H. E., Fölling, P. G. and Diamond, R. 2001. Metamorphism of the Permo-Triassic Cape fold belt and its basement, South Africa, *Mineralogy and Petrology*, 73(4), pp. 325– 346. doi: 10.1007/s007100170005.

Gat, J. R. 1971. Comments on the Stable Isotope Method in Regional Groundwater Investigations, *Water Resources Research*, 7(4), pp. 980–993. doi: 10.1029/WR007i004p00980.

Gat, J. R. 1996. Oxygen and hydrogen isotopes in the hydrologic cycle, *Annual Review of Earth and Planetary Sciences*, 24, pp. 225–262. doi: 10.1146/annurev.earth.24.1.225.

Good, S. P. Noone, D. Kurita, N. Benetti, M. Bowen, G. J. 2015. D/H isotope ratios in the global hydrologic cycle, *Geophysical Research Letters*, 42(12), pp. 5042–5050. doi: 10.1002/2015GL064117.

Harris, C. Faure, K. Diamond, R. E. Scheepers, R. 1997.Oxygen and hydrogen isotope geochemistry of S- and I-type granitoids: The Cape Granite suite, South Africa, *Chemical Geology*, 143(1–2), pp. 95–114. doi: 10.1016/S0009-2541(97)00103-4.

Harris, C. Burgers, C. Miller, J. Rawoot, F. 2010. O- and H-isotope record of Cape Town rainfall from 1996 to 2008, and its application to recharge studies of Table Mountain groundwater, South Africa, *South African Journal of Geology*, 113(1), pp. 33–56. doi: 10.2113/gssajg.113.1.33.

Harris, C., Oom, B. M. and Diamond, R. E. 1999. A preliminary investigation of the oxygen and hydrogen isotope hydrology of the greater Cape Town area and an assessment of the potential for using stable isotopes as tracers, *Water SA*, 25(1), pp. 15–24.

International Atomic Energy Agency and World Meteorological Organization. 2006. *Station 6881600 'Malan' (Cape Town) South Africa. Global Network of Isotopes in Precipitation. The GNIP database*. Available: http://isohis.iaea.org [2021, August 14].

Jat, M. K., Khare, D. and Garg, P. K. 2009. Urbanization and its impact on groundwater: A remote sensing and GIS-based assessment approach, *Environmentalist*, 29(1), pp. 17–32. doi: 10.1007/s10669-008-9176-2.

Johnston, S. T. 2000. The Cape Fold Belt and Syntaxis and the rotated Falkland Islands: Dextral transpressional tectonics along the southwest margin of Gondwana', *Journal of African Earth Sciences*, 31(1), pp. 51–63. doi: 10.1016/S0899-5362(00)00072-5.

Jørgensen, N. O., Andersen, M. S. and Engesgaard, P. 2008. Investigation of a dynamic seawater intrusion event using strontium isotopes (87Sr/86Sr), *Journal of Hydrology*, 348(3– 4), pp. 257–269. doi: 10.1016/j.jhydrol.2007.10.001.

Kjeldsen, P. 1993. Groundwater pollution source characterization of an old landfill, *Journal of Hydrology*, 142(1–4), pp. 349–371. doi: 10.1016/0022-1694(93)90018-5.

Koning, T. 2013. Fractured and Weathered Basement Reservoirs: Best Practices for Exploration and Production - Examples from USA, Venezuela, and Brazil. AAPG Annual Convention, Pittsburgh, Pennsylvania, May 21. Poster paper presentation.

Kotwicki, V. 2009. Water balance of Earth', *Hydrological Sciences Journal*, 54(5), pp. 829–840. doi: 10.1623/hysj.54.5.829.

Landwehr, J. M., Coplen, T. B. and Stewart, D. W. 2014. Spatial, seasonal, and source variability in the stable oxygen and hydrogen isotopic composition of tap waters throughout the USA, *Hydrological Processes*, 28(21), pp. 5382–5422. doi: 10.1002/hyp.10004.

Liu, Z. Tian, L. Yao, T. Yu, W 2008. Seasonal deuterium excess in Nagqu precipitation: Influence of moisture transport and recycling in the middle of Tibetan Plateau, *Environmental Geology*, 55(7), pp. 1501–1506. doi: 10.1007/s00254-007-1100-4.

Mauger, C. L. Compton, J. S. 2011. Formation of modern dolomite in hypersaline pans of the Western Cape, South Africa, *Sedimentology*, 58, pp. 1678-1692.

McMullen, C.C., Fritze, K. and Tomilson, R.H. 1966. The half-life of Rubidium- 87. *Canadian Journal of Physics,* 44(12): 3033-3038. https://doi.org/10.1139/p66-248

McNutt, R.H. 2000. Strontium isotopes, *Environmental tracers in subsurface hydrology*. P.G. Cook, and A.L. Herczeg, Eds. Glen Osmond, Australia.

Merlivat, L. and Jouzel, J. 1979. Global climatic interpretation of the deuterium-oxygen 16 relationship for precipitation, *Journal of Geophysical Research*, 84(C8), pp. 5029–5033. doi: 10.1029/JC084iC08p05029.

Midgley, G. F. Chapman, R.A., Hewitson, B., Johnston, P., De Wit, M., Ziervogel, G., Mukheibir, P., Van Niekerk, L., Tadross, M., Van Wilgen, B.W. and Kgope, B. 2005. 'A Status Quo , Vulnerability and Adaptation Assessment of the Physical and Socio-Economic Effects of Climate Change in the Western Cape, *CSIR Report No. ENV-S-C 2005-073*, (January 2005), p. 171.

Midgley, J. J. Harris, C. Harington, A. Potts, A. J. 2012. Geochemical perspective on origins and consequences of Heuweltjie Formation in the Southwestern Cape, South Africa, *South Africa Journal Of Geology*, 115(4), pp. 577-588

Miller, J. A., Dunford, A.J., Swana, K.A., Palcsu, L., Butler, M. and Clarke, C.E. 2017. Stable isotope and noble gas constraints on the source and residence time of spring water from the Table Mountain Group Aquifer, Paarl, South Africa and implications for large scale abstraction, *Journal of Hydrology*. Elsevier B.V., 551, pp. 100–115. doi: 10.1016/j.jhydrol.2017.05.036.

Miller, J. A. 2018. Groundwater quality, quantity, and recharge estimation on the West Coast of South Africa', *Biodiversity & Ecology*, 6(May), pp. 86–95. doi: 10.7809/b- e.00309.

de Montety, V. *et al.* 2008. Origin of groundwater salinity and hydrogeochemical processes in a confined coastal aquifer: Case of the Rhône delta (Southern France), *Applied Geochemistry*, 23(8), pp. 2337–2349. doi: 10.1016/j.apgeochem.2008.03.011.

Otto, F. E. L. Wolski, P., Lehner, F., Tebaldi, C., Van Oldenborgh, G.J., Hogesteeger, S., Singh, R., Holden, P., Fučkar, N.S., Odoulami, R.C. and New, M. 2018. Anthropogenic influence on the drivers of the Western Cape drought 2015-2017, *Environmental Research Letters*, 13(12). doi: 10.1088/1748- 9326/aae9f9.

Pfahl, S. and Sodemann, H. 2013. What controls deuterium excess in global precipitation?, *Climate of the Past Discussions*, 9(4), pp. 4745–4770. doi: 10.5194/cpd-9-4745-2013.

Pietersen, K. and Parsons, R. 2002. The need for Appropriate Research of the Table Mountain Group Aquifer systems, *Water Research Commission*, 158(1).

Riemann, K., Chimboza, N. and Fubesi, M. 2012. A proposed groundwater management framework for municipalities in South Africa, *Water SA*, 38(3), pp. 445–452. doi:10.4314/wsa.v38i3.10.

Rodriquez, K, Intawong, A, Hodgson, N et al. 2017. Fractured Basement – An Overlooked Play Type with Strong Indications of Significant Potential from a Global Seismic Database. First Break, 35 (7). pp. 77-82. ISSN 1365-2397

Rust, I.C. (1973). The Evolution of the Paleozoic Cape Basin, Southern Margin of Africa. In: Nairn, A.E.M., Stehli, F.G. (eds) The South Atlantic. Springer, Boston, MA. https://doi.org/10.1007/978-1-4684-3030-1_6

Scheepers, R. 1995. Geology, geochemistry and petrogenesis of Late Precambrian S-, I- and A-type granitoids in the Saldania belt, Western Cape Province, South Africa, Journal of African Earth Sciences, 21(1), pp. 35–58. doi: 10.1016/0899-5362(95)00087-A.

Scheepers, R. and Schoch, A.E. 2006. The Cape Granite Suite. In the geology of South Africa. M.R., Johnson, C.R., Anhaeusser and R.J., Thomas, Eds. Pretoria, South Africa: Geological Society of South Africa and the Council for Geoscience: 421-432.

Schoch, A., Leterrier, J. and de la Roche, H. 1997. Major element Geochemical Trends in the Cape Granites', *Trans Geol Soc South Afr*, 80, pp. 197–209. Available at: https://journals.co.za/doi/pdf/10.10520/AJA10120750_1262.

Schot, P. P. and van der Wal, J. 1992. Human impact on regional groundwater composition through intervention in natural flow patterns and changes in land use, *Journal of Hydrology*, 134(1–4), pp. 297–313. doi: 10.1016/0022-1694(92)90040-3.

Scott, M., le Roux, P., Sealy, J. and Pickering, R. 2020. Lead and strontium isotopes as palaeodietary indicators in the Western Cape of South Africa. South African Journal of Science, 116(5/6): 1-8. DOI: https://doi.org/10.17159/sajs.2020/6700

Spangenberg, J.E. and Vennemann, T.W. 2008. The stable hydrogen and oxygen isotope variation of water stored in polyethylene terephthalate (PET) bottles. *Rapid Communications in Mass Spectrometry*, 22: 672– 676. DOI: https://doi.org/10.1002/rcm.3415

Stapor Jr, F.W., May, J.P. and Barwis, J. 1983. Eolian Shape-Sorting and Aerodynamic Traction Equivalence in the Coastal Dunes of Hout Bay, Republic of South Africa. Developments in Sedimentology Volume 38, 149–164. http://dx.doi.org/10.1016/S0070-4571(08)70794-5

Stewart, M.K. 1975. Stable isotope fractionation due to evaporation and isotopic exchange of falling water drops, *Journal of Geophysical Research*, 80(9), pp. 1133–1146.

Tankard, A.J., Jackson, M.P.A., Eriksson, K.A., Hobday, D.K., Hunter, D.R., Minter, W.E.L. (1982). The Cape Trough: An Aborted Rift. *Crustal Evolution of Southern Africa*. https://doi.org/10.1007/978-1-4613-8147-1_10

Theron, J.N. 1984. *The geology of Cape Town and environs. Explanation of sheets 3318CD, DC, 3418AB, AD and BA.* Pretoria, South Africa: Department of Mineral and Energy Affairs.

Tredoux, G. Cave, L. Engelbrecht, P. 2004. Groundwater Pollution: Are we monitoring the appropriate parameters?. *Water SA,* 30(5), pp. 114-119

Weaver, J. M. C., Talma, A. S. and Cave, L. C. 1999. Geochemistry and isotopes for resource evaluation in the fractured rock aquifers of the Table Mountain Group, *Water Research Commission*, 481(481), pp. 1–121.

West, A. G., February, E. C. and Bowen, G. J. 2014. Spatial analysis of hydrogen and oxygen stable isotopes ("isoscapes") in ground water and tap water across South Africa, *Journal of Geochemical Exploration*. Elsevier B.V., 145, pp. 213–222. doi: 10.1016/j.gexplo.2014.06.009.

West, J. B. Bowen, J.B. Cerling, T.E. Ehleringer, J.R. 2006. Stable isotopes as one of nature's ecological recorders, *Trends in Ecology and Evolution*, 21(7), pp. 408–414. doi: 10.1016/j.tree.2006.04.002.

Weaver, J.M.C., Talma, A.S. and Cavé, L.C. 1999. Geochemistry and isotopes for resource evaluation in the fractured rock aquifers of the Table Mountain Group. *WRC report no. 481/1/99*. Pretoria, South Africa: Water Research Commission.

Zektser, I.S. and Loaigiga, H.A. 1993. Groundwater fluxes in the global hydrologic cycle: past, present, and future, *Journal of Hydrology,* pp. 405-427

Appendix:

Table 3.3 Picarro spectrometer analysis of 41 Evian water runs in 2020 at UCT

Run:	δD (‰):	$\delta^{18}O$ (‰):
PIC1	-72.0	-10.32
PIC1	-71.8	-10.34
PIC1	-71.7	-10.13
PIC2	-72.1	-10.24
PIC2	-71.7	-10.36
PIC2	-71.7	-10.24
PIC3	-71.8	-10.19
PIC3	-71.7	-10.40
PIC3	-71.7	-10.49
PIC3	-71.5	-10.24
PIC4.1	-71.6	-10.20
PIC4.2	-72.0	-10.05
PIC4.2	-71.7	-10.21
PIC4.2	-71.9	-10.27
PIC5.1	-72.1	-10.38
PIC5.1	-71.5	-10.39
PIC5.1	-71.8	-10.39
PIC5.2	-71.7	-10.32
PIC5.2	-71.7	-10.41
PIC7	-72.3	-10.04
PIC7	-72.0	-10.17
PIC7	-71.9	-10.27
PIC10	-72.2	-10.34
PIC10	-71.6	-10.30
PIC10	-72.1	-10.31
PIC14	-72.2	-10.14
PIC14	-71.8	-10.25
PIC14	-71.5	-10.25
PIC14	-70.4	-10.04
PIC15	-71.8	-10.29
PIC15	-71.1	-10.16
PIC15	-70.6	-9.97
PIC15	-71.0	-10.20
PIC16	-71.5	-10.24
PIC16	-71.4	-10.07
PIC16	-71.3	-10.33
PIC16	-70.2	-9.88
PIC17	-71.3	-10.12
PIC17	-71.7	-10.19
PIC17	-71.6	-10.35
PIC17	-71.8	-10.37
$\bar{x}$	**-71.6**	**-10.24**
σ	**0.4**	**0.13**

$\bar{x}$: mean
σ: standard deviation

Table 3.1 The coordinates (°S, °E), elevation (mamsl), borehole depth (m), and sampling dates of Hout Bay groundwater

Sample #:	Longitude:	Latitude:	Elevation (mamsl)	Borehole Depth (m):	1st Sample date:	2nd Sample date:
HB1	34° 1'27.53"S	18°21'58.35"E	76	75	04/02/2020	02/11/2020
HB2	*NA*	*NA*	*NA*	*NA*	*NA*	*NA*
HB3	34° 1'39.16"S	18°21'12.61"E	10	4	05/02/2020	03/11/2020
HB4	34° 2'28.01"S	18°21'59.53"E	79		05/02/2020	04/11/2020
HB5	34° 0'50.37"S	18°22'41.73"E	74		05/02/2020	17/11/2020
HB6	34° 0'40.74"S	18°23'11.03"E	87	20	05/02/2020	04/11/2020
HB7	34° 1'23.93"S	18°22'14.99"E	81		06/02/2020	05/11/2020
HB8	34° 1'26.08"S	18°22'6.41"E	83		06/02/2020	02/11/2020
HB9	34° 2'30.45"S	18°21'41.03"E	18		06/02/2020	10/11/2020
HB10	34° 0'50.67"S	18°21'50.20"E	86	80	08/02/2020	20/11/2020
HB11	34° 1'53.59"S	18°20'58.33"E	23	7	06/02/2020	05/11/2020
HB12	34° 1'45.42"S	18°21'12.65"E	9	4	06/02/2020	04/11/2020
HB13	34° 1'26.64"S	18°21'26.04"E	13	3	06/02/2020	03/11/2020
HB14	34° 1'13.48"S	18°21'26.23"E	31		06/02/2020	02/11/2020
HB15	34° 1'16.68"S	18°22'16.49"E	57	70	06/02/2020	02/11/2020
HB16	34° 1'4.16"S	18°21'26.87"E	60	76	06/02/2020	04/11/2020
HB17	34° 2'23.64"S	18°21'11.72"E	11	4	06/02/2020	05/11/2020
HB18	34° 0'43.28"S	18°22'29.43"E	122	100	07/02/2020	04/11/2020
HB19	34° 0'40.61"S	18°22'18.20"E	144	110	07/02/2020	04/11/2020
HB20	34° 0'48.90"S	18°23'21.45"E	95		07/02/2020	18/11/2020
HB21	34° 1'34.83"S	18°20'42.41"E	70	110	07/02/2020	19/11/2020
HB22	34° 1'23.92"S	18°22'39.94"E	118	46	07/02/2020	03/11/2020

mamsl: meters above mean sea level
NA means a value is unknown either due to technical reasons or because a sample was not acquired.

Sample #:	Longitude:	Latitude:	Elevation (mamsl):	Borehole Depth (m):	1st Sample date:	2nd Sample date:
HB23	34° 2'40.34"S	18°22'1.52"E	87		07/02/2020	05/11/2020
HB24	34° 2'40.03"S	18°22'2.44"E	90		07/02/2020	05/11/2020
HB25	34° 2'37.86"S	18°22'2.91"E	88		07/02/2020	05/11/2020
HB26	34° 2'37.86"S	18°22'2.91"E	88		07/02/2020	05/11/2020
HB27	34° 1'32.36"S	18°21'17.65"E	13	5	07/02/2020	03/11/2020
HB28	34° 1'11.25"S	18°21'29.95"E	36	45	08/02/2020	04/11/2020
HB29	34° 1'4.64"S	18°21'39.82"E	46	35	08/02/2020	04/11/2020
HB30	34° 0'53.52"S	18°23'13.12"E	100	48	08/02/2020	04/11/2020
HB31	34° 1'11.10"S	18°22'28.95"E	54	16	08/02/2020	17/11/2020
HB32	34° 2'22.81"S	18°20'53.69"E	37	47	08/02/2020	17/11/2020
HB33	34° 1'49.09"S	18°20'57.83"E	28		08/02/2020	05/11/2020
HB34	34° 1'56.16"S	18°20'58.92"E	24	20	10/02/2020	05/11/2020
HB35	34° 0'44.23"S	18°22'37.83"E	102	90	10/02/2020	10/11/2020
HB36	34° 0'41.10"S	18°21'7.70"E	162		10/02/2020	19/11/2020
HB37	34° 0'56.52"S	18°21'51.12"E	59	60	10/02/2020	20/11/2020
HB38	34° 0'56.62"S	18°21'49.92"E	58		12/02/2020	10/11/2020
HB39	34° 2'10.09"S	18°21'6.42"E	9	6	17/02/2020	05/11/2020
HB40	34° 1'59.62"S	18°21'1.15"E	21	3	18/02/2020	05/11/2020
HB41	34° 2'11.38"S	18°21'49.66"E	112	60	21/02/2020	04/11/2020
HB42	34° 1'2.34"S	18°23'2.97"E	108	80	21/02/2020	05/11/2020
HB43	34° 1'12.83"S	18°22'59.18"E	132	180	21/02/2020	04/11/2020
HB44	34° 2'10.81"S	18°21'42.50"E	76		23/02/2020	04/11/2020

mamsl: meters above mean sea level
NA means a value is unknown either due to technical reasons or because a sample was not acquired.

Sample #:	Longitude:	Latitude:	Elevation (mamsl):	Borehole Depth (m):	1st Sample date:	2nd Sample date:
HB44	34° 2'10.81"S	18°21'42.50"E	76		23/02/2020	04/11/2020
HB45	34° 2'9.84"S	18°21'38.06"E	61	70	23/02/2020	04/11/2020
HB46	34° 0'32.11"S	18°22'56.29"E	138	95	23/02/2020	17/11/2020
HB47	34° 1'57.84"S	18°21'17.58"E	6	40	26/02/2020	18/11/2020
HB48	34° 1'57.50"S	18°21'17.54"E	6	5	26/02/2020	18/11/2020
HB49	34° 2'27.20"S	18°20'59.47"E	16		26/02/2020	10/11/2020
HB50	34° 0'52.28"S	18°21'50.81"E	79	53	27/02/2020	20/11/2020
HB51	34° 1'1.45"S	18°21'55.31"E	49	42	27/02/2020	10/11/2020
HB52	34° 0'58.82"S	18°21'47.35"E	49	75	27/02/2020	10/11/2020
HB53	34° 0'49.26"S	18°21'51.57"E	87	75	27/02/2020	10/11/2020
HB54	34° 2'22.23"S	18°21'34.72"E	20	30	01/03/2020	18/11/2020
HB55	34° 1'41.06"S	18°21'12.87"E	9	2	01/03/2020	19/11/2020
HB56	34° 0'27.85"S	18°22'56.49"E	158		05/03/2020	17/11/2020
HB57	34° 1'31.66"S	18°20'39.64"E	86		05/03/2020	10/11/2020
HB58	34° 1'28.68"S	18°20'38.12"E	102		05/03/2020	10/11/2020
HB59	34° 1'33.21"S	18°21'28.74"E	15	6	05/03/2020	10/11/2020
HB60	*NA*	*NA*	*NA*	*NA*	*NA*	*NA*
HB61	34° 1'29.47"S	18°22'31.39"E	12		NA	12/11/2020
HB62	34° 1'50.97"S	18°20'55.29"E	30		NA	18/11/2020
HB63	34° 0'40.56"S	18°22'52.08"E	109		NA	10/11/2020
HB64	34° 1'32.68"S	18°20'41.02"E	81		NA	10/11/2020
HB65	34° 1'33.86"S	18°20'39.25"E	80		NA	10/11/2020

mamsl: meters above mean sea level
NA means a value is unknown either due to technical reasons or because a sample was not acquired.

Table 3.2 The coordinates (°S, °E), elevation (mamsl), and sampling dates (where applicable) of; Kirstenbosch, rain gauges (Hout Bay, UCT) , Hout Bay streams, and Terraclimate models (Hout Bay, UCT).

	Longitude:	Latitude:	Elevation (mamsl):	Date:
Rain Gauges:				
Hout Bay	34° 0'51.56"S	18°21'49.56"E	81	02/2020-02/2021 (monthly)
UCT	33°57'32.18"S	18°27'37.71"E	114	01/2001-02/2021 (monthly)
Terraclimate Models:				
Hout Bay	34°1'0.12"S	18°21'42.84"E	51	02/2020-12/2021 (monthly)
Kirstenbosch	33°59'15.51"S	18°25'57.90"E	132	01/1997-12/2007 (monthly)
Hout Bay Streams:				
S1	34° 0'23.68"S	18°24'2.14"E	254	17/08/2020
S2	34° 0'14.19"S	18°24'1.31"E	279	17/08/2020
S3	34° 0'3.96"S	18°24'1.94"E	323	17/08/2020
S4	33°59'54.31"S	18°24'2.11"E	334	17/08/2020
S5	33°59'36.84"S	18°24'9.19"E	382	17/08/2020
S6	33°59'32.25"S	18°24'1.66"E	377	17/08/2020
S7	33°59'28.91"S	18°23'13.31"E	405	17/08/2020
S8	33°59'37.15"S	18°23'12.61"E	358	17/08/2020
S9	33°59'58.81"S	18°23'10.74"E	290	17/08/2020
S10	34° 0'22.68"S	18°22'47.16"E	214	18/08/2020
S11	34° 0'29.70"S	18°22'33.78"E	208	18/08/2020
S12	34° 0'31.32"S	18°22'9.48"E	207	18/08/2020
S13	34° 2'35.89"S	18°22'38.29"E	239	18/08/2020
S14	34° 2'36.09"S	18°22'38.63"E	244	18/08/2020